

Study of the CKM angle γ sensitivity using flavor untagged $B_s^0 \rightarrow \tilde{D}^{(*)0} \phi$ decays*

D. Ao(敖冬)¹ D. Decamp² W. B. Qian(钱文斌)¹ S. Ricciardi³ H. Sazak⁴ S. T'Jampens² V. Tisserand⁴
Z. R. Wang(王子睿)⁵ Z. W. Yang(杨振伟)⁵ S. N. Zhang(张舒楠)⁶ X. K. Zhou(周晓康)^{1†}

¹University of Chinese Academy of Sciences, Beijing 100049, China

²Univ. Grenoble Alpes, Univ. Savoie Mont Blanc, CNRS, IN2P3-LAPP, Annecy, France

³STFC Rutherford Appleton Laboratory, Didcot, United Kingdom

⁴Université Clermont Auvergne, CNRS/IN2P3, LPC, Clermont-Ferrand, France

⁵Center for High Energy Physics, Tsinghua University, Beijing 100084, China

⁶School of Physics State Key Laboratory of Nuclear Physics and Technology, Peking University, Beijing 100871, China

Abstract: A sensitivity study on the measurement of the CKM angle γ from $B_s^0 \rightarrow \tilde{D}^{(*)0} \phi$ decays is conducted using the D -meson reconstructed in the quasi flavour-specific modes $K\pi$, $K3\pi$, and $K\pi\pi^0$, as well as CP -eigenstate modes KK and $\pi\pi$, where the notation \tilde{D}^0 corresponds to a D^0 or \bar{D}^0 meson. The LHCb experiment is presented as a use case. A statistical uncertainty of approximately $8^\circ - 19^\circ$ can be achieved with the pp collision data collected in the LHCb experiment from 2011 to 2018. The sensitivity to γ should be of the order $3^\circ - 8^\circ$ after accumulating 23 fb^{-1} of pp collision data by 2025, whereas it is expected to improve further by 300 fb^{-1} by the second half of the 2030 decade. The accuracy is dependent on the strong parameters $r_B^{(*)}$ and $\delta_B^{(*)}$, which together with γ describe the interference between the leading amplitudes of the $B_s^0 \rightarrow \tilde{D}^{(*)0} \phi$ decays.

Keywords: sensitivity study, CKM angle γ , $B_s^0 \rightarrow \tilde{D}^{(*)0} \phi$ decays

DOI: 10.1088/1674-1137/abd16d

I. INTRODUCTION

Precision measurement of the CKM [1] angle γ (which is defined as $\arg[-V_{ud}V_{ub}^*/V_{cd}V_{cb}^*]$) in various B -meson decay modes is one of the main goals of flavor physics. Such measurements can be achieved by exploiting the interference of the decays that proceed via the $b \rightarrow c\bar{u}s$ and $b \rightarrow u\bar{c}s$ tree-level amplitudes, in which the determination of the relative weak phase γ is not affected by theoretical uncertainties.

Several methods have been proposed to extract γ [2–11]. In LHCb, the best precision is obtained by combining the measurements of many decay modes, which yields $\gamma = (74.0_{-5.8}^{+5.0})^\circ$ [12]. This precision dominates the world average of γ from tree-level decays. LHCb has presented a new measurement based on the BPGGSZ method [7] using the full Run 1 and Run 2 data. The result is $\gamma = (68.7_{-5.1}^{+5.2})^\circ$ [13], and it constitutes the single best world measurement of γ . A 2σ difference between B^+

and B_s^0 results was observed since the summer of 2018. The B_s^0 measurement is based on a single decay mode with only Run 1 data, *i.e.*, $B_s^0 \rightarrow D_s^\mp K^\pm$,¹⁾ and exhibits large uncertainty [14]. In October 2020, LHCb included a similar analysis with the decay $B_s^0 \rightarrow D_s^\mp K^\pm \pi^+ \pi^-$ [15] based on Run 1 and Run 2 data, for which $\gamma - 2\beta_s = (42 \pm 10 \pm 4 \pm 5)^\circ$. The most recent LHCb combination is therefore $\gamma = (67 \pm 4)^\circ$ [16], and the new B^+ (B_s^0) result is $(64_{-5}^{+4})^\circ$ ($(82_{-20}^{+17})^\circ$). Additional B_s^0 decay modes will aid in improving the measurement precision of the B_s^0 modes and the understanding of a possible discrepancy with respect to the B^+ modes. The two analyses based on $B_s^0 \rightarrow D_s^\mp K^\pm (\pi^+ \pi^-)$ use time-dependent methods and are therefore strongly reliant on the B -tagging capabilities of the LHCb experiment. It should be noted that measurements exist at LHCb for B^0 mesons [17, 18], which also exhibit quite good prospects as their current average is $(82_{-9}^{+8})^\circ$. These are based on the decay $B^0 \rightarrow D^0 K^{*0}$, where the B^0 is self-tagged from the

Received 3 August 2020; Accepted 30 November 2020; Published online 18 January 2021

* Supported by National Natural Science Foundation of China (NSFC) (11925504, 11975015); the 65th batch of China Postdoctoral Fund; the Fundamental Research Funds for the Central Universities, CNRS/IN2P3 (France), and STFC (United Kingdom) national agencies. Part of this work was supported through exchanges between Annecy, Beijing, and Clermont-Ferrand, by the France China Particle Physics Laboratory (*i.e.* FCPLL)

[†] E-mail: xiaokang.zhou@cern.ch

1) The inclusion of charge-conjugated processes is implied throughout the paper, unless otherwise stated.



Content from this work may be used under the terms of the Creative Commons Attribution 3.0 licence. Any further distribution of this work must maintain attribution to the author(s) and the title of the work, journal citation and DOI. Article funded by SCOAP³ and published under licence by Chinese Physical Society and the Institute of High Energy Physics of the Chinese Academy of Sciences and the Institute of Modern Physics of the Chinese Academy of Sciences and IOP Publishing Ltd

$K^{*0} \rightarrow K^+\pi^-$ decay. As opposed to measurements with B_s^0 , those with B^0 and B^+ are also accessible at Belle II [19]. The prospects of these measurements at LHCb are provided in Ref. [20]. For the mode $B_s^0 \rightarrow D_s^\mp K^\pm$, one may anticipate a precision on γ of the order of 4° after the end of LHC Run 3 in 2025, and 1° by 2035-2038. In combination with the B^0 and B^+ modes, the expected sensitivities are 1.5° and 0.35° . The anticipated precision provided by Belle II is 1.5° .

In this work, $B_s^0 \rightarrow \bar{D}^{(*)0} \phi$ decays, the observations of which were published by the LHCb experiment in 2013 [21] and 2018 [22], are used to determine γ . A novel method presented in Ref. [22] also demonstrated the feasibility of measuring $B_s^0 \rightarrow \bar{D}^{(*)0} \phi$ decays with a high purity. A partial reconstruction method is used for the $\bar{D}^{(*)0}$ meson [23]. A time-integrated method [24-26] was investigated, in which it was shown that information regarding CP violation is preserved in the untagged rate of $B_s^0 \rightarrow \bar{D}^{(*)0} \phi$ (or of $B^0 \rightarrow \bar{D}^0 K_S^0$), and that if a sufficient number of different D -meson final states is included in the analysis, this decay alone can be used to measure γ in principle. The sensitivity to γ is expected to be much better with the case of the $B_s^0 \rightarrow \bar{D}^{(*)0} \phi$ decay than for $B^0 \rightarrow \bar{D}^0 K_S^0$, as it is proportional to the decay width difference $y = \Delta\Gamma/2\Gamma$ defined in Section II and is equal to $(6.3 \pm 0.3)\%$ for B_s^0 mesons and $(0.05 \pm 0.50)\%$ for B^0 [27]. The sensitivity to γ from the $B_s^0 \rightarrow \bar{D}^{(*)0} \phi$ modes arises from the interference between two colour-suppressed diagrams, as illustrated in Fig. 1. The relatively large expected value of the ratio of the $\bar{b} \rightarrow \bar{u}c\bar{s}$ and $\bar{b} \rightarrow \bar{c}u\bar{s}$ tree-level amplitudes (20%–40%; see Section IVA) serves as additional motivation for measuring γ in $B_s^0 \rightarrow \bar{D}^{(*)0} \phi$ decays. In this study, five neutral D -meson decay modes, namely $K\pi$, $K3\pi$, $K\pi\pi^0$, KK , and $\pi\pi$, are included, the event yields of which are estimated using realistic assumptions based on measurements from LHCb [22, 28, 29]. We justify the choice of these decays and also discuss the case of the two decay modes $\bar{D}^0 \rightarrow K_S^0 \pi^+ \pi^-$ and $K_S^0 K^+ K^-$ in Section III.

In Section II, the notations and the selection of the D -meson decay final states are introduced. In Section III, the expected signal yields and their uncertainties are presented. In Section IV, the sensitivity that can be achieved using solely these decays is presented, and fur-

ther improvements are briefly discussed. In Section V, the future expected precision on γ with $B_s^0 \rightarrow \bar{D}^{(*)0} \phi$ at LHCb is discussed for the dataset available after LHC Run 3 by 2025 and after a possible second upgrade of LHCb by 2038. Finally, conclusions are presented in Section VI.

II. FORMALISM

Following the formalism introduced in Refs. [24-26], we define the amplitudes

$$A(B_s^0 \rightarrow \bar{D}^{(*)0} \phi) = A_B^{(*)}, \quad (1)$$

$$A(B_s^0 \rightarrow \bar{D}^{(*)0} \phi) = A_B^{(*)} r_B^{(*)} e^{i(\delta_B^{(*)} + \gamma)}, \quad (2)$$

where $A_B^{(*)}$ and $r_B^{(*)}$ are the magnitude of the B_s^0 decay amplitude and amplitude magnitude ratio between the suppressed over the favored B_s^0 decay modes, respectively, whereas $\delta_B^{(*)}$ and γ are the strong and weak phases, respectively. Neglecting mixing and CP violation in the D decays (see, for example, Refs. [30, 31]), the amplitudes into the final state f (denoted below as $[f]_D$) and its CP conjugate \bar{f} are defined as

$$A(\bar{D}^0 \rightarrow f) = A(D^0 \rightarrow \bar{f}) = A_f, \quad (3)$$

$$A(D^0 \rightarrow f) = A(\bar{D}^0 \rightarrow \bar{f}) = A_f r_D^f e^{i\delta_D^f}, \quad (4)$$

where δ_D^f and r_D^f are the strong phase difference and relative magnitude, respectively, between the $D^0 \rightarrow f$ and $\bar{D}^0 \rightarrow f$ decay amplitudes.

The amplitudes of the full decay chains are given by

$$\begin{aligned} A_{Bf} &\equiv A(B_s^0 \rightarrow [f]_{D^{(*)}} \phi) \\ &= A_B^{(*)} A_f^{(*)} \left[1 + r_B^{(*)} r_D^f e^{i(\delta_B^{(*)} + \delta_D^f + \gamma)} \right], \end{aligned} \quad (5)$$

$$\begin{aligned} A_{B\bar{f}} &\equiv A(B_s^0 \rightarrow [\bar{f}]_{D^{(*)}} \phi) \\ &= A_B^{(*)} A_f^{(*)} \left[r_B^{(*)} e^{i(\delta_B^{(*)} + \gamma)} + r_D^f e^{i\delta_D^f} \right]. \end{aligned} \quad (6)$$

The amplitudes of the CP -conjugate decays are obtained

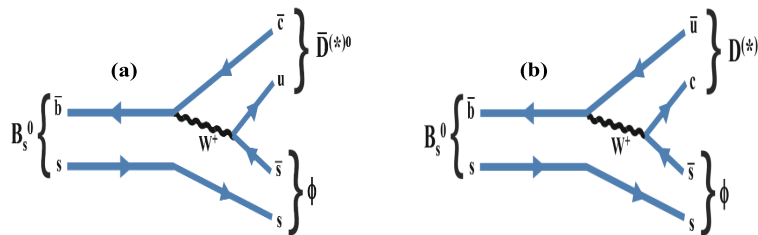


Fig. 1. (color online) Feynman diagrams for (a) $B_s^0 \rightarrow \bar{D}^{(*)0} \phi$ and (b) $B_s^0 \rightarrow D^{(*)0} \phi$ decays.

by changing the sign of the weak phase γ

$$\bar{A}_{Bf} \equiv A(\bar{B}_s^0 \rightarrow [f]_{D^{(*)}\phi}) = A_B^{(*)} A_f^{(*)} \left[r_B^{(*)} e^{i(\delta_B^{(*)}-\gamma)} + r_D^f e^{i\delta_D^f} \right], \quad (7)$$

$$\bar{A}_{B\bar{f}} \equiv A(\bar{B}_s^0 \rightarrow [\bar{f}]_{D^{(*)}\phi}) = A_B^{(*)} A_f^{(*)} \left[1 + r_B^{(*)} r_D^f e^{i(\delta_B^{(*)}+\delta_D^f-\gamma)} \right]. \quad (8)$$

$$\frac{d\Gamma(B_s^0(\tau) \rightarrow [f]_{D^{(*)}\phi})}{d\tau} + \frac{d\Gamma(\bar{B}_s^0(\tau) \rightarrow [f]_{D^{(*)}\phi})}{d\tau} \propto e^{-\tau} |A_{Bf}|^2 \times \left[(1 + |\lambda_f|^2) \cosh(y\tau) - 2\text{Re}(\lambda_f) \sinh(y\tau) \right]. \quad (9)$$

A. Time acceptance

Experimentally, owing to the trigger and selection requirements as well as inefficiencies in the reconstruction, the decay time distribution is affected by the acceptance effects. The acceptance correction has been estimated from pseudoexperiments based on a related publication by the LHCb collaboration [34]. It is described by an empirical acceptance function

$$\varepsilon_{ta}(\tau) = \frac{(\alpha\tau)^\beta}{1 + (\alpha\tau)^\beta} (1 - \xi\tau), \quad (10)$$

with $\alpha = 1.5$, $\beta = 2.5$, and $\xi = 0.01$.

Taking into account this effect, the time-integrated untagged decay rate is

$$\Gamma(\bar{B}_s^0 \rightarrow [f]_{D^{(*)}\phi}) = \int_0^\infty \left[\frac{d\Gamma(B_s^0(\tau) \rightarrow [f]_{D^{(*)}\phi})}{d\tau} + \frac{d\Gamma(\bar{B}_s^0(\tau) \rightarrow [f]_{D^{(*)}\phi})}{d\tau} \right] \varepsilon_{ta}(\tau) d\tau. \quad (11)$$

By defining the function

$$g(x) = \int_0^\infty \frac{e^{-x\tau} (1 + \xi\tau(\alpha\tau)^\beta)}{1 + (\alpha\tau)^\beta} d\tau, \quad (12)$$

and using Eq. (9), one obtains

$$\Gamma(B_s^0 \rightarrow [f]_{D\phi}) \propto |A_{Bf}|^2 \left[(1 + |\lambda_f|^2) \mathcal{A} - 2y\text{Re}(\lambda_f) \mathcal{B} \right], \quad (13)$$

where $\mathcal{A} = 1 - [g(1-y) + g(1+y)]/2$ and $\mathcal{B} = 1 - [g(1-y) - g(1+y)]/2y$. With $y = (0.128 \pm 0.009)/2$ for the B_s^0 meson

Using the standard notations

$$\tau = \Gamma_s t, \quad \Gamma_s = \frac{\Gamma_L + \Gamma_H}{2}, \quad \Delta\Gamma_s = \Gamma_L - \Gamma_H, \\ y = \frac{\Delta\Gamma_s}{2\Gamma_s}, \quad \lambda_f = \frac{q}{p} \cdot \frac{\bar{A}_{Bf}}{A_{Bf}},$$

and assuming that $|q/p| = 1$ ($|q/p| = 1.0003 \pm 0.0014$ [32]), the untagged decay rate for the decay $B_s^0/\bar{B}_s^0 \rightarrow [f]_{D^{(*)}\phi}$ is obtained by Eq. (10) of Ref. [33]:

[27], one obtains $\mathcal{A} = 0.488 \pm 0.005$ and $\mathcal{B} = 0.773 \pm 0.008$. Examples of decay-time acceptance distributions are displayed in Fig. 2.

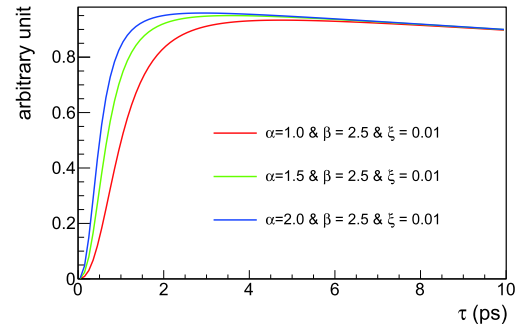


Fig. 2. (color online) Examples of decay-time acceptance distributions for three different sets of parameters α , β , and ξ (nominal in green).

B. Observables for D^0 decays

The D -meson decays are reconstructed in quasi flavor-specific modes $f^-(\equiv f) = K^-\pi^+$, $K^-\pi^+\pi^0$, and $K^-\pi^+\pi^0$; their CP -conjugate modes $f^+(\equiv \bar{f}) = K^+\pi^-$, $K^+\pi^-\pi^0$, and $K^+\pi^-\pi^0$; and CP -eigenstate modes $f_{CP} = K^+K^-$ and $\pi^+\pi^-$.

In the following, we introduce the weak phase β_s that is defined as $\beta_s = \arg\left(-\frac{V_{ts}V_{tb}^*}{V_{cs}V_{cb}^*}\right)$. From Eqs. (5), (7), and (13) and with $\lambda_f = e^{2i\beta_s} \frac{\bar{A}_{Bf}}{A_{Bf}}$, for a given number of un-

tagged B_s^0 mesons produced in the pp collisions at the LHCb interaction point, $N(B_s^0)$, we can compute the number of $B_s^0 \rightarrow \bar{D}^0\phi$ decays with the D meson decaying into the final state f^- . For the reference decay mode $f^- \equiv K^-\pi^+$, we obtain

$$N(B_s^0 \rightarrow [K^-\pi^+]_D [K^+K^-]_\phi) = C_{K\pi} \left[-2\mathcal{B}y r_B \cos(\delta_B + 2\beta_s - \gamma) + \mathcal{A}(1 + r_B^2 + 4r_B r_D^{K\pi} \cos\delta_B \cos(\delta_D^{K\pi} + \gamma)) \right], \quad (14)$$

in which the terms proportional to $(r_D^{K\pi})^2 \ll 1$ and $yr_D^{K\pi} \ll 1$ have been neglected ($r_D^{K\pi} = 5.90_{-0.25}^{+0.34} \%$ [27]). The best approximation for the scale factor $C_{K\pi}$ is

$$C_{K\pi} = N(B_s^0 \rightarrow \varepsilon(B_s^0 \rightarrow [K^- \pi^+]_D [K^+ K^-]_\phi) \times Br(B_s^0 \rightarrow [K^- \pi^+]_D [K^+ K^-]_\phi), \quad (15)$$

where $\varepsilon(B_s^0 \rightarrow [K^- \pi^+]_D [K^+ K^-]_\phi)$ is the global detection efficiency of this decay mode, and $Br(B_s^0 \rightarrow [K^- \pi^+]_D [K^+ K^-]_\phi)$ is its branching fraction. The value of the scale

factor $C_{K\pi}$ is estimated from the LHCb Run 1 data [22], the average f_s/f_d of the b -hadron production fraction ratio measured by LHCb [35], and the different branching fractions [32].

For better numerical behavior, we use the Cartesian coordinate parameterization

$$x_\pm^{(*)} = r_B^{(*)} \cos(\delta_B^{(*)} \pm \gamma) \quad \text{and} \quad y_\pm^{(*)} = r_B^{(*)} \sin(\delta_B^{(*)} \pm \gamma). \quad (16)$$

Subsequently, Eq. (14) becomes

$$N(B_s^0 \rightarrow [K^- \pi^+]_D [K^+ K^-]_\phi) = C_{K\pi} \left[-2\mathcal{B}y[x_- \cos(2\beta_s) - y_- \sin(2\beta_s)] + \mathcal{A}(1 + x_-^2 + y_-^2 + 2r_D^{K\pi}[(x_+ + x_-) \cos \delta_D^{K\pi} - (y_+ - y_-) \sin \delta_D^{K\pi}]) \right]. \quad (17)$$

For three and four body final states $K3\pi$ and $K\pi\pi^0$, multiple interfering amplitudes exist; therefore, their amplitudes and phases δ_D^f vary across the decay phase space. However, an analysis that is integrated over the phase space can be performed in a very similar manner to two body decays with the inclusion of an additional para-

meter, namely the so-called coherence factor R_D^f , which has been measured in previous experiments [36]. The strong phase difference δ_D^f is then treated as an effective phase that is averaged over all amplitudes. For these modes, we obtain an expression similar to (17):

$$N(B_s^0 \rightarrow [f^-]_D [K^+ K^-]_\phi) = C_{K\pi} F_f \left[-2\mathcal{B}y[x_- \cos(2\beta_s) - y_- \sin(2\beta_s)] + \mathcal{A}(1 + x_-^2 + y_-^2 + 2r_D^f R_D^f [(x_+ + x_-) \cos \delta_D^f - (y_+ - y_-) \sin \delta_D^f]) \right], \quad (18)$$

where F_f is the scale factor of the f decay relative to the $K\pi$ decay and depends on the ratios of detection efficiencies and branching fractions of the corresponding modes

$$F_f = \frac{C_f}{C_{K\pi}} = \frac{\varepsilon(D \rightarrow f)}{\varepsilon(D \rightarrow K\pi)} \times \frac{[Br(D^0 \rightarrow f) + Br(\bar{D}^0 \rightarrow f)]}{[Br(D^0 \rightarrow K^- \pi^+) + Br(\bar{D}^0 \rightarrow K^- \pi^+)]}. \quad (19)$$

The value of F_f for the different modes used in this study is determined from the LHCb measurements in the $B^\pm \rightarrow DK^\pm$ and $B^\pm \rightarrow D\pi^\pm$ modes, with two or four-body D decays [28, 29].

The time-integrated untagged decay rate for $B_s^0 \rightarrow [f]_D \phi$ is given by Eq. (13) by substituting $A_{Bf} \rightarrow \bar{A}_{B\bar{f}}$ and $\lambda_f \rightarrow \bar{\lambda}_{\bar{f}} = \lambda_f^{-1} = e^{-2i\beta_s} (A_{B\bar{f}}/\bar{A}_{B\bar{f}})$, which is equivalent to the change $\beta_s \rightarrow -\beta_s$ and $\gamma \rightarrow -\gamma$ (*i.e.*, $x_\pm \rightarrow x_\mp$ and $y_\pm \rightarrow y_\mp$). Therefore, the observables are

$$N(B_s^0 \rightarrow [K^+ \pi^-]_D [K^+ K^-]_\phi) = C_{K\pi} \left[-2\mathcal{B}y[x_+ \cos(2\beta_s) + y_+ \sin(2\beta_s)] + \mathcal{A}(1 + x_+^2 + y_+^2 + 2r_D^{K\pi} [(x_+ + x_-) \cos \delta_D^{K\pi} + (y_+ - y_-) \sin \delta_D^{K\pi}]) \right], \quad (20)$$

and for the modes $f^+ \equiv K^+ 3\pi$, $K^+ \pi^- \pi^0$

$$N(B_s^0 \rightarrow [f^+]_D [K^+ K^-]_\phi) = C_{K\pi} F_f \left[-2\mathcal{B}y[x_+ \cos(2\beta_s) + y_+ \sin(2\beta_s)] + \mathcal{A}(1 + x_+^2 + y_+^2 + 2r_D^f R_f^f [(x_+ + x_-) \cos \delta_D^f + (y_+ - y_-) \sin \delta_D^f]) \right]. \quad (21)$$

Obviously, any significant asymmetries on the yield of the observable corresponding to Eq. (17) with respect to Eq. (20), or Eq. (18) with respect to Eq. (21), are a clear signature for CP violation.

For the CP -eigenstate modes $D \rightarrow h^+ h^-$ ($h \equiv K, \pi$), we have $r_D = 1$ and $\delta_D = 0$. By following the same approach as that for quasi flavor-specific modes, the observables can be written as

$$N(B_s^0 \rightarrow [h^+ h^-]_D [K^+ K^-]_\phi) = 4C_{K\pi} F_{hh} \left[\mathcal{A} \left(1 + x_+^2 + y_+^2 + x_+ + x_- \right) - \mathcal{B}y \left((1 + x_+ + x_- + x_+ x_- + y_+ y_-) \cos(2\beta_s) \right. \right. \\ \left. \left. + (y_+ - y_- + y_+ x_- - x_+ y_-) \sin(2\beta_s) \right) \right]. \quad (22)$$

Analogous to F_f , F_{hh} is defined as

$$F_{hh} = \frac{C_{hh}}{C_{K\pi}} = \frac{\varepsilon(D \rightarrow hh)}{\varepsilon(D \rightarrow K\pi)} \times \frac{Br(D^0 \rightarrow hh)}{[Br(D^0 \rightarrow K^- \pi^+) + Br(\bar{D}^0 \rightarrow K^- \pi^+)]} \quad (23)$$

and their values are determined in the same manner as F_f .

For the modes $K_S^0 \pi^+ \pi^-$ and $K_S^0 K^+ K^-$ (i.e., $K_S^0 hh$), we obtain

$$N(B_s^0 \rightarrow [K_S^0 hh]_D [K^+ K^-]_\phi) = 2C_{K\pi} F_{K_S^0 hh} \times \left[-\mathcal{B}y \left[(x_+ + x_-) \cos(2\beta_s) + (y_+ - y_-) \sin(2\beta_s) \right] + \mathcal{A} \left(1 + x_-^2 + y_-^2 + 2(x_+ + x_-) \right. \right. \\ \left. \left. \times r_D^{K_S^0 hh}(m_+^2, m_-^2) \kappa_D^{K_S^0 hh}(m_+^2, m_-^2) \cos \delta_D^{K_S^0 hh}(m_+^2, m_-^2) \right) \right], \quad (24)$$

where $F_{K_S^0 hh}$ is defined as in Eq. (23). The strong parameters $r_D^{K_S^0 hh}(m_+^2, m_-^2)$, $\kappa_D^{K_S^0 hh}(m_+^2, m_-^2)$, and $\cos \delta_D^{K_S^0 hh}(m_+^2, m_-^2)$ vary over the Dalitz plot $(m_+^2, m_-^2) \equiv (m^2(K_S^0 \pi^+), m^2(K_S^0 \pi^-))$ and are defined in Section III.

C. Observables for D^{*0} decays

For the D^{*0} decays, we consider the two modes $D^{*0} \rightarrow D^0 \pi^0$ and $D^{*0} \rightarrow D^0 \gamma$, where the D^0 mesons are re-

constructed, as in the above, in quasi flavor-specific modes $K\pi$, $K3\pi$, and $K\pi\pi^0$ as well as CP -eigenstate modes $\pi\pi$ and KK . As demonstrated in Ref. [37], the formalism for the cascade $B_s^0 \rightarrow \bar{D}^{*0} \phi$, $\bar{D}^{*0} \rightarrow \bar{D}^0 \pi^0$ is similar to that of $B_s^0 \rightarrow \bar{D}^0 \phi$. Therefore, the relevant observables can be written similarly to Eqs. (17), (18), (20), (21), and (22), by substituting $C_{K\pi} \rightarrow C_{K\pi, D\pi^0}$, $r_B \rightarrow r_B^*$, and $\delta_B \rightarrow \delta_B^*$ ($x_\pm \rightarrow x_\pm^*$ and $y_\pm \rightarrow y_\pm^*$):

$$N(B_s^0 \rightarrow [K^- \pi^+]_D \pi^0]_{D^*} [K^+ K^-]_\phi) = C_{K\pi, D\pi^0} \left[-2\mathcal{B}y [x_-^* \cos(2\beta_s) - y_-^* \sin(2\beta_s)] \right. \\ \left. + \mathcal{A} \left(1 + x_-^{*2} + y_-^{*2} + 2r_D^{K\pi} [(x_+^* + x_-^*) \cos \delta_D^{K\pi} - (y_+^* - y_-^*) \sin \delta_D^{K\pi}] \right) \right], \quad (25)$$

$$N(B_s^0 \rightarrow [K^+ \pi^-]_D \pi^0]_{D^*} [K^+ K^-]_\phi) = C_{K\pi, D\pi^0} \left[-2\mathcal{B}y [x_+^* \cos(2\beta_s) + y_+^* \sin(2\beta_s)] \right. \\ \left. + \mathcal{A} \left(1 + x_+^{*2} + y_+^{*2} + 2r_D^{K\pi} [(x_+^* + x_-^*) \cos \delta_D^{K\pi} + (y_+^* - y_-^*) \sin \delta_D^{K\pi}] \right) \right], \quad (26)$$

$$N(B_s^0 \rightarrow [f^-]_D \pi^0]_{D^*} [K^+ K^-]_\phi) = C_{K\pi, D\pi^0} F_f \left[-2\mathcal{B}y [x_-^* \cos(2\beta_s) - y_-^* \sin(2\beta_s)] \right. \\ \left. + \mathcal{A} \left(1 + x_-^{*2} + y_-^{*2} + 2r_D^f R_f [(x_+^* + x_-^*) \cos \delta_D^f - (y_+^* - y_-^*) \sin \delta_D^f] \right) \right], \quad (27)$$

$$N(B_s^0 \rightarrow [f^+]_D \pi^0]_{D^*} [K^+ K^-]_\phi) = C_{K\pi, D\pi^0} F_f \left[-2\mathcal{B}y [x_+^* \cos(2\beta_s) + y_+^* \sin(2\beta_s)] \right. \\ \left. + \mathcal{A} \left(1 + x_+^{*2} + y_+^{*2} + 2r_D^f R_f [(x_+^* + x_-^*) \cos \delta_D^f + (y_+^* - y_-^*) \sin \delta_D^f] \right) \right], \quad (28)$$

$$N(B_s^0 \rightarrow [h^+ h^-]_D \pi^0]_{D^*} [K^+ K^-]_\phi) = 4C_{K\pi, D\pi^0} F_{hh} \left[\mathcal{A} \left(1 + x_+^{*2} + y_+^{*2} + x_+^* + x_-^* \right) - \mathcal{B}y \left((1 + x_+^* + x_-^* + x_+^* x_-^* + y_+^* y_-^*) \cos(2\beta_s) \right. \right. \\ \left. \left. + (y_+^* - y_-^* + y_+^* x_-^* - x_+^* y_-^*) \sin(2\beta_s) \right) \right]. \quad (29)$$

In the case of $D^{*0} \rightarrow D^0 \gamma$, the formalism is very similar, except that there is an effective strong phase shift of π with respect to $D^{*0} \rightarrow D^0 \pi^0$ [37]. The observables can be

derived from the previous ones by substituting $C_{K\pi, D\pi^0} \rightarrow C_{K\pi, D\gamma}$ and $\delta_B^* \rightarrow \delta_B^* + \pi$ (i.e. $x_\pm^* \rightarrow -x_\pm^*$ and $y_\pm^* \rightarrow -y_\pm^*$):

$$N(B_s^0 \rightarrow [[K^- \pi^+]_D \gamma]_{D^*} [K^+ K^-]_\phi) = C_{K\pi, D\gamma} [2\mathcal{B}y[x_-^* \cos(2\beta_s) - y_-^* \sin(2\beta_s)] + \mathcal{A}(1 + x_-^{*2} + y_-^{*2} + 2r_D^{K\pi} [-(x_+^* + x_-^*) \cos \delta_D^{K\pi} + (y_+^* - y_-^*) \sin \delta_D^{K\pi}])], \quad (30)$$

$$N(B_s^0 \rightarrow [[K^+ \pi^-]_D \gamma]_{D^*} [K^+ K^-]_\phi) = C_{K\pi, D\gamma} [2\mathcal{B}y[x_+^* \cos(2\beta_s) + y_+^* \sin(2\beta_s)] + \mathcal{A}(1 + x_+^{*2} + y_+^{*2} + 2r_D^{K\pi} [-(x_+^* + x_-^*) \cos \delta_D^{K\pi} - (y_+^* - y_-^*) \sin \delta_D^{K\pi}])], \quad (31)$$

$$N(B_s^0 \rightarrow [[f^-]_D \gamma]_{D^*} [K^+ K^-]_\phi) = C_{K\pi, D\gamma} F_f [2\mathcal{B}y[x_-^* \cos(2\beta_s) - y_-^* \sin(2\beta_s)] + \mathcal{A}(1 + x_-^{*2} + y_-^{*2} + 2r_D^f R_f [-(x_+^* + x_-^*) \cos \delta_D^f + (y_+^* - y_-^*) \sin \delta_D^f])], \quad (32)$$

$$N(B_s^0 \rightarrow [[f^+]_D \gamma]_{D^*} [K^+ K^-]_\phi) = C_{K\pi, D\gamma} F_f [2\mathcal{B}y[x_+^* \cos(2\beta_s) + y_+^* \sin(2\beta_s)] + \mathcal{A}(1 + x_+^{*2} + y_+^{*2} + 2r_D^f R_f [-(x_+^* + x_-^*) \cos \delta_D^f - (y_+^* - y_-^*) \sin \delta_D^f])], \quad (33)$$

$$N(B_s^0 \rightarrow [[h^+ h^-]_D \gamma]_{D^*} [K^+ K^-]_\phi) = 4C_{K\pi, D\gamma} F_{hh} [\mathcal{A}(1 + x_+^{*2} + y_+^{*2} - x_+^* - x_-^*) - \mathcal{B}y((1 - x_+^* - x_-^* + x_+^* x_-^* + y_+^* y_-^*) \cos(2\beta_s) + (-y_+^* + y_-^* + y_+^* x_-^* - x_+^* y_-^*) \sin(2\beta_s))]. \quad (34)$$

$C_{K\pi, D\pi^0}$ and $C_{K\pi, D\gamma}$ are determined in the same manner as $C_{K\pi}$, *i.e.*, from the LHCb Run 1 data [22] and taking into account the fraction of longitudinal polarization in the decay $B_s^0 \rightarrow D^{*0} \phi$, $f_L = (73 \pm 15 \pm 4)\%$ [22], and the branching fractions $Br(\bar{D}^{*0} \rightarrow \bar{D}^0 \pi^0)$ and $Br(\bar{D}^{*0} \rightarrow \bar{D}^0 \gamma)$ [32].

III. EXPECTED YIELDS

The LHCb collaboration has measured the yields of the $B_s^0 \rightarrow \bar{D}^{*0} \phi$ and $\bar{D}^0 \rightarrow K\pi$ modes using Run 1 data, corresponding to an integrated luminosity of 3 fb^{-1} (Ref. [22]). Taking into account the cross-section differences among different center-of-mass energies, the equivalent integrated luminosities in different data over several years from LHCb are summarized in Table 1. The corresponding expected yields of the \bar{D}^0 meson decaying into other modes are also estimated according to Refs. [28], [29], and [41]. The scaled results are listed in Table 2, where the longitudinal polarization fraction $f_L = (73 \pm 15 \pm 4)\%$ [22] of $B_s^0 \rightarrow \bar{D}^{*0} \phi$ is considered so that the CP eigen-

value of the final state is well defined and is similar to that of the $B_s^0 \rightarrow \bar{D}^0 \phi$ mode.

Several additional parameters are used in the sensitivity study, as indicated in Table 3. Most of these originate from D decays, and the scale factors F are calculated by using the data from Refs. [28] and [29], as well as the branching fractions from PDG [32].

The expected numbers of signal events are also calculated from the full expressions provided in Sections IIB and IIC by using the detailed branching fraction derivations explained in Ref. [22], as well as scaling by the LHCb Run 1 and Run 2 integrated luminosities, as listed in Table 1. The obtained normalization factors $C_{K\pi}$, $C_{K\pi, D\pi^0}$, and $C_{K\pi, D\gamma}$ are 608 ± 67 , 347 ± 56 , and 189 ± 31 , respectively. To compute the uncertainty on the normalization factors, we assume that it is possible to improve the global uncertainty on the measurement of the branching fraction of the decay modes $B_s^0 \rightarrow \bar{D}^{*0} \phi$, and of the polarization of the mode $B_s^0 \rightarrow \bar{D}^{*0} \phi$, by a factor of 2 when adding the LHCb data from Run 2 [22]. The values of the three

Table 1. Integrated luminosities and cross-sections of LHCb Run 1 and Run 2 data. The integrated luminosities are obtained from Ref. [38] and the cross-sections are obtained from Refs. [39, 40].

Years/Run	\sqrt{s} /TeV	Int. lum./fb ⁻¹	Cross section	Equiv. 7 TeV data
2011	7	1.1	$\sigma_{2011} = 38.9 \text{ } \mu\text{b}$	1.1
2012	8	2.1	$1.17 \times \sigma_{2011}$	2.4
Run 1	—	3.2	—	3.5
2015 to 2018 (Run 2)	13	5.9	$2.00 \times \sigma_{2011}$	11.8
Total	—	9.1	—	15.3

Table 2. Expected yield of each mode for 9.1fb^{-1} (Run 1 and Run 2 data). The expected yields for the $B_s^0 \rightarrow \bar{D}^{*0}\phi$ sub-modes are scaled by the longitudinal fraction of polarization $f_L = (73 \pm 15)\%$. To be scaled by 6.3 (90) for prospects after 2025 (2038) (see Section V).

	Expect. yield (Run 1 only)	
$B_s^0 \rightarrow \bar{D}^0(K\pi)\phi$	577 (132 \pm 13 [22])	
$B_s^0 \rightarrow \bar{D}^0(K3\pi)\phi$	218	
$B_s^0 \rightarrow \bar{D}^0(K\pi\pi^0)\phi$	58	
$B_s^0 \rightarrow \bar{D}^0(KK)\phi$	82	
$B_s^0 \rightarrow \bar{D}^0(\pi\pi)\phi$	24	
$B_s^0 \rightarrow \bar{D}^0(K_S^0\pi\pi)\phi$	54	
$B_s^0 \rightarrow \bar{D}^0(K_S^0KK)\phi$	8	
$B_s^0 \rightarrow \bar{D}^{*0}\phi$ mode	$D^0\pi^0$	$D^0\gamma$
$B_s^0 \rightarrow \bar{D}^{*0}(K\pi)\phi$	337	184
	(119 [22])	
$B_s^0 \rightarrow \bar{D}^{*0}(K3\pi)\phi$	127	69
$B_s^0 \rightarrow \bar{D}^{*0}(K\pi\pi^0)\phi$	34	18
$B_s^0 \rightarrow \bar{D}^{*0}(KK)\phi$	48	26
$B_s^0 \rightarrow \bar{D}^{*0}(\pi\pi)\phi$	14	8

Table 3. Other external parameters used in sensitivity study. The scale factors F are also listed.

Parameter	Value
$-2\beta_S$ [mrad]	-36.86 ± 0.82 [42]
$y = \Delta\Gamma_S/2\Gamma_S$ (%)	6.40 ± 0.45 [27]
$r_D^{K\pi}$ (%)	$5.90^{+0.34}_{-0.25}$ [27]
$\delta_D^{K\pi}$ [deg]	$188.9^{+8.2}_{-8.9}$ [27]
$r_D^{K3\pi}$ (%)	5.49 ± 0.06 [36]
$R_D^{K3\pi}$ (%)	43^{+17}_{-13} [36]
$\delta_D^{K3\pi}$ [deg]	128^{+28}_{-17} [36]
$r_D^{K\pi\pi^0}$ (%)	4.47 ± 0.12 [36]
$R_D^{K\pi\pi^0}$ (%)	81 ± 6 [36]
$\delta_D^{K\pi\pi^0}$ [deg]	198^{+14}_{-15} [36]
Scale factor (w.r.t. $K\pi$)	(Stat. uncertainty only)
$F_{K3\pi}$ (%)	37.8 ± 0.1 [28]
$F_{K\pi\pi^0}$ (%)	10.0 ± 0.1 [29]
F_{KK} (%)	14.2 ± 0.1 [28]
$F_{\pi\pi}$ (%)	4.2 ± 0.1 [28]

normalization factors are in good agreement with the yields listed in Table 2.

The number of expected event yields and the value of the coherence factor R_D listed in Tables 2 and 3 justify a

posteriori our choice of performing the sensitivity study on γ with the D -meson decay modes $K\pi$, $K3\pi$, $K\pi\pi^0$, KK and $\pi\pi$. By definition, the value of R_D is 1 for two-body decays and $r_D = 1$ for CP -eigenstates, whereas for $K3\pi$, R_D is approximately 43% and larger, namely 81%, for $K\pi\pi^0$. A larger R_D results in stronger sensitivity to γ . According to Eqs. (20), (21), and (22), it is clear that the largest sensitivity to γ is expected to originate from the ordered D^0 decay modes: KK , $\pi\pi$, $K\pi$, $K\pi\pi^0$, and $K3\pi$, for the same number of selected events. Therefore, even with lower yields, the modes $K\pi\pi^0$ and $\pi\pi$ should be of interest; this is discussed in Section IV I.

Returning to the modes $D^0 \rightarrow K_S^0\pi\pi$ and K_S^0KK , the scale factors are $F_{K_S^0\pi\pi} = (9.3 \pm 0.1)\%$ and $F_{K_S^0KK} = (1.4 \pm 0.1)\%$ [41]. The strong parameters $r_D^{K_S^0hh}(m_+^2, m_-^2)$, $\kappa_D^{K_S^0hh}(m_+^2, m_-^2)$, and $\cos\delta_D^{K_S^0hh}(m_+^2, m_-^2)$ can be defined according the effective method presented in Ref. [43], by using quantum-correlated \bar{D}^0 decays, in which the phase space (m_+^2, m_-^2) is divided into \mathcal{N} tailored regions or “bins” [44], such that in the bin of index i ,

$$\sqrt{K_i/K_{-i}} = r_{D,i}^{K_S^0hh}, \quad c_i = \kappa_{D,i}^{K_S^0hh} \cos\delta_{D,i}^{K_S^0hh},$$

$$\text{and } s_i = \kappa_{D,i}^{K_S^0hh} \sin\delta_{D,i}^{K_S^0hh},$$

where $\delta_{D,i}^{K_S^0hh}$ is the strong phase difference and $\kappa_{D,i}^{K_S^0hh}$ is the coherence factor. A recent publication by the BES-III collaboration [45] combines its data with the results of CLEO-c [44], while applying the same technique to obtain the values of the c_i , s_i , and $K_{\pm i}$ parameters varying with the phase space. The binning schemes are symmetric with respect to the diagonal in the Dalitz plot (m_+^2, m_-^2) (*i.e.* $\pm i$). These results have also been compared to an amplitude model from the B -factories BaBar and Belle [46]. When porting the result between the BES-III/CLEO-c combination, obtained using quantum correlated \bar{D}^0 decays, and LHCb for $B_s^0 \rightarrow \bar{D}^{(*)0}\phi$ measurements, care should be taken with the bin conventions so that there may be a minus sign in the phase (which only affects s_i). The expected yield listed in Table 2 for the mode $D^0 \rightarrow K_S^0\pi\pi$ is 54 events, whereas it is 8 events for the decay $D^0 \rightarrow K_S^0KK$. Although the binning scheme in the latter case is only 2×2 , its expected yield is definitely too small to be considered further. For $D^0 \rightarrow K_S^0\pi\pi$, the binned method of Refs. [44, 45] splits the selected \bar{D}^0 events over 2×8 bins, such that with Run 1 and Run 2, only approximately three events may populate each bin. This is the reason that, although the related observable is presented in Eq. (24), we decide not include that mode in the sensitivity study. This choice could eventually be revisited after Run 3, when approximately 340 $B_s^0 \rightarrow D^0(K_S^0\pi\pi)\phi$ events should be available, at which point approximately 20 events may populate each bin.

IV. SENSITIVITY STUDY FOR RUN 1 & 2 LHCb DATASET

The sensitivity study consists of testing and measuring the value of the unfolded γ , $r_B^{(*)}$, and $\delta_B^{(*)}$ parameters and their expected resolution, after having computed the values of the observables according to various initial configurations and given the external inputs for the other involved physics parameters or associated experimental observables. To achieve this, a procedure involving global χ^2 fit based on the CKMfitter package [47] has been established to generate pseudoexperiments and to fit samples of $B_s^0 \rightarrow \tilde{D}^{(*)0}\phi$ events.

This section is organized as follows: In Section IVA, we explain the various configurations that we tested for the nuisance strong parameters $r_B^{(*)}$, and $\delta_B^{(*)}$, as well as the value of γ . In Section IVB, we explain how the pseudoexperiments have been generated. In Section IVC, the first step of the method is illustrated with one- and two-dimensional (1-D and 2-D) p -value profiles for the γ , $r_B^{(*)}$, and $\delta_B^{(*)}$ parameters. Before showing how the γ , $r_B^{(*)}$, and $\delta_B^{(*)}$ parameters are unfolded from the generated pseudoexperiments in Section IVF, we discuss the stability of the former 1-D p -value profile for γ when changing the time acceptance parameters (Section IVD) and for a newly available binning scheme for the $D \rightarrow K3\pi$ decay (Section IVE). Thereafter, the unfolded values for γ and precisions (sensitivity) for the Run 1 & 2 LHCb dataset for the various generated configurations of $\delta_B^{(*)}$ and $r_B^{(*)}$ are presented in Section IVG. We conclude with Sections IVH and IVI, in which we study the intriguing case where $\gamma = 74^\circ$ (see LHCb 2018 combination [12], recently superseded by [16]), and we test the effect of dropping or not dropping the least abundant expected decays modes $B_s^0 \rightarrow \tilde{D}^{(*)0}(\pi\pi)\phi$ and $B_s^0 \rightarrow \tilde{D}^{(*)0}(K\pi\pi^0)\phi$ in the Run 1 & 2 LHCb dataset.

A. Various configurations of γ , $r_B^{(*)}$, and $\delta_B^{(*)}$ parameters

The sensitivity study was performed with the CKM angle γ true value set to $(65.66_{-2.65}^{+0.90})^\circ$ (1.146 rad), as obtained by the CKMfitter group, while excluding any measured values of γ in its global fit [42]. As a reminder, the average of the LHCb measurements is $\gamma = (74.0_{-5.8}^{+5.0})^\circ$ [12]; therefore, the value $\gamma = 74^\circ$ was also tested (see Subsection IVH).

The value of the strong phases $\delta_B^{(*)}$ is a nuisance parameter that cannot be predicted or guessed by any argument, and therefore, six different values are assigned thereto: 0, 1, 2, 3, 4, and 5 rad (0° , 57.3° , 114.6° , 171.9° , 229.2° , and 286.5°). This corresponds to 36 tested configurations (6×6).

As both interfering diagrams displayed in Fig. 1 are

color-suppressed, the value of the ratio of the $\bar{b} \rightarrow \bar{u}c\bar{s}$ and $\bar{b} \rightarrow \bar{c}u\bar{s}$ tree-level amplitudes $r_B^{(*)}$ is expected to be $|V_{ub}V_{cs}|/|V_{cb}V_{us}| \sim 0.4$. This assumption is well supported by the study performed with $B_s^0 \rightarrow D_s^\mp K^\pm$ decays by the LHCb collaboration, for which a value of $r_B = 0.37_{-0.09}^{+0.10}$ has been measured [14]. However, as the decay $B_s^0 \rightarrow D_s^\mp K^\pm$ is color-favored, it is important to test other values obtained from already measured colour-suppressed B -meson decays, as non-factorizing final state interactions can modify the decay dynamics [48]. Among these, the decay $B^0 \rightarrow DK^{*0}$ plays such a role, for which the LHCb has obtained $r_B = 0.22_{-0.27}^{+0.17}$ [42], which has been confirmed by a more recent and accurate computation: $r_B = 0.265 \pm 0.023$ [18]. The value of r_B is known to impact the precision on γ measurements strongly as $1/r_B$ [49]. Therefore, the two extreme values 0.22 and 0.40 for $r_B^{(*)}$ were tested for the sensitivity study, whereas the values for r_B and r_B^* are expected to be similar.

This leads to a total of 72 tested configurations for the $r_B^{(*)}$, δ_B , and δ_B^* parameters ($2 \times 6 \times 6$).

B. Generation of pseudoexperiments for various parameter configurations

As the first step, different configurations for the observables corresponding to Sections IIB and IIC are computed. The observables are obtained with the value of the angle γ and with the values of the four nuisance parameters $r_B^{(*)}$ and $\delta_B^{(*)}$ fixed to various sets of initial true values (see Section IVA), whereas the external parameters listed in Table 3 and the normalization factors $C_{K\pi}$, $C_{K\pi,D\pi^0}$, and $C_{K\pi,D\gamma}$ are left free to vary within their uncertainties. In the second step, for the obtained observables, including their uncertainties that we assume to be their square root, as well as all the other parameters except for γ , $r_B^{(*)}$, and $\delta_B^{(*)}$, a global χ^2 fit is performed to compute the resulting p -value distributions of the γ , $r_B^{(*)}$, and $\delta_B^{(*)}$ parameters. As the third step, for the obtained observables, including their uncertainties, as well as all the other parameters except for γ , $r_B^{(*)}$, and $\delta_B^{(*)}$, 4000 pseudoexperiments are generated according to Eqs. (14)-(34) for the various tested configurations. As the fourth step, for each of the generated pseudoexperiments, all of the quantities are varied within their uncertainties. Thereafter, a global χ^2 fit is performed to unfold the value of the parameters γ , $r_{B_0}^{(*)}$, and $\delta_{B_0}^{(*)}$ for each of the 4000 generated pseudoexperiments. As the fifth step, for the distribution of the 4000 values of the fitted γ , $r_B^{(*)}$, and $\delta_B^{(*)}$, an extended unbinned maximum likelihood fit is performed to compute the most probable value for each of the former five parameters, together with their dispersions. The resulting values are compared to their injected initial true values. Finally, the sensitivity to γ , $r_B^{(*)}$, and $\delta_B^{(*)}$ is deduced, and any bias correlation is eventually highlighted and studied.

C. 1-D and 2-D p -value profiles for γ , $r_B^{(*)}$, and $\delta_B^{(*)}$ parameters

Figure 3 displays the 1-D p -value profiles of γ at step 2 of the procedure described in Section IVB. The figure is obtained for an example set of initial parameters: $\gamma = 65.66^\circ$ (1.146 rad), $r_B^{(*)} = 0.4$, $\delta_B = 3.0$ rad, and $\delta_B^* = 2.0$ rad. The assumed integrated luminosity in this case is that of the LHCb data collected in Run 1 & 2. The corresponding fitted value is $\gamma = (65.7_{-33.8}^{+6.3})^\circ$, which is thus in excellent agreement with the initial tested true value. Figure 3 also depicts the corresponding distributions obtained from a full frequentist treatment on the Monte-Carlo simulation basis [50], where $\gamma = (65.7_{-34.9}^{+6.9})^\circ$. This is considered as a demonstration that the two estimates on γ are in quite fair agreement, at least at the 68.3% confidence level (CL), such that no obvious under-coverage is experienced with the nominal method, based on the ROOT function TMath::Prob [51]. On the upper part of the distribution, the relative under-coverage of the “Prob” method is approximately $6.3/6.9 \approx 91\%$. As opposed to the full frequentist treatment on the Monte-Carlo simulation basis, the nominal retained method allows performing computations of a very large number of pseudoexperiments within a reasonable amount of time and with non-prohibitive CPU resources. For the LHCb Run 1 & 2 dataset, 72 configurations of 4000 pseudoexperiments were generated (288000 pseudoexperiments in total). The entire study was repeated another two times for prospective studies with future anticipated LHCb data, such that more than approximately 864000 pseudoexperiments were generated for this publication (see Section V). In the

same figure, one can also observe the effect of modifying the value of $r_B^{(*)}$ from 0.4 to 0.22, for which $\gamma = (65.7_{-60.7}^{+12.0})^\circ$, where the upper uncertainty scales are roughly as expected: $1/r_B^{(*)}$ ($6.3 \times 0.4/0.22 = 12.6$). Compared to the full frequentist treatment on the Monte-Carlo simulation, where $\gamma = (65.7_{-\infty}^{+13.2})^\circ$, the relative under-coverage of the “Prob” method is approximately $12.0/13.2 \approx 91\%$. Finally, the p -value profile of γ is also displayed when dropping the information provided by the $B_s^0 \rightarrow \bar{D}^{*0} \phi$ mode, thus retaining only that of the $B_s^0 \rightarrow \bar{D}^0 \phi$ mode. In this case, γ is equal to $(65.7_{-\infty}^{+6.3(12.0)})^\circ$, $r_B^{(*)} = 0.4$ (0.22), such that the CL interval is noticeably enlarged on the lower side of the γ angle distribution (further details can be found in Section VC).

Figure 4 displays the 1-D p -value profile of the nuisance parameters $r_B^{(*)}$ and $\delta_B^{(*)}$ for the same set of initial parameters ($\gamma = 65.66^\circ$ (1.146 rad), $r_B^{(*)} = 0.4$, $\delta_B = 3.0$ rad, and $\delta_B^* = 2.0$ rad) and the same projected integrated luminosity. It can be observed that the p -value is the maximum at the initial tested value, as expected.

The 2-D p -value profiles of the nuisance parameters $r_B^{(*)}$ and $\delta_B^{(*)}$ as a function of γ are presented in Figs. 5-8. Figures 5 and 6 correspond to two other example configurations $\gamma = 1.146$ rad, $\delta_B = 1.0$ rad, and $\delta_B^* = 5.0$ rad, and $r_B^{(*)} = 0.4$ and $r_B^{(*)} = 0.22$, respectively. Figures 7 and 8 represent the configurations $\gamma = 1.146$ rad, $\delta_B = 3.0$ rad, and $\delta_B^* = 2.0$ rad, and $r_B^{(*)} = 0.4$ and $r_B^{(*)} = 0.22$, respectively. These 2-D views allow the correlation between the different parameters to be observed. In general, large correlations between $\delta_B^{(*)}$ and γ are observed. In the case of

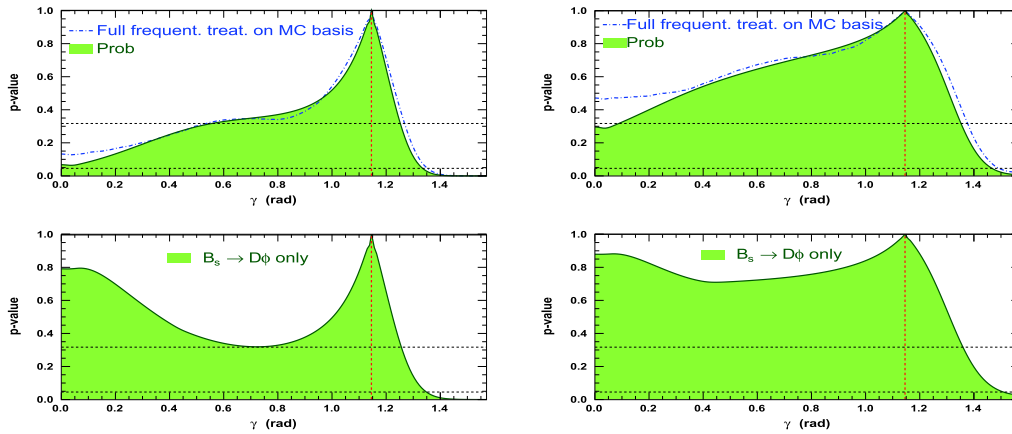


Fig. 3. (color online) Profile of p -value of global χ^2 fit to γ after computing observables (top left) for a set of true initial parameters: $\gamma = 1.146$ rad, $r_B^{(*)} = 0.4$, $\delta_B = 3.0$ rad, and $\delta_B^* = 2.0$ rad (the corresponding distribution obtained from the full frequentist treatment on the Monte-Carlo simulation basis [50] is superimposed on the same distribution). The related p -value profile for $r_B^{(*)} = 0.22$ is also presented (top right). The assumed integrated luminosity assumed is that of the LHCb data collected in Run 1 & 2. Profile of p -value of global χ^2 fit to γ after computing observables, where only decay mode $B_s^0 \rightarrow \bar{D}^0 \phi$ is used, and for a set of true initial parameters: $\gamma = 1.146$ rad, $r_B^{(*)} = 0.4$ (bottom left) and 0.22 (bottom right), $\delta_B = 3.0$ rad, and $\delta_B^* = 2.0$ rad. In each figure, the vertical dashed red line indicates the initial γ true value, and the two horizontal dashed black lines refer to 68.3 and 95.4% CLs.

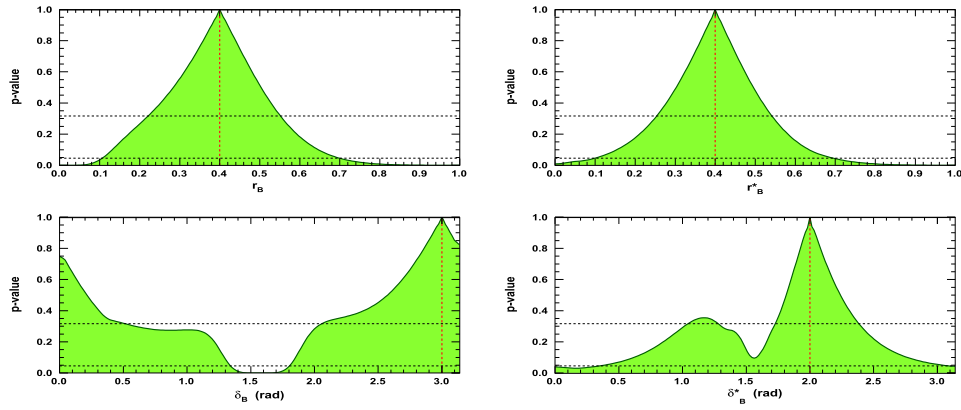


Fig. 4. (color online) Profiles of p -value distributions of global χ^2 fit to $r_B^{(*)}$ (top left (right)) and $\delta_B^{(*)}$ (bottom left (right)) after computing observables for set of initial true parameters: $\gamma = 65.66^\circ$ (1.146 rad), $r_B^{(*)} = 0.4$, $\delta_B = 3.0$ rad, and $\delta_B^* = 2.0$ rad. In each figure, the vertical dashed red line indicates the initial $r_B^{(*)}$ and $\delta_B^{(*)}$ true values, and the two horizontal dashed black lines refer to 68.3 and 95.4% CLs.

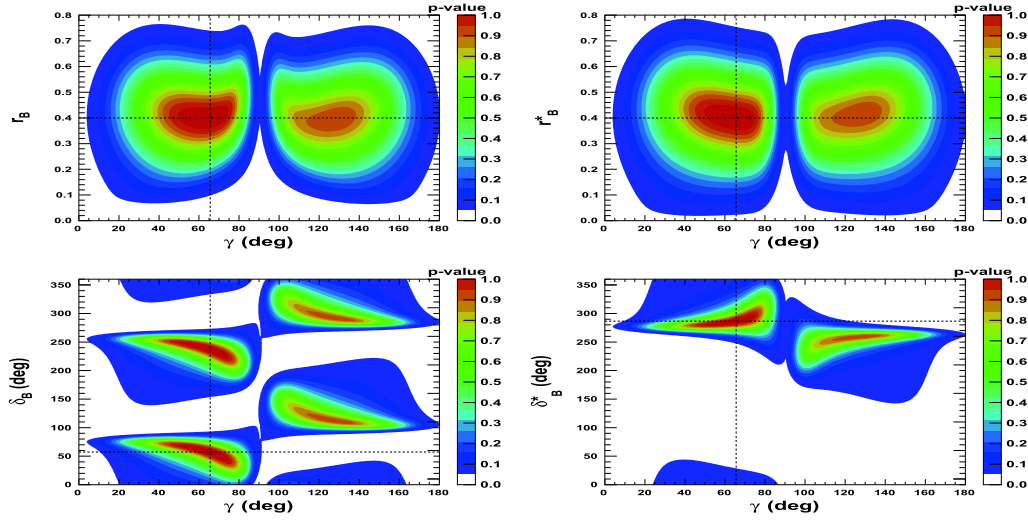


Fig. 5. (color online) 2-D p -value profile distribution of nuisance parameters $r_B^{(*)}$ and $\delta_B^{(*)}$ as a function of γ . In each figure, the dashed black lines indicate the initial true values: $\gamma = 65.66^\circ$ (1.146 rad), $\delta_B = 57.3^\circ$ (1.0 rad), and $\delta_B^* = 286.5^\circ$ (5.0 rad), as well as $r_B^{(*)} = 0.4$.

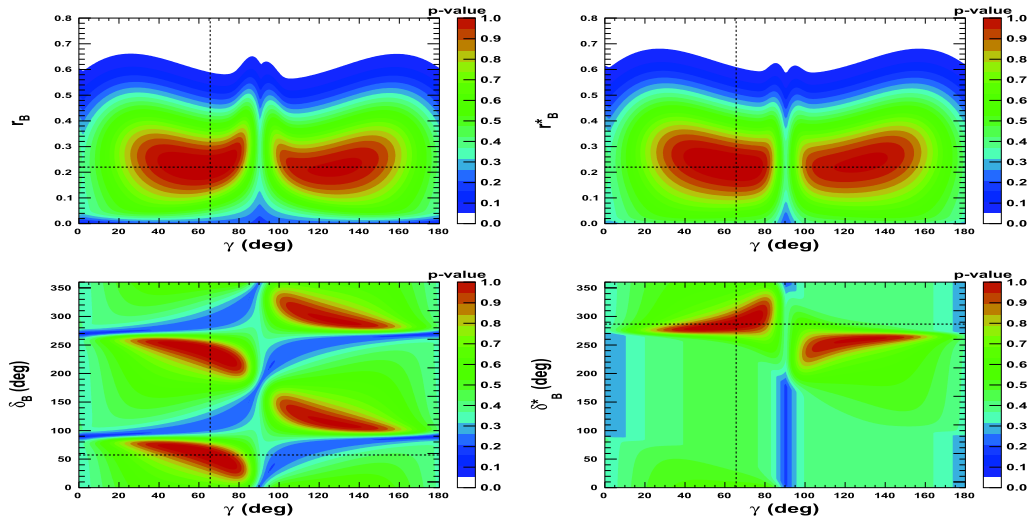


Fig. 6. (color online) 2-D p -value profile distribution of nuisance parameters $r_B^{(*)}$ and $\delta_B^{(*)}$ as a function of γ . In each figure, the dashed black lines indicate the initial true values: $\gamma = 65.66^\circ$ (1.146 rad), $\delta_B = 57.3^\circ$ (1.0 rad), and $\delta_B^* = 286.5^\circ$ (5.0 rad), as well as $r_B^{(*)} = 0.22$.

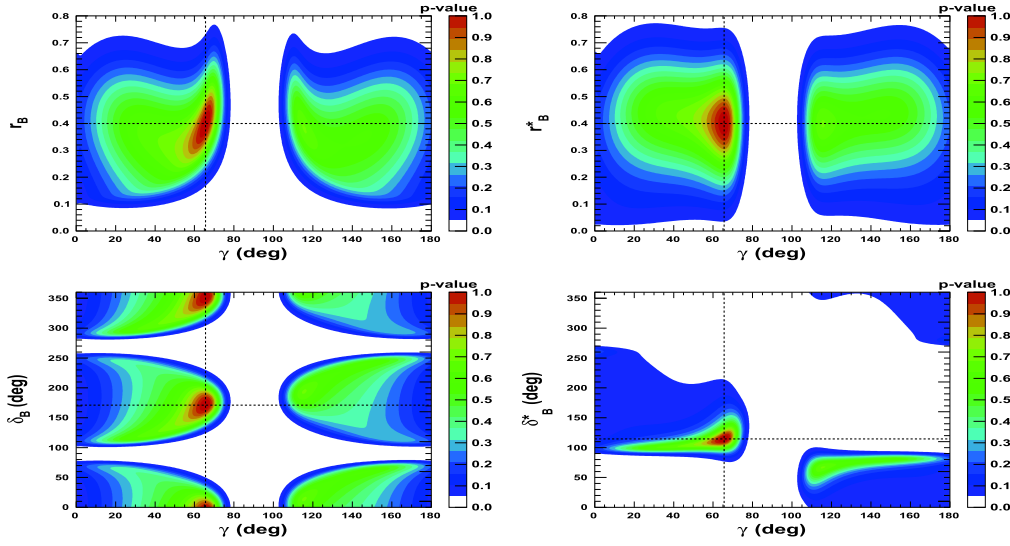


Fig. 7. (color online) 2-D p -value profile distribution of nuisance parameters $r_B^{(*)}$ and $\delta_B^{(*)}$ as a function of γ . In each figure, the dashed black lines indicate the initial true values: $\gamma = 65.66^\circ$ (1.146 rad), $\delta_B = 171.9^\circ$ (3.0 rad), and $\delta_B^* = 114.6^\circ$ (2.0 rad), as well as $r_B^{(*)} = 0.4$.

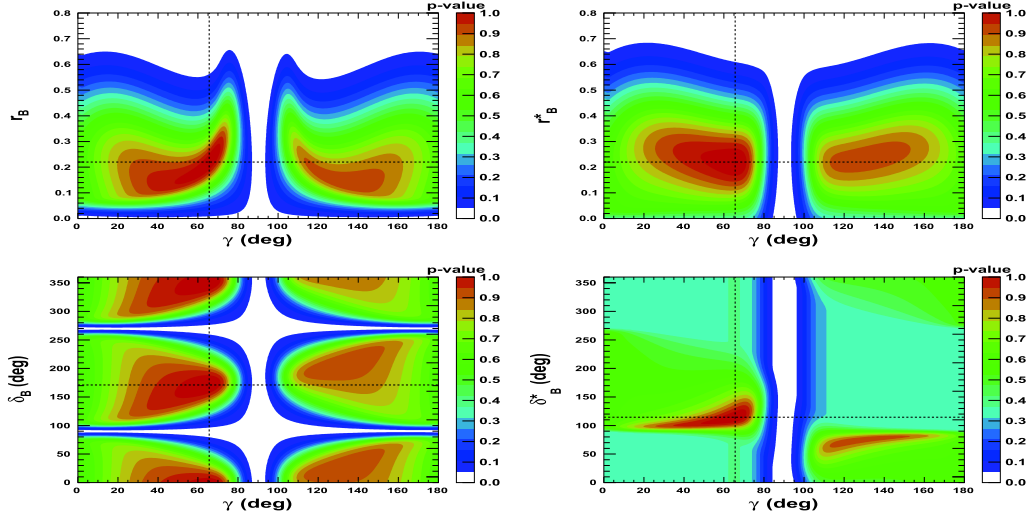


Fig. 8. (color online) 2-D p -value profile distribution of nuisance parameters $r_B^{(*)}$ and $\delta_B^{(*)}$ as a function of γ . In each figure, the dashed black lines indicate the true values: $\gamma = 65.66^\circ$ (1.146 rad), $\delta_B = 171.9^\circ$ (3.0 rad), and $\delta_B^* = 114.6^\circ$ (2.0 rad), as well as $r_B^{(*)} = 0.22$.

configurations where $r_B^{(*)} = 0.4$, a large fraction of the $\delta_B^{(*)}$ vs. γ plane can be excluded at a 95% CL, whereas the fraction is significantly reduced for the corresponding $r_B^{(*)} = 0.22$ configurations. For the δ_B^* vs. γ plane, the advantage of our Cartesian coordinate approach (see Section IIB and IIC) can easily be observed, together with the fact that in the case of the mode $D^{*0} \rightarrow D^0 \gamma$, there is an effective strong phase shift of π with respect to the $D^{*0} \rightarrow D^0 \pi^0$ [37], such that additional constraints enable the fold ambiguities with respect to the associated δ_B vs. γ plane to be removed.

D. Effect of time acceptance parameters

Figure 9 demonstrates that for a tested configuration

of $\gamma = 1.146$ rad, $r_B^{(*)} = 0.4$, and $\delta_B^{(*)} = 1.0$ rad, the impact of the time acceptance parameters \mathcal{A} and \mathcal{B} can eventually be non negligible and the parameters affect the profile distribution of the p -value of the global χ^2 fit to γ . For the given example, the fitted value of γ is either $(65.3^{+14.3}_{-38.4})^\circ$ or $(66.5^{+13.8}_{-51.0})^\circ$ when the time acceptance is either accounted for or not. The reason due to which the precision improves when the time acceptance is taken into account may not be intuitive. This is because, for $\mathcal{B}/\mathcal{A} \simeq 1.6$, as opposed to the case of $\mathcal{B}/\mathcal{A} \simeq 1.0$, the impact of the first term in Eq. (14), which is directly proportional to $\cos(\delta_B + 2\beta_s - \gamma)$, is amplified with respect to the second term, for which the sensitivity to γ is more diluted.

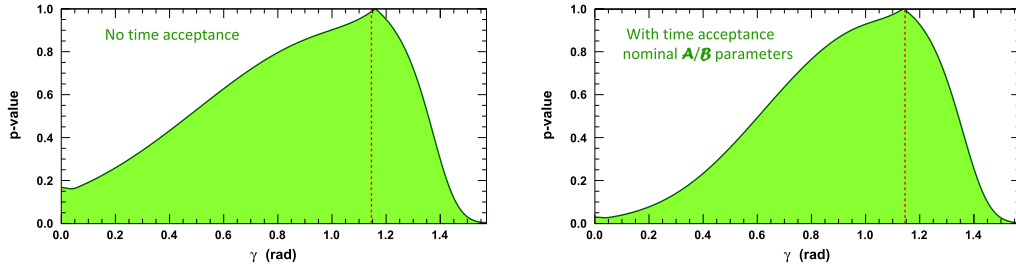


Fig. 9. (color online) Profile of p -value distribution of global χ^2 fit to γ for a set of true initial parameters: $\gamma = 1.146$ rad, $r_B^{(*)} = 0.4$, and $\delta_B^{(*)} = 1.0$ rad. The assumed integrated luminosity is that of the LHCb data collected in Run 1 & 2 when the time acceptance values \mathcal{A} and \mathcal{B} are set to 1 in Eqs. (14) to (34): no time acceptance (top left) or to their nominal values $\mathcal{A} = 0.488 \pm 0.005$ and $\mathcal{B} = 0.773 \pm 0.008$ (top right), as computed in Section IIA. The dashed red line indicates the initial γ true value $\gamma = 65.66^\circ$ (1.146 rad).

Even if the parameters \mathcal{A} and \mathcal{B} are computed to a precision at the percentage level (Section IIA), we further investigate the effect of changing their values. Note that for this study, the overall efficiency is maintained constant, whereas the shape of the acceptance function is varied. The values α , β , and ξ are changed in Eq. (10), and the results of those changes are listed in Table 4. When α increases, both \mathcal{A} and \mathcal{B} become larger, but the value of the ratio \mathcal{B}/\mathcal{A} decreases. When β or ξ decreases, the three values of \mathcal{A} , \mathcal{B} , and \mathcal{B}/\mathcal{A} increase. The effect of changing β or ξ alone is small. A modification of α has a much greater impact on \mathcal{A} and \mathcal{B} . However, all of these changes have a weak impact on the precision of the fitted γ value. This is quite encouraging, as it means that the relative efficiency loss caused by the time acceptance effects will not cause a significant change in the sensitivity to the CKM γ angle. As a result, the time acceptance requirements can be varied without substantial concern to improve the signal purity and statistical significance when analyzing the $B_s^0 \rightarrow \bar{D}^{(*)0} \phi$ decays with LHCb data.

E. Effect of new binning scheme for $D \rightarrow K3\pi$ decay

According to Ref. [46], the averaged values of the $K3\pi$ input parameters over the phase space, which are

Table 4. Expected value of γ as a function of different time acceptance parameters. The second line corresponds to the nominal values. The nominal set of parameters \mathcal{A} and \mathcal{B} is indicated in bold.

α	β	ξ	\mathcal{A}	\mathcal{B}	\mathcal{B}/\mathcal{A}	Fitted γ ($^\circ$)
1.0	2.5	0.01	0.367	0.671	1.828	$66.5^{+13.8}_{-40.1}$
1.5	2.5	0.01	0.488	0.773	1.584	$65.3^{+14.3}_{-38.4}$
2.0	2.5	0.01	0.570	0.851	1.493	$65.3^{+13.2}_{-37.8}$
1.5	2.0	0.01	0.484	0.751	1.552	$65.9^{+13.2}_{-39.0}$
1.5	3.0	0.01	0.491	0.789	1.607	$66.5^{+13.2}_{-38.4}$
1.5	2.5	0.02	0.480	0.755	1.573	$66.5^{+13.8}_{-39.5}$
1.5	2.5	0.005	0.492	0.783	1.591	$65.3^{+13.8}_{-36.7}$

defined as

$$R_D^{K3\pi} e^{-i\delta_D^{K3\pi}} = \frac{\int A_{\bar{D}^0 \rightarrow K3\pi}^*(x) A_{D^0 \rightarrow K3\pi}(x) dx}{A_{\bar{D}^0 \rightarrow K3\pi} A_{D^0 \rightarrow K3\pi}}, \quad (35)$$

are used here and correspond to a relatively limited value for the coherence factor: $R_D^{K3\pi} = (43^{+17}_{-13})\%$ [36]. A more attractive approach may be to perform the analysis in disjoint bins of the phase space. In this case, the parameters are re-defined within each bin. New values for $R_D^{K3\pi}$ and $\delta_D^{K3\pi}$ in each bin from Ref. [52] have alternatively been employed. No noticeable changes were observed in the γ and $r_B^{(*)}$ fitted p -value profiles, but it is possible that certain fold-effects on $\delta_B^{(*)}$, *e.g.*, as observed in Figs. 5-7, become less probable. The lack of significant improvement is expected as the $\bar{D}^0 \rightarrow K3\pi$ mode is not the dominant decay, and also because the new measurements of $R_D^{K3\pi}$ and $\delta_D^{K3\pi}$ in each bin still have large uncertainties.

F. Unfolding γ , $r_B^{(*)}$, and $\delta_B^{(*)}$ parameters from generated pseudoexperiments

As explained in Section IVB, for each of the tested γ , $r_B^{(*)}$, and $\delta_B^{(*)}$ configurations, 4000 pseudoexperiments are generated, for which the values of γ , $r_B^{(*)}$, and $\delta_B^{(*)}$ are unfolded from the global χ^2 fits (see Section IVC for illustrations). Figure 10 displays the extended unbinned maximum likelihood fits to the nuisance parameters $r_B^{(*)}$ and $\delta_B^{(*)}$. The initial configuration is $\gamma = 65.66^\circ$ (1.146 rad), $r_B^{(*)} = 0.4$, $\delta_B = 171.9^\circ$ (3 rad), and $\delta_B^* = 114.6^\circ$ (2 rad), with an integrated luminosity that is equivalent to that of the LHCb Run 1 & 2 data. It can be compared with Fig. 4. All of the distributions are fitted with the *Novosibirsk* empirical function, the description of which contains a Gaussian core part and a left or right tail, depending on the sign of the tail parameter [53]. The fitted values of $r_B^{(*)}$ are centered at their initial tested values of 0.4, with a resolution of 0.14, and no bias is observed. For $\delta_B^{(*)}$, the fitted value is $(176 \pm 42)^\circ$ ($(104 \pm 13)^\circ$) for an initial true

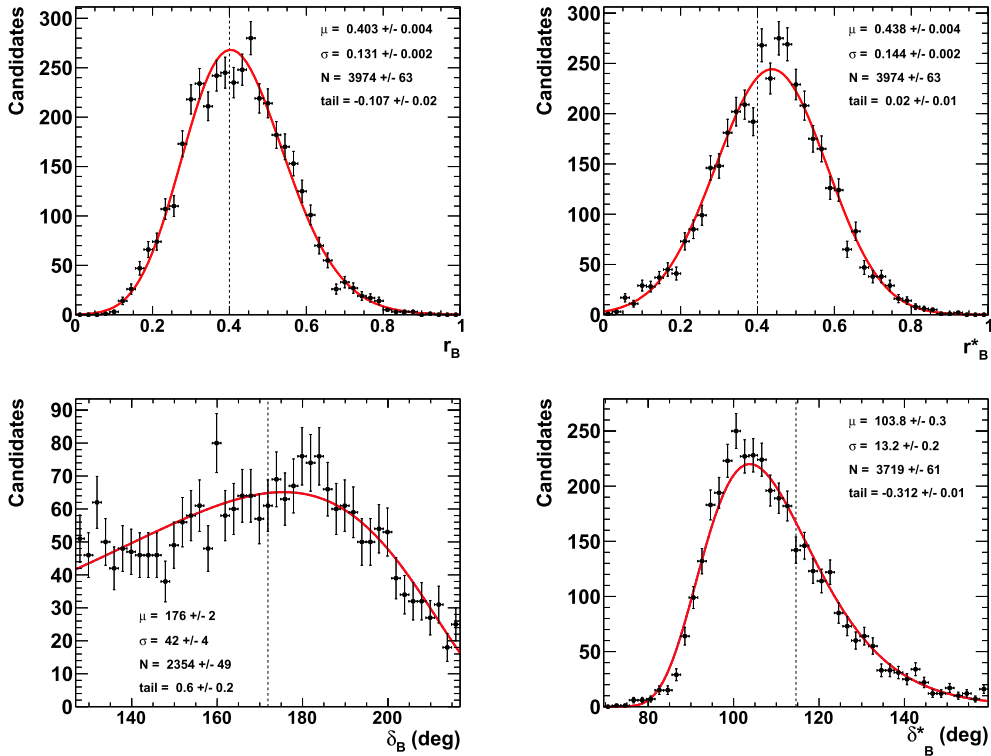


Fig. 10. (color online) Fit to distributions of nuisance parameters $r_B^{(*)}$ (top left (right)) and $\delta_B^{(*)}$ (bottom left (right)) obtained from 4000 pseudoexperiments. The initial configuration is $\gamma = 65.66^\circ$ (1.146 rad), $r_B^{(*)} = 0.4$, $\delta_B = 171.9^\circ$ (3 rad), and $\delta_B^{(*)} = 114.6^\circ$ (2 rad). The distributions of $\delta_B^{(*)}$ are plotted and fitted within $\pm 45^\circ$ of their initial true values. In the distributions, only the candidates with values of $\gamma \in [0^\circ, 90^\circ]$ are considered.

value that is equal to 171.9° (114.6°). The fitted value for $\delta_B^{(*)}$ is slightly shifted by approximately 2/3 of a standard deviation, but its measurement is much more precise than that of δ_B , as it is measured from both the $D^{*0} \rightarrow D^0 \gamma$ and $D^{*0} \rightarrow D^0 \pi^0$ observables.

Figure 11 presents the corresponding fit to the CKM angle γ , where the value $r_B^{(*)} = 0.22$ is also tested. This figure can be compared to the initial p -value profiles illustrated in Fig. 3. As shown in Figs. 7 and 8, γ is correlated with the nuisance parameters $r_B^{(*)}$ and $\delta_B^{(*)}$. Such correlations may generate long tails in the distributions, as obtained from the 4000 pseudoexperiments. To account for these tails, extended unbinned maximum likelihood fits, constituting two *Novosibirsk* functions with opposite-side tails, are performed on the γ distributions. With an initial value of 65.66° , the fitted value for γ returns a central value equal to $\mu_\gamma = (65.9 \pm 0.3)^\circ$ with a resolution of $\sigma_\gamma = (8.8 \pm 0.2)^\circ$ when $r_B^{(*)} = 0.4$, and $\mu_\gamma = (66.6 \pm 0.7)^\circ$ with a resolution of $\sigma_\gamma = (14.4 \pm 0.5)^\circ$ when $r_B^{(*)} = 0.22$. The worse resolution obtained with $r_B^{(*)} = 0.22$ follows the empirical behavior $1/r_B^{(*)}$ ($8.8 \times 0.4/0.22 \simeq 16.0$). Again, no bias is observed.

Finally, Fig. 12 displays the 2-D distributions of the nuisance parameters $r_B^{(*)}$ and $\delta_B^{(*)}$ as a function of γ obtained from 4000 pseudoexperiments. This figure can be

compared with the corresponding p -value profiles presented in Fig. 7.

G. Varying $\delta_B^{(*)}$ and $r_B^{(*)}$

According to Section IVA, 72 configurations of nuisance parameters $\delta_B^{(*)}$ and $r_B^{(*)}$ have been tested for $\gamma = 65.66^\circ$ (1.146 rad) and 4000 pseudoexperiments have been generated for each set, following the procedure described in Section IVB and illustrated in Section IVF. The assumed integrated luminosity in this section is that of the LHCb data collected in Run 1 & 2.

The fitted mean values of γ (μ_γ) for $r_B^{(*)} = 0.4$ and 0.22 as a function of $\delta_B^{(*)}$, for an initial true value of 65.66° (1.146 rad), are displayed in Table 5, whereas the corresponding resolutions (σ_γ) are listed in Table 6. In general, the fitted means are compatible with the true γ values within less than one standard deviation. For $r_B^{(*)} = 0.4$, the resolution varies from $\sigma_\gamma = 8.3^\circ$ to 12.9° . For $r_B^{(*)} = 0.22$, the resolution is worse, as expected, and it varies from $\sigma_\gamma = 13.9^\circ$ to 18.7° . For $r_B^{(*)} = 0.22$, the distribution of γ of the 4000 pseudoexperiments has its maximum above 90° for $\delta_B^{(*)} = 286.5^\circ$ and it is therefore not considered.

The obtained values for μ_γ and σ_γ are also displayed in Figs. 13 and 14. It is clear that the resolution on γ de-

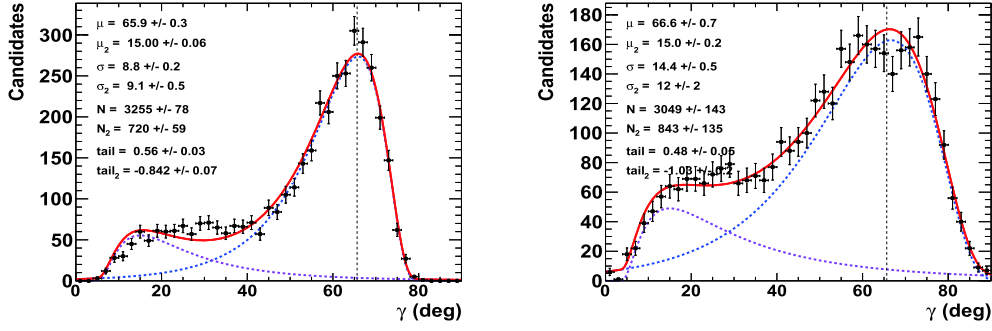


Fig. 11. (color online) Fit to distributions of nuisance parameters γ obtained from 4000 pseudoexperiments. The initial configuration is $\gamma = 65.66^\circ$ (1.146 rad), $r_B^{(*)} = 0.4$ (left) and 0.22 (right), $\delta_B = 171.9^\circ$ (3 rad), and $\delta_B^* = 114.6^\circ$ (2 rad). In the distributions, only the candidates with a value of $\gamma \in [0^\circ, 90^\circ]$ are considered. The purple dashed curve represents tails generated by the correlations with the nuisance parameters $r_B^{(*)}$ and $\delta_B^{(*)}$, whereas the blue dashed curve indicates the core part of the distribution, and the plain red line is the sum of the two components of the fit.

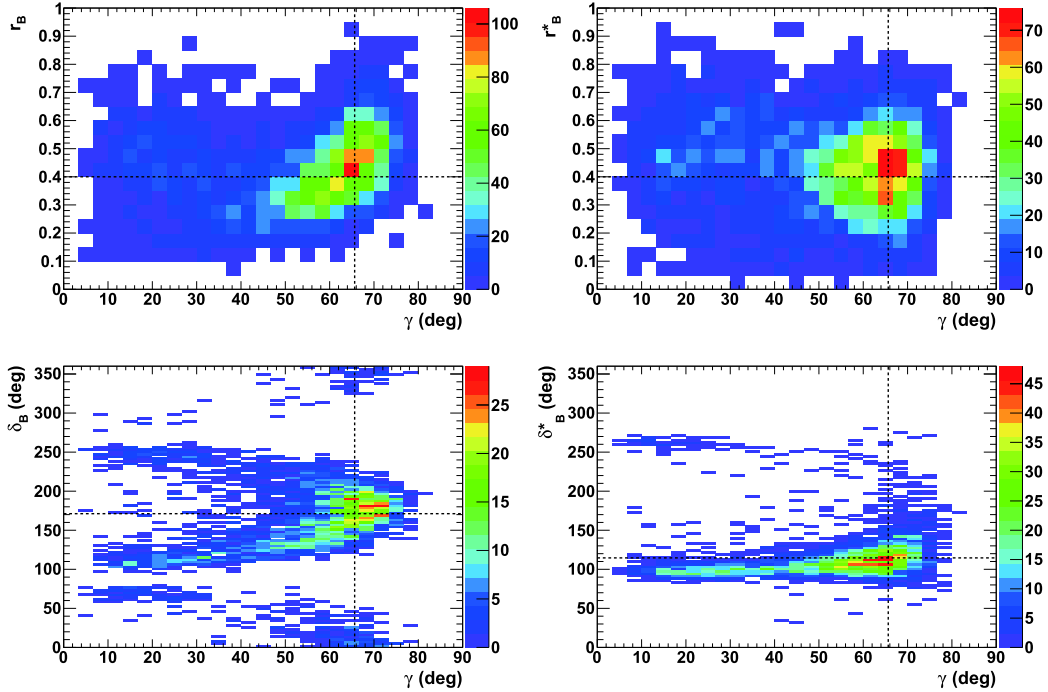


Fig. 12. (color online) 2-D distributions of nuisance parameters $r_B^{(*)}$ and $\delta_B^{(*)}$ as a function of γ obtained from 4000 pseudoexperiments. In each figure, the horizontal dashed black lines indicate the initial true values: $\gamma = 65.66^\circ$ (1.146 rad), $\delta_B = 171.9^\circ$ (3.0 rad), and $\delta_B^* = 114.6^\circ$ (2.0 rad), as well as $r_B^{(*)} = 0.4$.

depends to the first order on $r_B^{(*)}$, and then to the second order on $\delta_B^{(*)}$. The best agreement with respect to the tested initial true value of γ is obtained when $\delta_B^{(*)} = 0^\circ$ (0 rad) or 180° (π rad), and the best resolutions (the lowest values of σ_γ) are also obtained in this case. The largest CP violation effects and best sensitivity to γ are observed. In contrast, the worst sensitivity is obtained when $\delta_B^{(*)} = 90^\circ$ ($\pi/2$ rad) or 270° ($3\pi/2$ rad). The other best and worst positions for $\delta_B^{(*)}$ can easily be deduced from Eq. (14). In most cases, for $r_B^{(*)} = 0.4$ (0.22), the value of the resolution is $\sigma_\gamma \sim 10^\circ$ (15°) and the fitted mean value

$\mu_\gamma \sim 65.66^\circ$ or slightly larger.

For completeness, the fitted means and resolutions for the nuisances parameters $r_B^{(*)}$ and $\delta_B^{(*)}$ are presented in Figs. A1-A4 in Appendix A. It can be observed that the fitted mean values of $r_B^{(*)}$ and $\delta_B^{(*)}$ are in good agreement with their initial tested true values, within one standard deviation of their fitted resolutions.

H. Case where γ equals 74°

Configurations in which $\gamma = 74^\circ$ (see Ref. [12]) have also been tested. The potential problem in this case is

Table 5. Fitted mean values of γ (μ_γ) (in [deg]) for $r_B^{(*)} = 0.4$ (top) and 0.22 (bottom), as a function of $\delta_B^{(*)}$, for initial true value of 65.66° .

δ_B	δ_B^*					
	0	57.3	114.6	171.9	229.2	286.5
$r_B^{(*)} = 0.4$						
0.0	66.2 ± 0.4	65.9 ± 0.4	67.4 ± 0.4	65.9 ± 0.4	65.9 ± 0.4	67.4 ± 0.4
57.3	65.4 ± 0.4	69.2 ± 0.4	71.4 ± 0.4	65.5 ± 0.3	67.7 ± 0.4	72.6 ± 0.4
114.6	65.8 ± 0.4	70.5 ± 0.4	72.9 ± 0.4	65.9 ± 0.3	69.3 ± 0.4	73.8 ± 0.4
171.9	$65.6^{+0.5}_{-0.4}$	65.2 ± 0.3	65.9 ± 0.3	65.5 ± 0.3	65.2 ± 0.4	66.1 ± 0.3
229.2	64.9 ± 0.4	67.6 ± 0.4	68.9 ± 0.4	65.0 ± 0.4	67.1 ± 0.4	69.0 ± 0.4
286.5	66.1 ± 0.4	71.0 ± 0.4	75.7 ± 0.4	65.7 ± 0.3	69.8 ± 0.4	78.8 ± 0.4
δ_B	δ_B^*					
	0	57.3	114.6	171.9	229.2	286.5
$r_B^{(*)} = 0.22$						
0.0	$67.2^{+0.9}_{-1.0}$	$68.1^{+1.0}_{-0.9}$	$68.3^{+0.9}_{-0.8}$	67.1 ± 0.8	68.4 ± 0.9	69.0 ± 0.8
57.3	67.4 ± 0.9	72.2 ± 0.8	$74.1^{+0.8}_{-0.7}$	66.6 ± 0.7	71.5 ± 0.8	75.5 ± 0.8
114.6	65.7 ± 0.9	71.8 ± 0.6	74.9 ± 0.6	68.0 ± 0.6	71.2 ± 0.7	74.9 ± 0.6
171.9	65.4 ± 0.7	66.9 ± 0.7	66.6 ± 0.7	64.7 ± 0.7	65.2 ± 0.6	68.3 ± 0.6
229.2	$65.9^{+0.9}_{-1.0}$	69.1 ± 0.8	$70.1^{+0.7}_{-0.8}$	67.7 ± 0.7	67.4 ± 0.7	$71.0^{+0.6}_{-0.7}$
286.5	67.5 ± 0.9	75.8 ± 0.8	$77.5^{+0.8}_{-0.7}$	68.1 ± 0.6	$72.8^{+0.9}_{-0.8}$	$83.5^{+2.4}_{-1.5}$

Table 6. Fitted resolution of γ (σ_γ) (in [deg]) for $r_B^{(*)} = 0.4$ (top) and 0.22 (bottom), as a function of $\delta_B^{(*)}$.

δ_B	δ_B^*					
	0	57.3	114.6	171.9	229.2	286.5
$r_B^{(*)} = 0.4$						
0.0	9.6 ± 0.4	11.2 ± 0.3	11.2 ± 0.3	9.4 ± 0.4	12.2 ± 0.4	11.2 ± 0.3
57.3	11.2 ± 0.3	12.6 ± 0.3	11.8 ± 0.3	10.2 ± 0.3	12.4 ± 0.3	12.9 ± 0.3
114.6	11.4 ± 0.3	11.9 ± 0.3	11.1 ± 0.3	10.0 ± 0.3	11.3 ± 0.3	11.9 ± 0.3
171.9	8.3 ± 0.4	9.8 ± 0.3	8.8 ± 0.2	8.9 ± 0.3	9.5 ± 0.3	9.0 ± 0.2
229.2	10.8 ± 0.3	11.7 ± 0.3	10.8 ± 0.3	10.3 ± 0.3	12.4 ± 0.3	11.7 ± 0.3
286.5	11.0 ± 0.3	12.9 ± 0.3	11.6 ± 0.3	9.2 ± 0.2	11.7 ± 0.3	$13.2^{+0.6}_{-0.5}$
δ_B	δ_B^*					
	0	57.3	114.6	171.9	229.2	286.5
$r_B^{(*)} = 0.22$						
0.0	16.5 ± 0.7	16.8 ± 0.7	16.0 ± 0.6	$16.8^{+0.8}_{-0.7}$	$15.9^{+0.0}_{-0.6}$	16.0 ± 0.7
57.3	16.7 ± 0.6	$18.1^{+0.9}_{-0.8}$	$17.1^{+1.0}_{-0.9}$	14.3 ± 0.5	16.8 ± 0.7	$17.6^{+1.3}_{-1.1}$
114.6	$16.1^{+0.6}_{-0.7}$	15.9 ± 0.6	13.9 ± 0.5	14.1 ± 0.5	15.1 ± 0.6	14.9 ± 0.6
171.9	$15.7^{+0.7}_{-0.6}$	14.5 ± 0.5	14.4 ± 0.5	15.5 ± 0.6	$15.7^{+0.0}_{-0.5}$	14.0 ± 0.5
229.2	15.9 ± 0.6	$15.7^{+0.5}_{-0.6}$	15.4 ± 0.6	$14.6^{+0.6}_{-0.5}$	15.6 ± 0.5	14.4 ± 0.6
286.5	$16.9^{+0.7}_{-0.6}$	$18.0^{+1.3}_{-1.1}$	$16.7^{+1.2}_{-1.0}$	$14.9^{+0.5}_{-0.6}$	16.1 ± 0.7	$18.7^{+2.8}_{-2.1}$

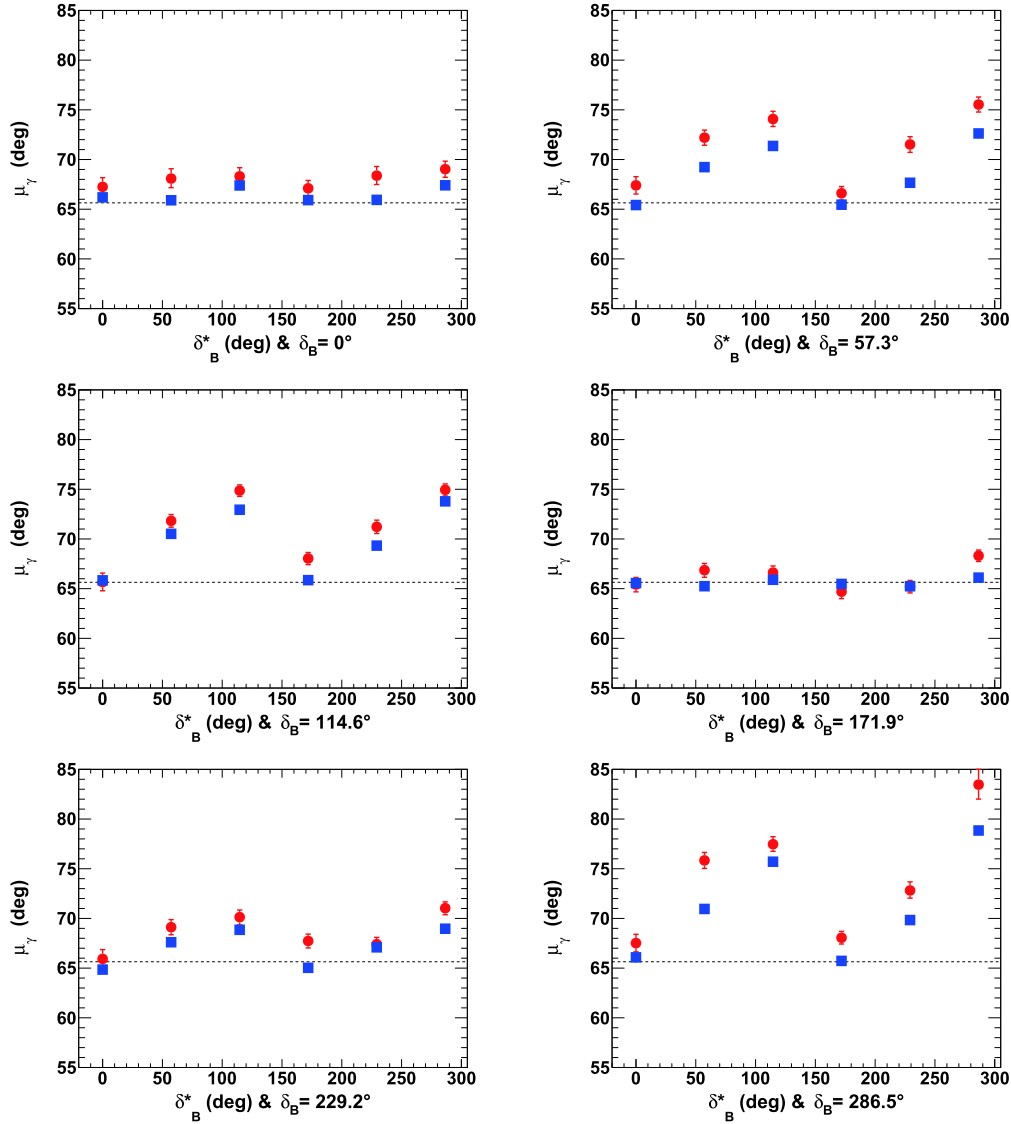


Fig. 13. (color online) Fitted mean values of γ (μ_γ) for $r_B^{(*)} = 0.22$ (red circles) and 0.4 (blue squares) as a function of $\delta_B^{(*)}$ for initial true value of 65.66° (1.146 rad). All of the listed values are in [deg]. In each figure, the horizontal dashed black line indicates the initial γ true value. All of the plotted uncertainties are statistical only.

that, as the true value of γ is closer to the 90° boundary, the unfolding of this parameter may become more difficult for many configurations of the nuisance parameters $r_B^{(*)}$ and $\delta_B^{(*)}$. It is clear from Eq. (14) that the sensitivity to γ is null at 90° . This is illustrated in Fig. B1 in Appendix B, which can be compared with Fig. 11. In this case, the initial tested configuration is $\gamma = 74^\circ$, $r_B^{(*)} = 0.4$ and 0.22 , $\delta_B = 171.9^\circ$ (3 rad), and $\delta_B^* = 114.6^\circ$ (2 rad). For these configurations, $\mu_\gamma = (73.7 \pm 0.3)^\circ$ ($(74.2 \pm 0.7)^\circ$) and $\sigma_\gamma = (7.7 \pm 0.3)^\circ$ ($(14.7 \pm 0.6)^\circ$) for $r_B^{(*)} = 0.4$ (0.22). There is limited degradation of the resolution compared to the corresponding configuration when the true value of γ is 65.66° . The fit to γ for the pseudoexperiments corresponding to the configuration $\gamma = 74^\circ$, $r_B^{(*)} = 0.4$ and 0.22 ,

$\delta_B = 57.3^\circ$ (1 rad), and $\delta_B^* = 286.5^\circ$ (5 rad) is presented in Fig. B2 in Appendix B. For $r_B^{(*)} = 0.22$, it can clearly be observed that the fitted γ value approaches the boundary limit of 90° , and the corresponding resolution is approximately 18° . Such behavior can be clearly understood from the 2-D distribution presented in Fig. 6. This is comparable to the case listed in Tables 5 and 6 when $\delta_B^{(*)} = 286.5^\circ$ (near $3\pi/2$ rad) and $r_B^{(*)} = 0.22$.

I. Effect of using or not the $B_s^0 \rightarrow \tilde{D}^{(*)0}(\pi\pi)\phi$ and

$B_s^0 \rightarrow \tilde{D}^{(*)0}(K\pi\pi^0)\phi$ decays or not

As listed in Table 2 the expected yields for the D -meson decays to $\pi\pi$ and $K\pi\pi^0$ are somewhat lower than those for the other modes, down to a few tens of events.

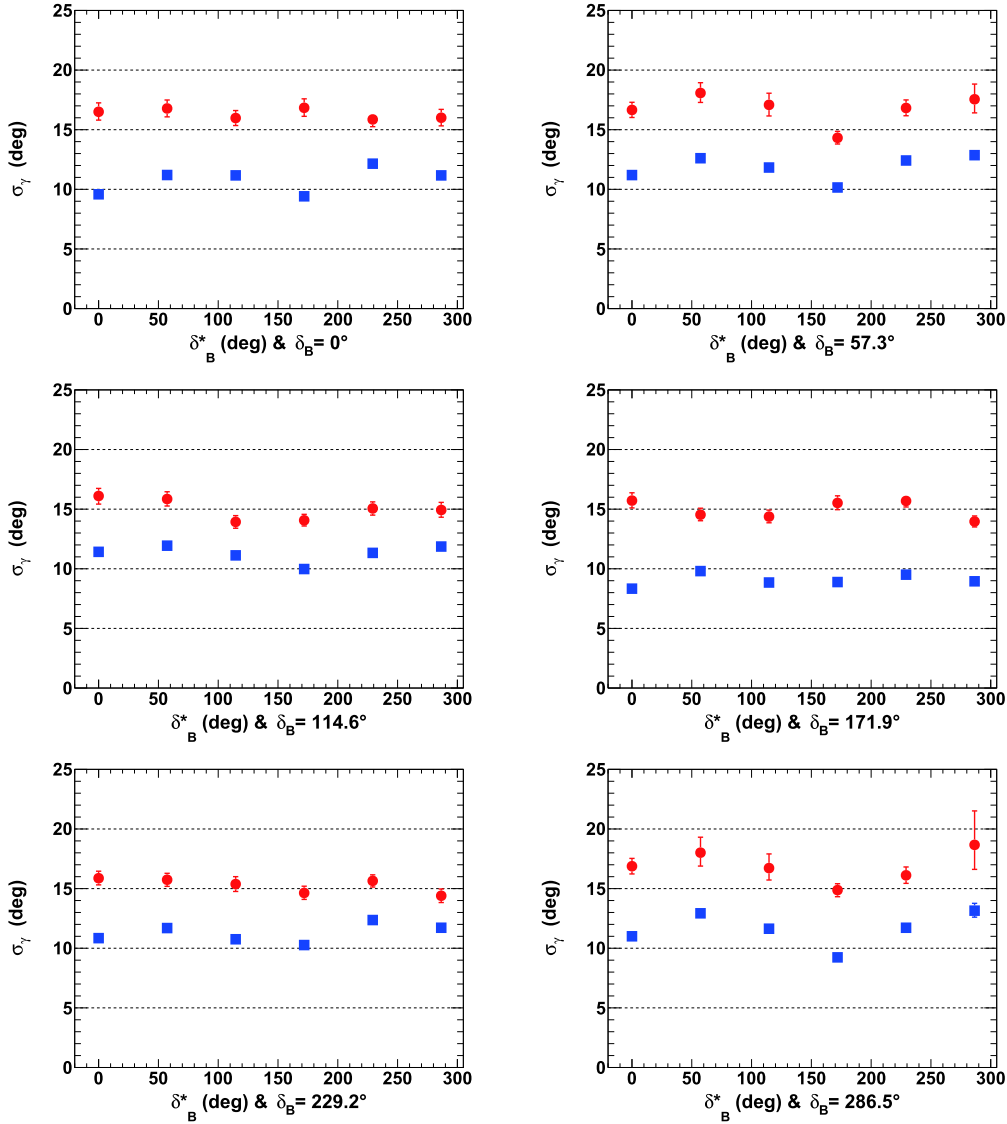


Fig. 14. (color online) Fitted resolutions of γ (σ_γ), for $r_B^{(*)} = 0.22$ (red circles) and 0.4 (blue squares) as a function of $\delta_B^{(*)}$ for initial true value of 65.66° (1.146 rad). All of the listed values are in [deg]. In each figure, the horizontal dashed black lines are guides for the eye at $\sigma_\gamma = 5^\circ, 10^\circ, 15^\circ$, and 20° . All of the plotted uncertainties are statistical only.

Again, these yields have been computed from LHCb studies on $B^\pm \rightarrow \tilde{D}^0(\pi/K)^\pm$, as reported in Refs. [28] and [29], and normalized to Ref. [22] with respect to the mode $B_s^0 \rightarrow \tilde{D}^{(*)0}(K\pi)\phi$. Therefore, the selections are not necessarily against the signals $B_s^0 \rightarrow \tilde{D}^{(*)0}(\pi\pi)\phi$ and $B_s^0 \rightarrow \tilde{D}^{(*)0}(K\pi\pi^0)\phi$, and the expected yields may be underestimated, as well as all the sub-decays listed in Table 2. Furthermore, it should be noted that the mode $\pi\pi$ is a CP -eigenstate, whereas the $K\pi\pi^0$ 3-body decay also has a large coherence factor value $R_D^{K\pi\pi^0} = (81 \pm 6)\%$ [36]. Nevertheless, the effect of using the $B_s^0 \rightarrow \tilde{D}^{(*)0}(\pi\pi)\phi$ and $B_s^0 \rightarrow \tilde{D}^{(*)0}(K\pi\pi^0)\phi$ decays or not has been studied and is reported here, and in Section VC, the effect of including the decays $B_s^0 \rightarrow \tilde{D}^{*0}\phi$ or not is also discussed for future more abundant datasets.

According to Fig. C1 in Appendix C, there is a relative loss on the precision in the unfolded value of γ of approximately 3 to 15%, when the $B_s^0 \rightarrow \tilde{D}^{(*)0}(\pi\pi)\phi$ decays are not used. Figure C2 in Appendix C indicates that a relative loss in precision of approximately 3 to 22% is observed when the $B_s^0 \rightarrow \tilde{D}^{(*)0}(K\pi\pi^0)\phi$ decays are not used.

V. PROSPECTIVE ON SENSITIVITY TO γ FOR RUNS 1–3 AND FULL HIGH-LUMINOSITY LHC (HL-LHC) LHCb DATASETS

The perspectives on the sensitivity to the CKM angle γ with $B_s^0 \rightarrow \tilde{D}^{(*)0}\phi$ decays have also been studied for the foreseen LHCb integrated luminosities at the end of LHC

Run 3 and for the possible full HL-LHC future LHCb program. According to Ref. [20], the LHCb trigger efficiency will be improved by a factor of 2 at the beginning of LHC Run 3. The full expected LHCb dataset of pp collisions at $\sqrt{s} = 13$ TeV corresponding to the sum of the Run 1, 2, and 3 LHCb dataset should be equal to 23 fb^{-1} by 2025, whereas it is expected to be 300 fb^{-1} by the second half of the 2030 decade. The final integrated LHCb luminosity accounts for an LHCb detector upgrade phase II. In the following, the projected event yields, as listed in Table 2, after 2025 and after 2038 have been scaled by a factor $F_{\text{later}} = 6.3$ and 90, respectively, and with uncertainties on observables of $1/\sqrt{F_{\text{later}}}$.

A. Projected precision on γ determination with

$$B_s^0 \rightarrow \tilde{D}^{(*)0} \phi \text{ decays}$$

For this prospective sensitivity study, we have made the conservative assumption that the precision on the strong parameters of the D -meson decays to $K\pi$, $K3\pi$, and $K\pi\pi^0$ listed in Table 3 should be improved by a factor of 2 at the end of the LHCb program (see the BES-III experiment perspectives [54]). The procedure described for the LHCb Run 1 & 2 data in Section IV has been repeated. The values of the normalization factors $C_{K\pi}$, $C_{K\pi,D\pi^0}$, and $C_{K\pi,D\gamma}$ obtained for Run 1 & 2 (see Section III) have been scaled to their expected equivalent rate for Runs 1 to 3 and full HL-LHC LHCb datasets. The statistical uncertainties of the computed observables (see Section IVC) obtained for the Run 1 & 2 LHCb data

have been scaled by the square root of a factor two times (trigger improvement) the relative increase in the anticipated collected B_s^0 -meson yield: 2.2 (8.8) for the Run 1 to 3 (full HL-LHC) LHCb dataset. Thereafter, for the Run 1 & 2 sensitivity studies, the same $2 \times 6 \times 6$ configurations of the $r_B^{(*)}$, and $\delta_B^{(*)}$ nuisance parameters have been tested ($r_B^{(*)} = 0.22$ or 0.4 and $\delta_B^{(*)} = 0, 1, 2, 3, 4, 5$ rad, and $\gamma = 65.66^\circ$ (1.146 rad)).

The 2-D p -value distribution profiles of the nuisance parameters $r_B^{(*)}$ and $\delta_B^{(*)}$ as a function of γ are presented in Figs. 15 and 16 for the expected Run1–3 LHCb dataset, and in Figs. 17 and 18 for the full HL-LHC LHCb dataset. For the purpose of these illustrations, the initial configuration of true values is $\gamma = 65.66^\circ$ (1.146 rad), $\delta_B = 171.9^\circ$ (3.0 rad), and $\delta_B^* = 114.6^\circ$ (2.0 rad), as well as $r_B^{(*)} = 0.4$ (0.22). Therefore, the distributions can be directly compared to those depicted in Figs. 7 and 8. The surface of the excluded regions at a 95.4% CL in $r_B^{(*)}$ vs. γ and $\delta_B^{(*)}$ vs. γ clearly increases with the additional data, but even in the semi-asymptotic regime, for the full expected HL-LHC LHCb dataset, one can clearly observe possible strong correlations between γ and the nuisance parameters $r_B^{(*)}$ and $\delta_B^{(*)}$. This is also visible in Figs. D1 and D2 in Appendix D, which are the equivalent version for the full expected HL-LHC LHCb dataset of the Run 1 & 2 LHCb dataset presented in Figs. 5 and 6 for the configurations $\gamma = 65.66^\circ$ (1.146 rad), $\delta_B = 57.3^\circ$ (1.0 rad), and $\delta_B^* = 286.5^\circ$ (5.0 rad), as well as $r_B^{(*)} = 0.4$ (0.22).

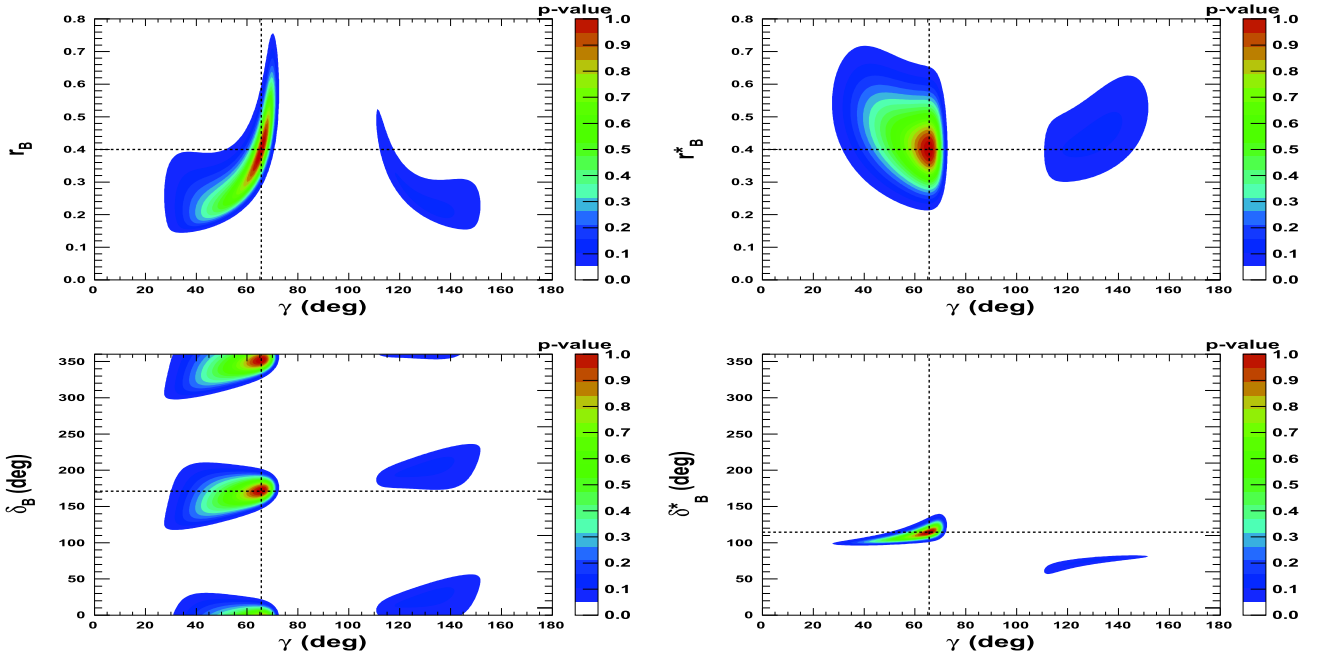


Fig. 15. (color online) 2-D p -value profiles of nuisance parameters $r_B^{(*)}$ and $\delta_B^{(*)}$ (Runs 1–3) as a function of γ . In each figure, the dashed black lines indicate the initial true values $\gamma = 65.66^\circ$ (1.146 rad), $\delta_B = 171.9^\circ$ (3.0 rad), and $\delta_B^* = 114.6^\circ$ (2.0 rad), as well as $r_B^{(*)} = 0.4$.

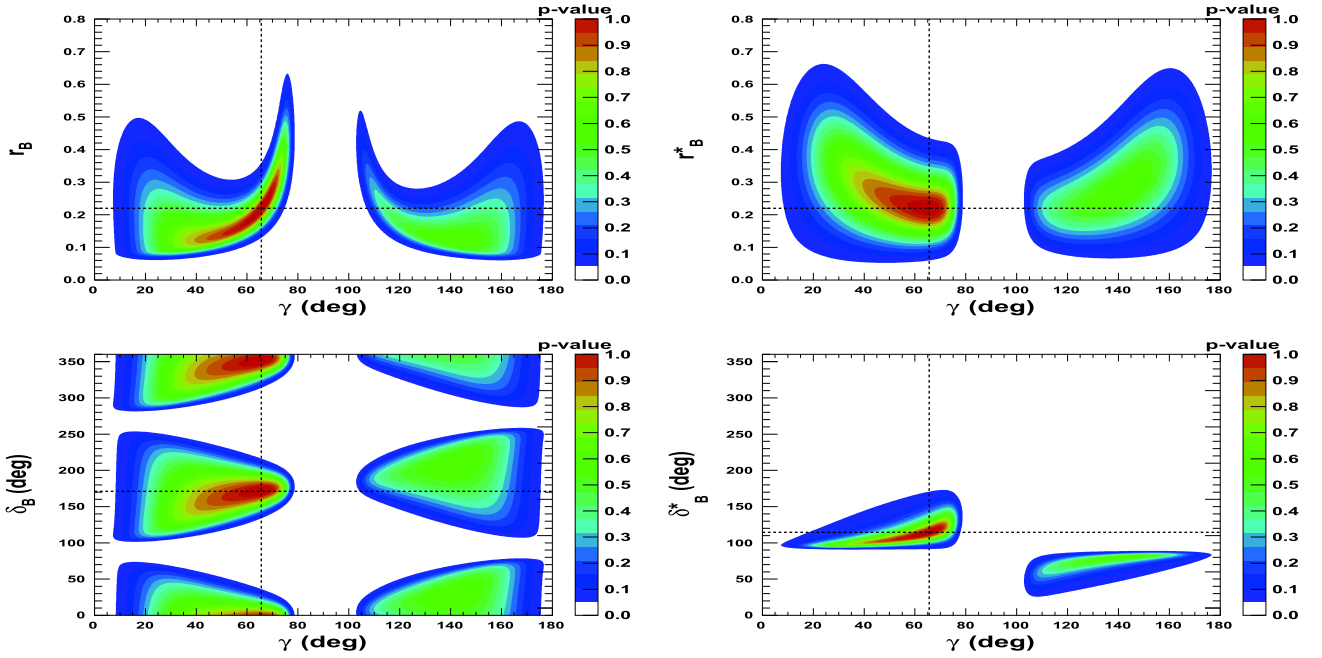


Fig. 16. (color online) 2-D p -value profiles of nuisance parameters $r_B^{(*)}$ and $\delta_B^{(*)}$ for Run 1–3 LHCb dataset as a function of γ . In each figure, the dashed black lines indicate the initial true values $\gamma = 65.66^\circ$ (1.146 rad), $\delta_B = 171.9^\circ$ (3.0 rad), and $\delta_B^* = 114.6^\circ$ (2.0 rad), as well as $r_B^{(*)} = 0.22$.

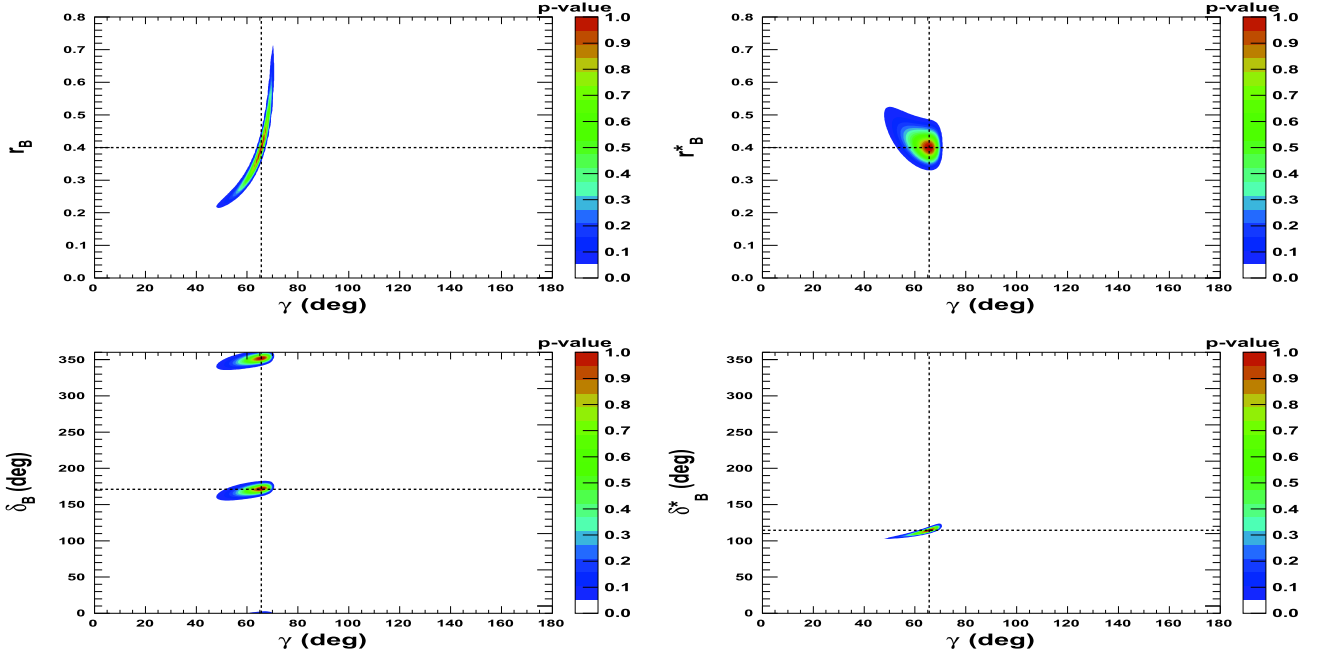


Fig. 17. (color online) 2-D p -value profiles of nuisance parameters $r_B^{(*)}$ and $\delta_B^{(*)}$ for full HL-LHC LHCb dataset as a function of γ . In each figure, the dashed black lines indicate the initial true values $\gamma = 65.66^\circ$ (1.146 rad), $\delta_B = 171.9^\circ$ (3.0 rad), and $\delta_B^* = 114.6^\circ$ (2.0 rad), as well as $r_B^{(*)} = 0.4$.

For the configuration $\gamma = 65.66^\circ$ (1.146 rad), $\delta_B = 171.9^\circ$ (3.0 rad), and $\delta_B^* = 114.6^\circ$ (2.0 rad), as well as $r_B^{(*)} = 0.4$ (0.22), Fig. 19 presents the fitted γ distribution obtained for 4000 pseudoexperiments for the expected

Run 1–3 LHCb dataset. The fitted values are $\mu_\gamma = (67.7 \pm 0.1)^\circ$ ($(73.5 \pm 0.2)^\circ$) and $\sigma_\gamma = (3.5 \pm 0.1)^\circ$ ($(5.5 \pm 0.2)^\circ$) for $r_B^{(*)} = 0.4$ (0.22). The fitted values presented in Fig. 21 are $\mu_\gamma = (68.1 \pm 0.1)^\circ$ ($(71.1 \pm 0.1)^\circ$)

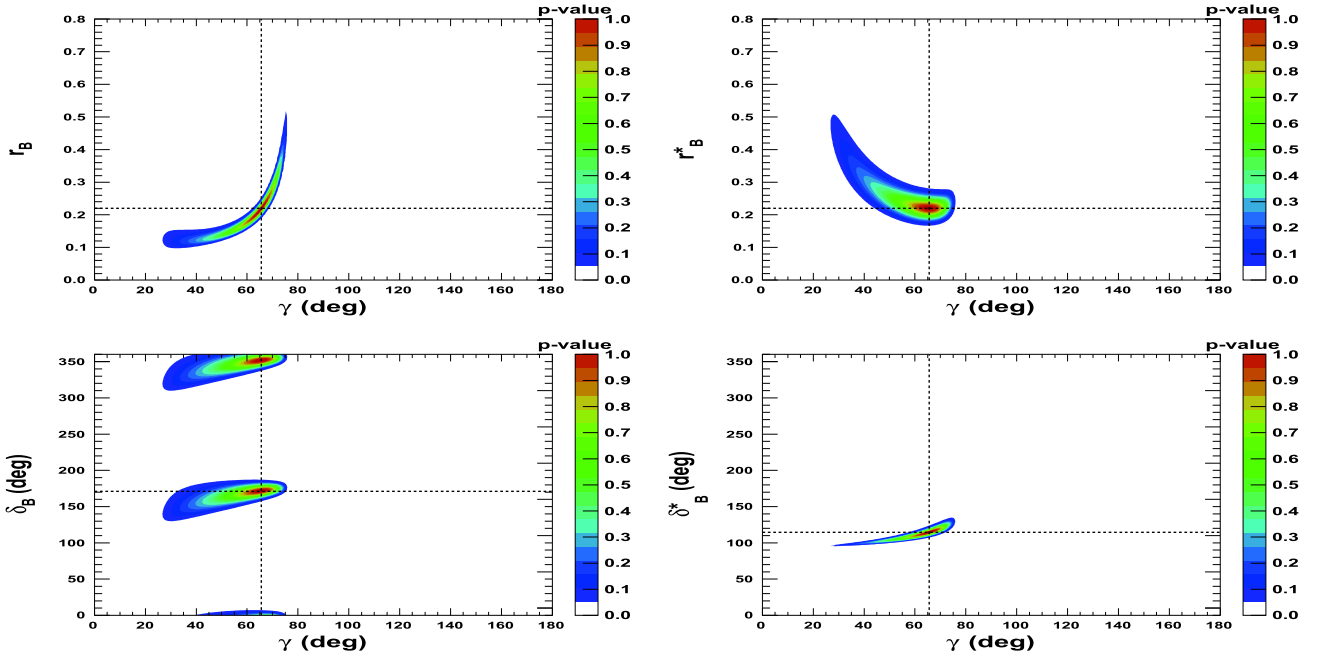


Fig. 18. (color online) 2-D p -value profiles of nuisance parameters $r_B^{(*)}$ and $\delta_B^{(*)}$ for full HL-LHC LHCb dataset as a function of γ . In each figure, the dashed black lines indicate the initial true values $\gamma = 65.66^\circ$ (1.146 rad), $\delta_B = 171.9^\circ$ (3.0 rad), and $\delta_B^{(*)} = 114.6^\circ$ (2.0 rad), as well as $r_B^{(*)} = 0.22$.

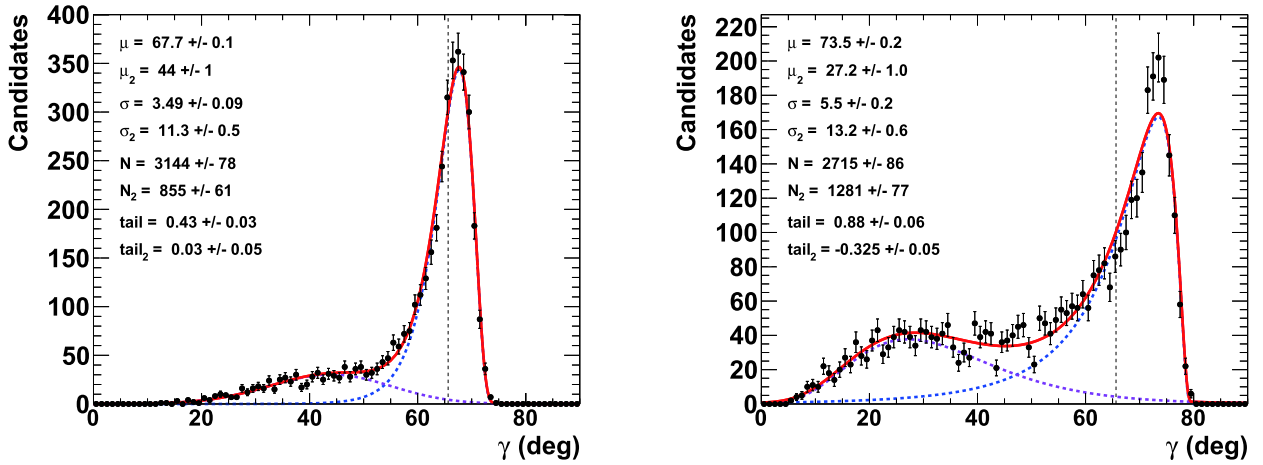


Fig. 19. (color online) Fit to distributions of γ obtained from 4000 pseudoexperiments for expected Run 1–3 LHCb dataset. The initial configuration is $\gamma = 65.66^\circ$, $r_B^{(*)} = 0.4$ (left) and 0.22 (right), $\delta_B = 171.9^\circ$ (3 rad), and $\delta_B^{(*)} = 114.6^\circ$ (2 rad). The purple dashed curve represents the tails generated by the correlations with the nuisance parameters $r_B^{(*)}$ and $\delta_B^{(*)}$, whereas the blue dashed curve indicates the core part of the distribution, and the plain red line is the sum of the two components of the fit.

and $\sigma_\gamma = (2.5 \pm 0.1)^\circ$ ($(5.3 \pm 0.1)^\circ$) for $r_B^{(*)} = 0.4$ (0.22), respectively, for the expected full HL-LHC LHCb dataset. The fitted values are slightly shifted up with respect to the initial γ true value but are compatible within one standard deviation. When comparing with the numbers listed in Table 6, it can be observed that the resolution improves as $8.8/3.5 = 2.5$ ($14.4/5.5 = 2.6$) for $r_B^{(*)} = 0.4$ (0.22) when moving from the Run 1 & 2 to the expected

Run 1–3 LHCb datasets, whereas a factor of 2.2 is expected. However, when moving from the expected Run 1–3 to the full expected HL-LHC LHCb datasets, the improvement is only $3.5/2.5 = 1.4$ ($5.5/5.3 = 1.040$) for $r_B^{(*)} = 0.4$ (0.22), whereas one may naively expect an improvement $8.8/2.2 = 4.0$. This is certainly partially owing to the strong correlations between the nuisance parameters $r_B^{(*)}$ and $\delta_B^{(*)}$. A more sophisticated simultaneous global fit to

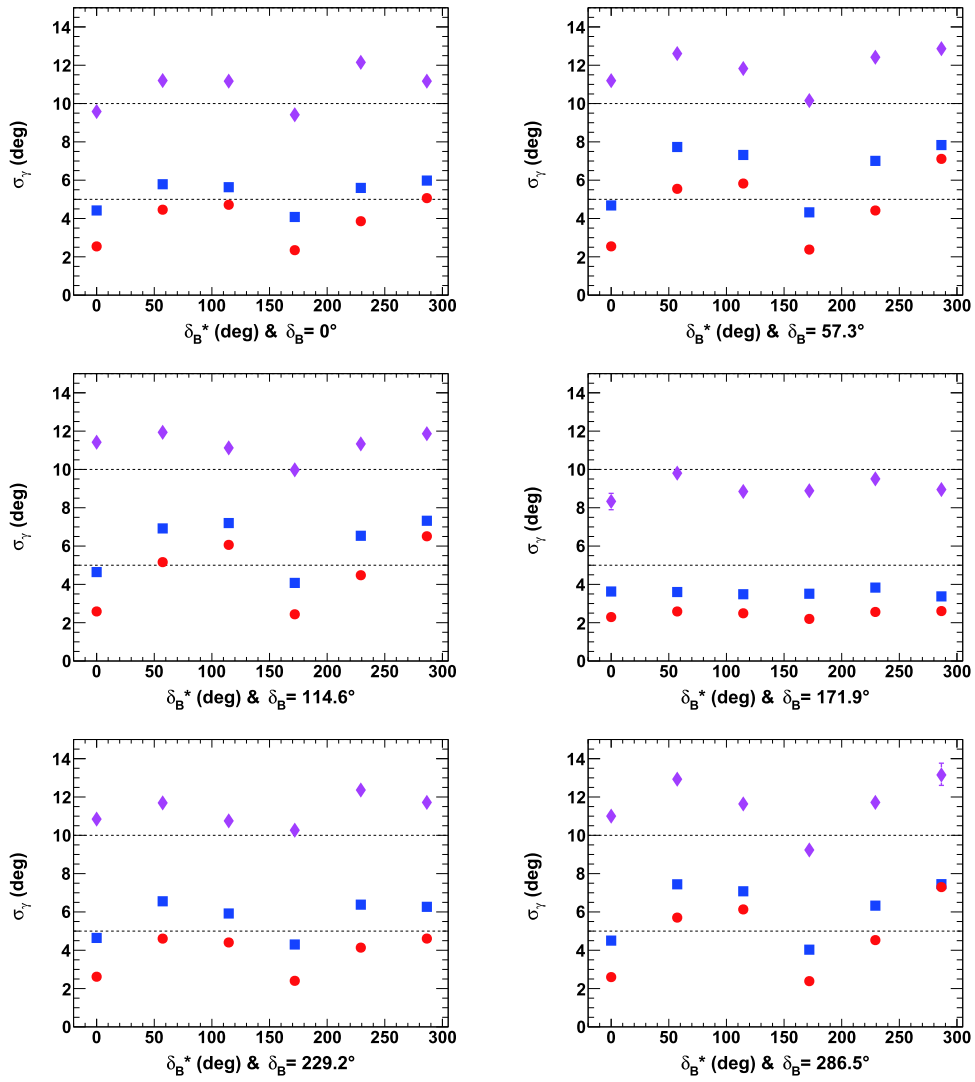


Fig. 20. (color online) Fitted mean values of γ (σ_γ) for Run 1 & 2 (pink lozenges), Run 1–3 (blue squares), and full HL-LHC (red circles) LHCb dataset as a function of δ_B^* , for $r_B^{(*)} = 0.4$ and initial true value of 65.66° (1.146 rad). In each figure, the horizontal dashed black lines are guides for the eye at $\sigma_\gamma = 5^\circ$ and 10° .

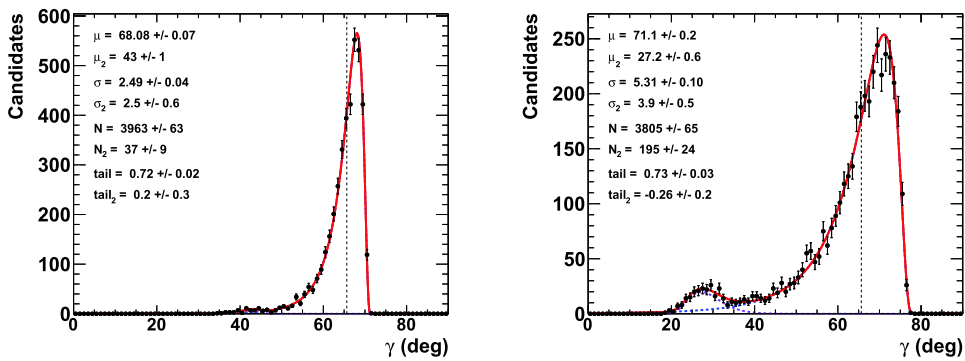


Fig. 21. (color online) Fit to distributions of γ obtained from 4000 pseudoexperiments for expected full HL-LHC LHCb dataset. The initial configuration is $\gamma = 65.66^\circ$, $r_B^{(*)} = 0.4$ (left) and 0.22 (right), $\delta_B = 171.9^\circ$ (3 rad), and $\delta_B^* = 114.6^\circ$ (2 rad). The purple dashed curve represents the tails generated by the correlations with the nuisance parameters $r_B^{(*)}$ and δ_B^* , whereas the blue dashed curve is the core part of the distribution, and the plain red line is the sum of the two components of the fit.

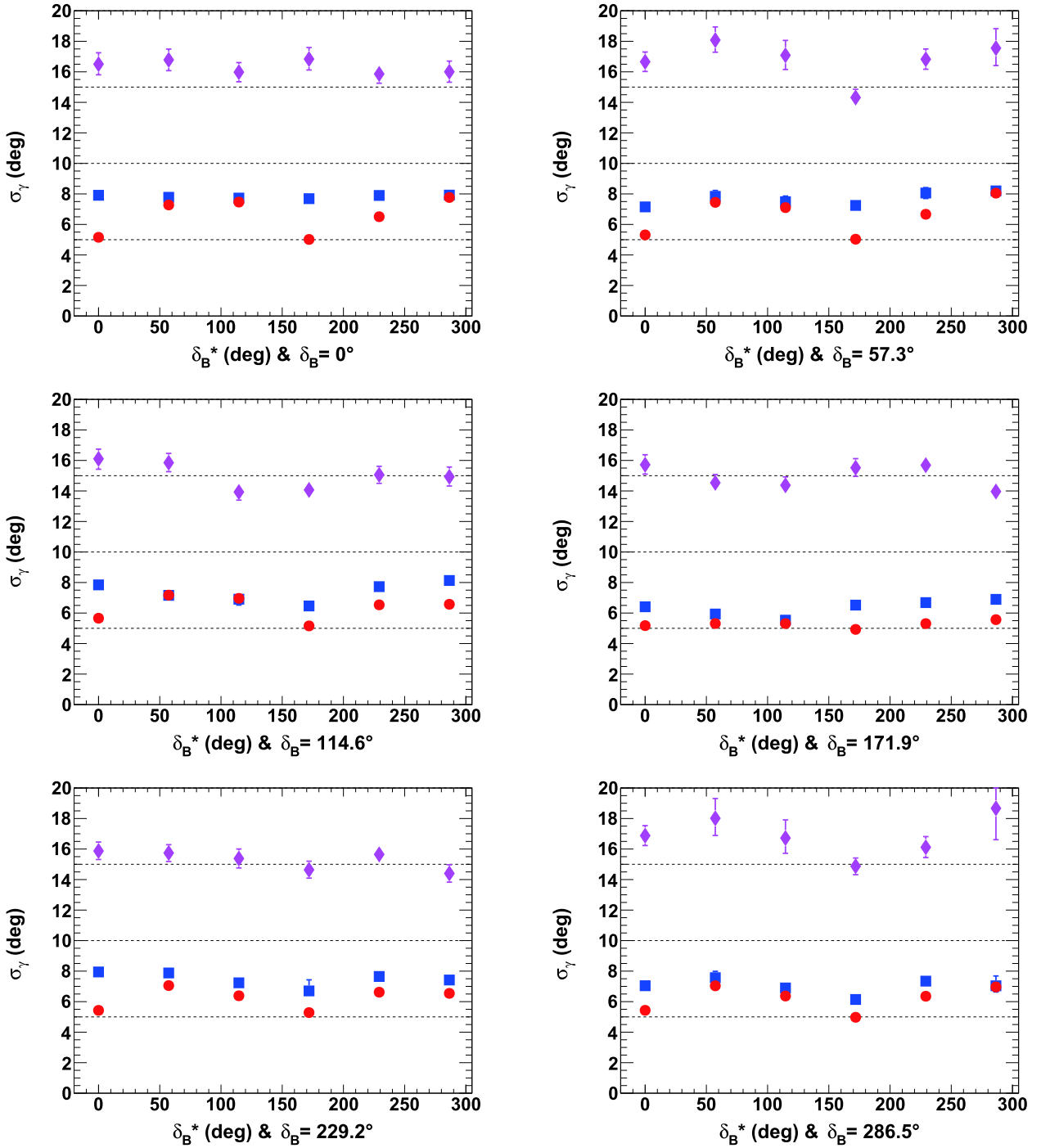


Fig. 22. (color online) Fitted resolutions of γ (σ_γ) for Run 1 & 2 (pink lozenges), Run 1–3 (blue squares), and full HL-LHC (red circles) LHCb dataset as a function of $\delta_B^{(*)}$, for $r_B^{(*)}=0.22$ and initial true value of 65.66° (1.146 rad). In each figure, the horizontal dashed black lines are guides for the eye at $\sigma_\gamma = 5^\circ$, 10° , and 15° .

the nuisance parameters $r_B^{(*)}$ and $\delta_B^{(*)}$, and γ may be useful.

It must also be remembered that TMath::Probstill exhibits some under-coverage, *namely* 79 (91)% and 94 (89)% for $r_B^{(*)}=0.4$ (0.22), with respect to the full frequentist treatment on the Monte-Carlo simulation basis [50], as presented in Fig. 23, with the Run 1–3 and full

expected HL-LHC LHCb datasets, respectively. The relative scale factors $F_{K3\pi}$, $F_{K\pi\pi^0}$, F_{KK} , and $F_{\pi\pi}$ used in this study already have a precision above 2%. The precision on the normalization factors $C_{K\pi}$, $C_{K\pi,D\pi^0}$, and $C_{K\pi,D\gamma}$ may also benefit from another improved precision of the branching fraction of the decay modes $B_s^0 \rightarrow \bar{D}^{(*)0}\phi$ and of

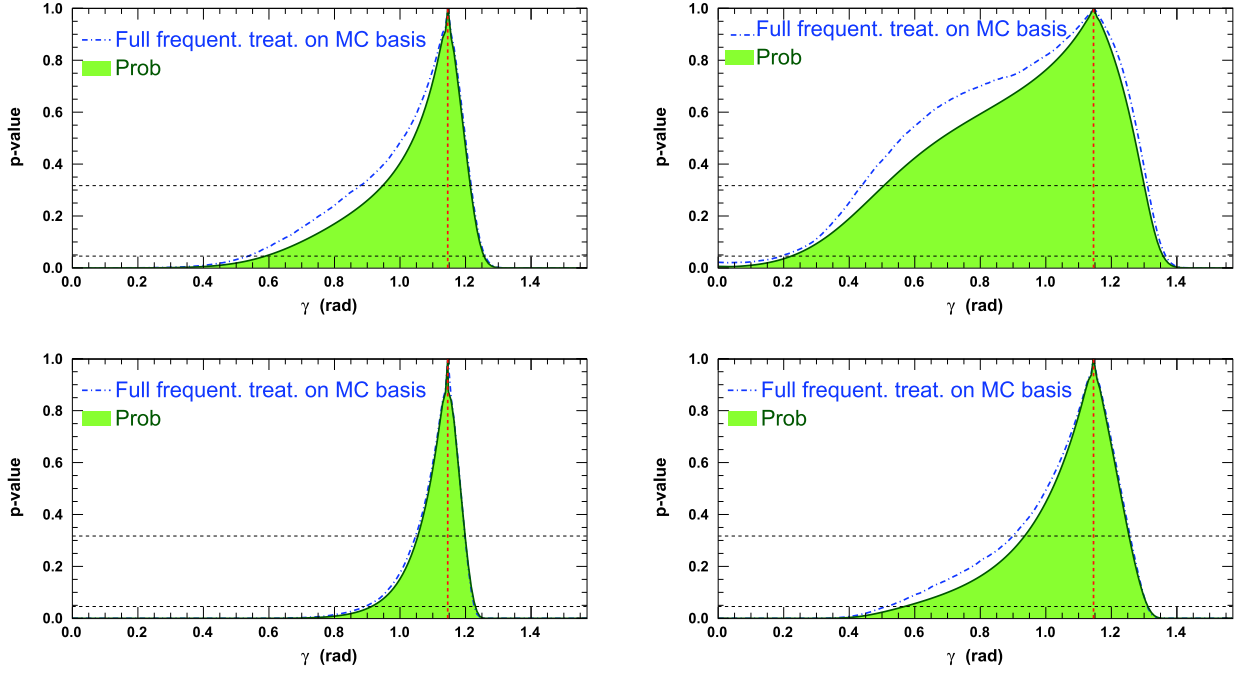


Fig. 23. (color online) Profiles of p -value distributions of global χ^2 fit to γ for set of true initial parameters $\gamma = 1.146$ rad, $r_B^{(*)} = 0.4$ (left) 0.22 (right), $\delta_B = 3.0$ rad, and $\delta_B^* = 2.0$ rad. The assumed integrated luminosity is that of the LHCb data expected to be collected after LHC Run 3 (top) and after the full HL-LHC (bottom) period. The corresponding distribution obtained from the full frequentist treatment on the Monte Carlo simulation basis [50] is superimposed on the profile obtained with TMath::Prob. In each figure, the vertical dashed red line indicates the initial γ true value, and the two horizontal dashed black lines refer to 68.3 and 95.4% CLs.

the longitudinal polarization fraction in the mode $B_s^0 \rightarrow \bar{D}^{*0} \phi$. However, the normalization factors are the same for all sets of Eqs. (14)-(34) for $B_s^0 \rightarrow \bar{D}^0 \phi$ or $\bar{D}^{*0}(\pi^0, \gamma) \phi$, and their improved precision should be a second order effect. All of the above listed improvements are expected to occur to benefit from the total expected HL-LHC LHCb dataset fully.

The expected resolutions on γ for the other usual configuration ($\delta_B^{(*)} = 0, 1, 2, 3, 4, 5$ rad, and $\gamma = 65.66^\circ$ (1.146 rad)) are presented in Fig. 20 for $r_B^{(*)} = 0.4$ and in Fig. 22 for $r_B^{(*)} = 0.22$, for the Run 1 & 2, Run 1–3, and full HL-LHC LHCb datasets. For $r_B^{(*)} = 0.4$, the resolution mainly ranges from 3.4° to 7.8° for Run 1–3 and from 2.2° to 7.1° , or better, for the full HL-LHC dataset. For $r_B^{(*)} = 0.22$, the resolution ranges from 5.5° to 8.2° for Run 1–3 and from 3.3° to 7.8° , or better, for the full HL-LHC dataset.

Another expected improvement could arise from a time-dependent CP Dalitz plane analysis of the decay $B_s^0 \rightarrow \bar{D}_{CP}^{*0} K^+ K^-$, as anticipated in Ref. [55]. With the ultimate HL-LHC LHCb dataset, it should be possible to perform such an analysis, thus including the $B_s^0 \rightarrow \bar{D}^{*0} \phi$ decay, to extract the CKM angle γ , as proposed a few years ago in [56].

For completeness, an alternate definition of the resolu-

tion as half of the 68.3% CL frequentist intervals of the 1-D p -value profiles of a 68.3% CL is provided in Appendix E in Figs. E1 and E2. A better scaling of the performances is observed with the size of the datasets, whereas relatively worse resolutions are obtained with respect to those displayed in Figs. 20 and 22. However, the effects of the nuisance parameters $r_B^{(*)}$ and $\delta_B^{(*)}$ are treated in a simplified manner compared to the full treatment by the generated pseudoexperiments.

B. Effect of strong parameters from D -meson decays and of $y = \Delta\Gamma_s/2\Gamma_s$

Most of the strong parameters of the D -meson decays to $K\pi$, $K3\pi$, and $K\pi\pi^0$ are external parameters and are obtained from beauty- or charm-factories, such as BaBar, Belle, CLEO-c, and LHCb [27]. Improvements in their determination are expected soon from the updated BES-III experiment [50] or later, from future super τ -charm factories [57–59]. Several scenarios have been tested to verify the effects of these improvements to the γ sensitivity. With the set of parameters $\gamma = 1.146$ rad (65.66°), $r_B^{(*)} = 0.4$, and $\delta_B = 3.0$ rad, as well as $\delta_B^* = 2.0$, the uncertainties of the current measurements of the D -meson parameters listed in Table 3 have been scaled down, and their effects on the fitted γ values from pseudoexperiments are listed in Table 7. As the uncertainties of the ex-

ternal parameters are not yet dominant (Run 1 & 2 data), a study has also been performed for the expected full HL-LHC dataset. However, with substantially more data, future improvements in the measurements of the strong parameters from the D -meson decays do not appear to influence the sensitivity to the CKM angle γ significantly.

This exercise was repeated using the same initial configuration of the parameters γ , $r_B^{(*)}$, and $\delta_B^{(*)}$, for the uncertainty on $y = \Delta\Gamma_s/2\Gamma_s$. The results of this study are listed in Table 8. Again, no obvious sensitivity to these changes is highlighted, neither for Run 1 & 2 nor for the full HL-LHC dataset. To our knowledge, it should be stressed that the tested improvements in y have not been supported by any published prospective studies.

From the above studies, it can be concluded that the possibly large correlations of γ with respect to the nuisance parameters $r_B^{(*)}$ and $\delta_B^{(*)}$ definitely dominate the ultimate precision on γ for the extraction with the $B_s^0 \rightarrow \tilde{D}^{(*)0}\phi$ modes.

C. Effect of using $B_s^0 \rightarrow \tilde{D}^{(*)0}\phi$ decays or not

It has been demonstrated in Ref. [22] that the decays $B_s^0 \rightarrow \tilde{D}^{(*)0}\phi$ can be reconstructed in a clean manner together with $B_s^0 \rightarrow \tilde{D}^0\phi$, with a similar rate and a partial reconstruction method, where the γ or π^0 produced in the decay of \tilde{D}^{*0} are omitted. Thus far, these modes have been included in the sensitivity studies. Figures F1-F6 in Appendix F present the 2-D p -value profiles of the nuisance parameters r_B and δ_B as a function of γ as well as the fit to the distributions of γ obtained from 4000 pseudoexperiments for the Run 1 & 2, Run 1–3, and full HL-LHC LHCb datasets for the initial true values $\gamma = 65.66^\circ$ (1.146 rad), $\delta_B = 171.9^\circ$ (3.0 rad), $\delta_B = 114.6^\circ$ (2.0 rad), and

$r_B^{(*)} = 0.4$ (0.22). The information from $B_s^0 \rightarrow \tilde{D}^{*0}\phi$ decays has not been included in these figures. According to Figs. F2, F4, and F6 in Appendix F, there is a relative loss in the precision of the unfolded value of γ of approximately 20 (40%) when the $B_s^0 \rightarrow \tilde{D}^{*0}\phi$ decays are not used for $r_B^{(*)} = 0.4$ (0.22). For future datasets, the improvement obtained by including the $B_s^0 \rightarrow \tilde{D}^{*0}\phi$ modes is less significant, but not negligible, and aids in improving the measurement of γ .

VI. CONCLUSIONS

Untagged $B_s^0 \rightarrow \tilde{D}^{(*)0}\phi$ decays provide another theoretically clean pathway to the measurement of the CKM-angle γ . By using the expected event yields for D decays on $K\pi$, $K3\pi$, $K\pi\pi^0$, KK , and $\pi\pi$, we have demonstrated that a precision on γ of approximately 8° to 19° can be achieved with LHCb Run 1 & 2 data. With additional data, a precision on γ of $3^\circ - 8^\circ$ can be achieved with the LHCb Run 1–3 dataset (23 fb^{-1} in 2025). Ultimately, a precision of the order of $2^\circ - 7^\circ$ is expected with the full HL-LHC LHCb dataset (300 fb^{-1} in 2038). The asymptotic sensitivity is dominated by the possibly large correlations of γ with respect to the nuisance parameters $r_B^{(*)}$ and $\delta_B^{(*)}$. The use of this method can improve our knowledge of γ from B_s^0 decays and aid in understanding the discrepancy of γ between measurements with B^+ and B_s^0 modes.

We are grateful to all members of the CKMfitter group for their comments and providing us with their private software based on a frequentist approach for computing the many pseudoexperiments performed for this study. In particular, we would like to thank J. Charles for his helpful comments on starting this analysis.

Table 7. Fitted resolutions of γ (σ_γ) in [deg] obtained from 4000 pseudoexperiments as a function of decreasing uncertainties of strong D -meson parameters (see Table 3).

Uncertainties of D -meson params.	Now	$\times 1/2$	$\times 1/5$	$\times 1/10$
Run 1 & 2 ($r_B^{(*)} = 0.4$)	8.8 ± 0.2	8.1 ± 0.3	8.0 ± 0.3	7.8 ± 0.2
Run 1 & 2 ($r_B^{(*)} = 0.22$)	12.9 ± 0.3	13.2 ± 0.5	13.1 ± 0.5	12.8 ± 0.9
Full HL-LHC ($r_B^{(*)} = 0.4$)	2.6 ± 0.1	2.5 ± 0.1	2.5 ± 0.1	2.5 ± 0.1
Full HL-LHC ($r_B^{(*)} = 0.22$)	5.4 ± 0.1	5.3 ± 0.1	5.2 ± 0.1	5.1 ± 0.1

Table 8. Fitted resolutions of γ (σ_γ) in [deg] obtained from 4000 pseudoexperiments as function of decreasing uncertainties of $y = \Delta\Gamma_s/2\Gamma_s$. For the full HL-LHC dataset, the uncertainties for the strong D -meson parameters are divided by 2 with respect to the current measurements (see Table 3).

Uncertainty on $y = \Delta\Gamma_s/2\Gamma_s$	Now	$\times 1/2$	$\times 1/5$	$\times 1/10$
Run 1 & 2 ($r_B^{(*)} = 0.4$)	8.8 ± 0.2	8.3 ± 0.2	8.2 ± 0.2	8.1 ± 0.3
Run 1 & 2 ($r_B^{(*)} = 0.22$)	12.9 ± 0.3	12.6 ± 0.4	12.5 ± 0.5	12.5 ± 0.5
Full HL-LHC ($r_B^{(*)} = 0.4$)	2.5 ± 0.1	2.5 ± 0.1	2.5 ± 0.1	2.5 ± 0.1
Full HL-LHC ($r_B^{(*)} = 0.22$)	5.3 ± 0.1	5.3 ± 0.1	5.2 ± 0.1	5.2 ± 0.1

Appendix A: Fitted nuisance parameters $r_B^{(*)}$ and $\delta_B^{(*)}$

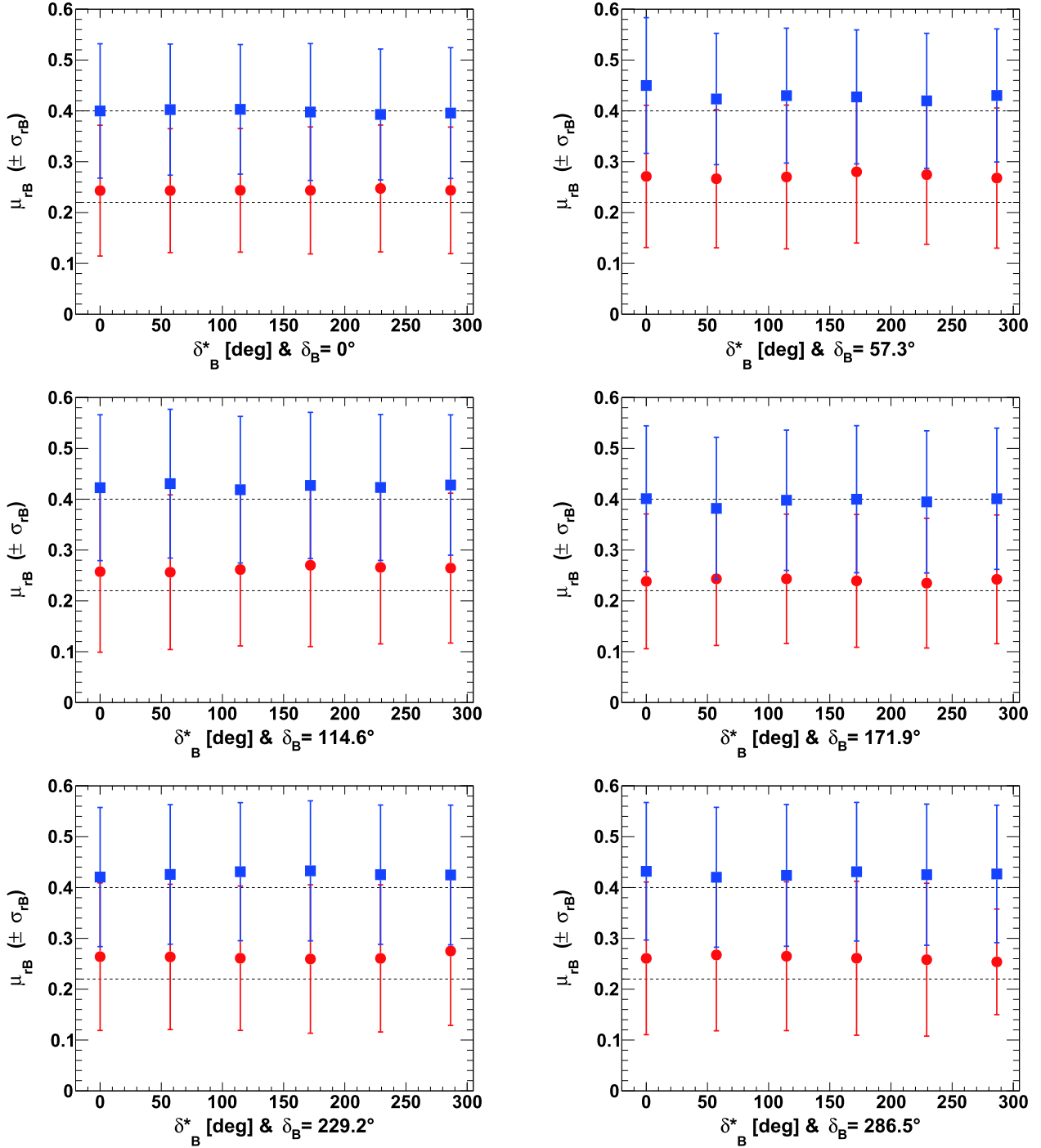


Fig. A1. (color online) Fitted mean values of r_B (μ_{r_B}), for $r_B^{(*)} = 0.22$ (red circles) and 0.4 (blue squares) as a function of $\delta_B^{(*)}$ for initial true value of γ of 65.66° (1.146 rad). In each figure, the horizontal dashed black line indicates the initial r_B true value, and the displayed uncertainties are the fitted resolutions on r_B (*i.e.* σ_{r_B}).

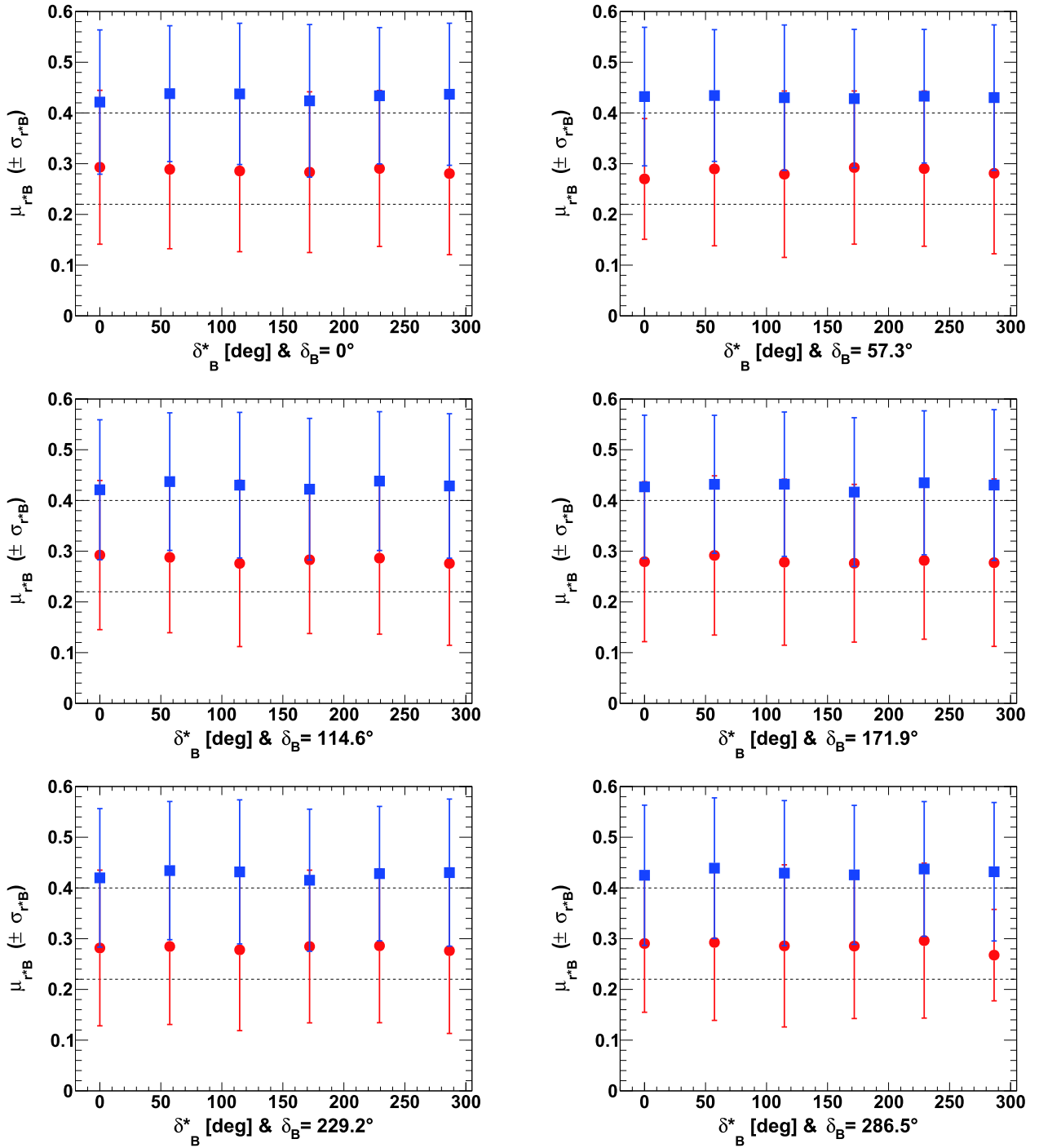


Fig. A2. (color online) Fitted mean values of r_B^* ($\mu_{r_B^*}$), for $r_B^* = 0.22$ (red circles) and 0.4 (blue squares) as a function of δ_B^* for initial true value of γ of 65.66° (1.146 rad). In each figure, the horizontal dashed black line indicates the initial r_B^* true value, and the displayed uncertainties are the fitted resolutions on r_B^* (*i.e.* $\sigma_{r_B^*}$).

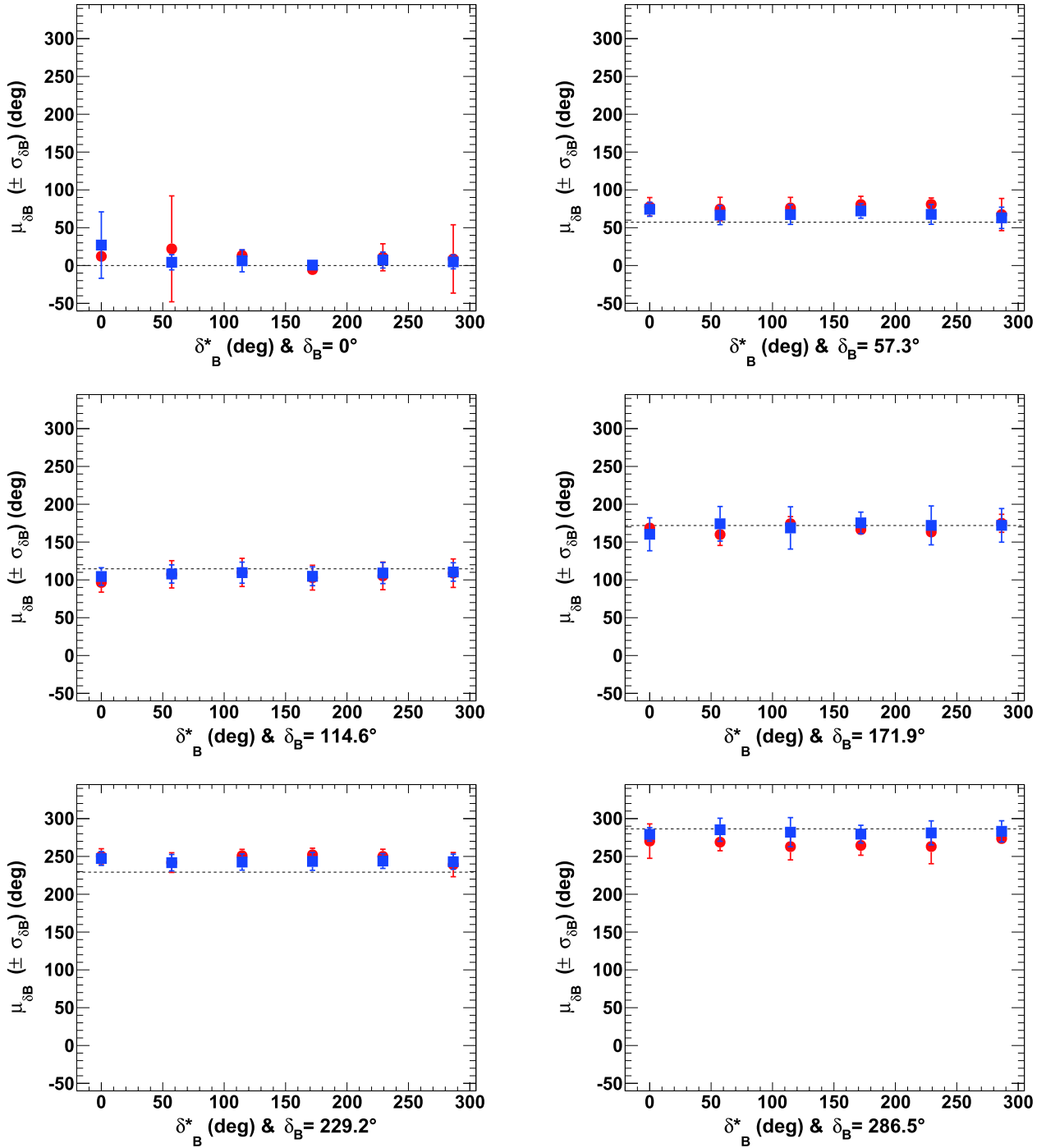


Fig. A3. (color online) Fitted mean values of δ_B (μ_{δ_B}), for $r_B^{(*)} = 0.22$ (red circles) and 0.4 (blue squares) as a function of δ_B^* for initial true value of γ of 65.66° (1.146 rad). In each figure, the horizontal dashed black line indicates the initial δ_B true value, and the displayed uncertainties are the fitted resolutions on δ_B (*i.e.* σ_{δ_B}).

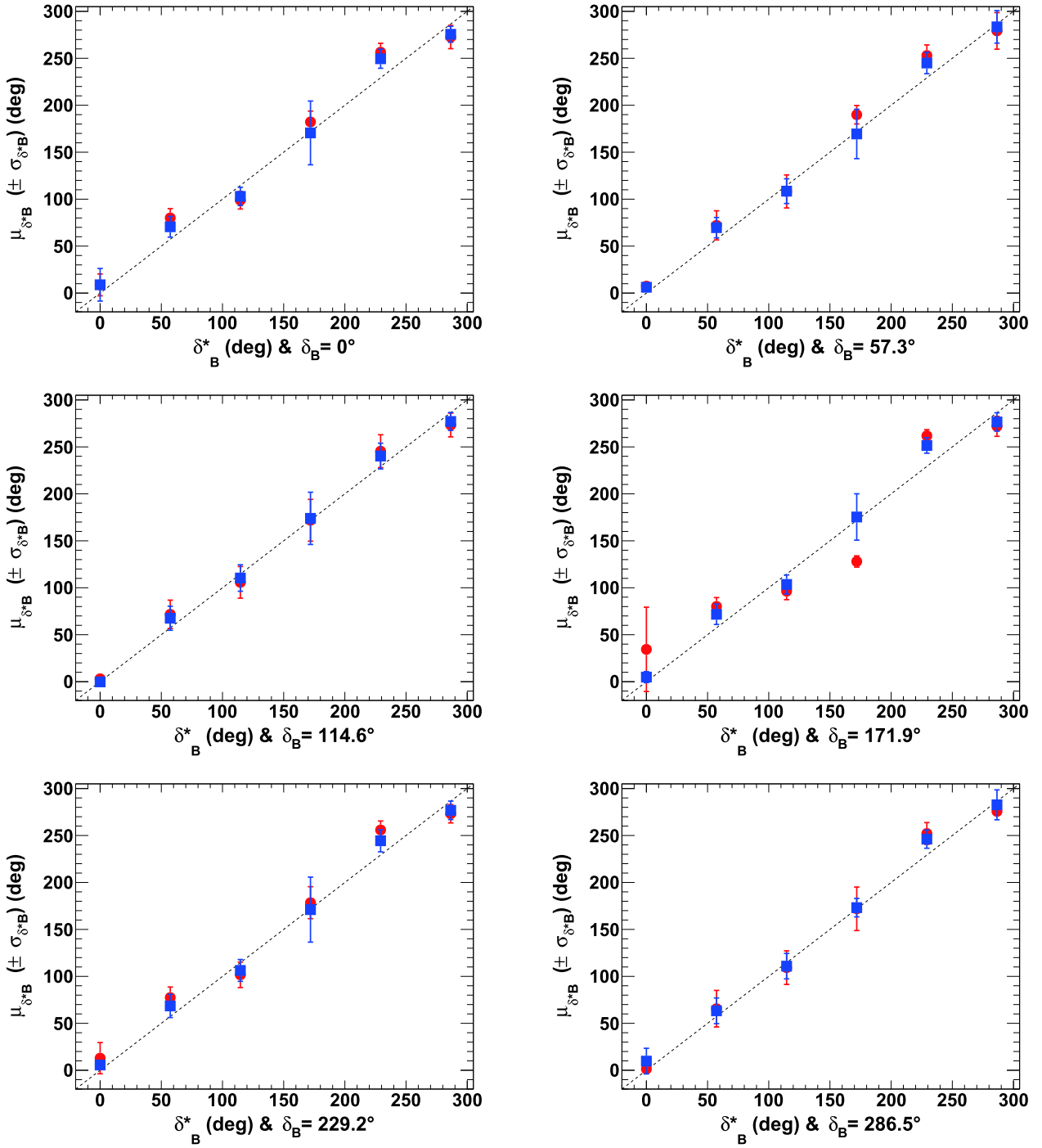


Fig. A4. (color online) Fitted mean values of δ_B^* ($\mu_{\delta_B^*}$), for $r_B^{(*)} = 0.22$ (red circles) and 0.4 (blue squares) as a function of $\delta_B^{(*)}$ for initial true value of γ of 65.66° (1.146 rad). In each figure, the dashed black line indicates the initial δ_B^* true value, and the displayed uncertainties are the fitted resolutions on δ_B^* (*i.e.* $\sigma_{\delta_B^*}$).

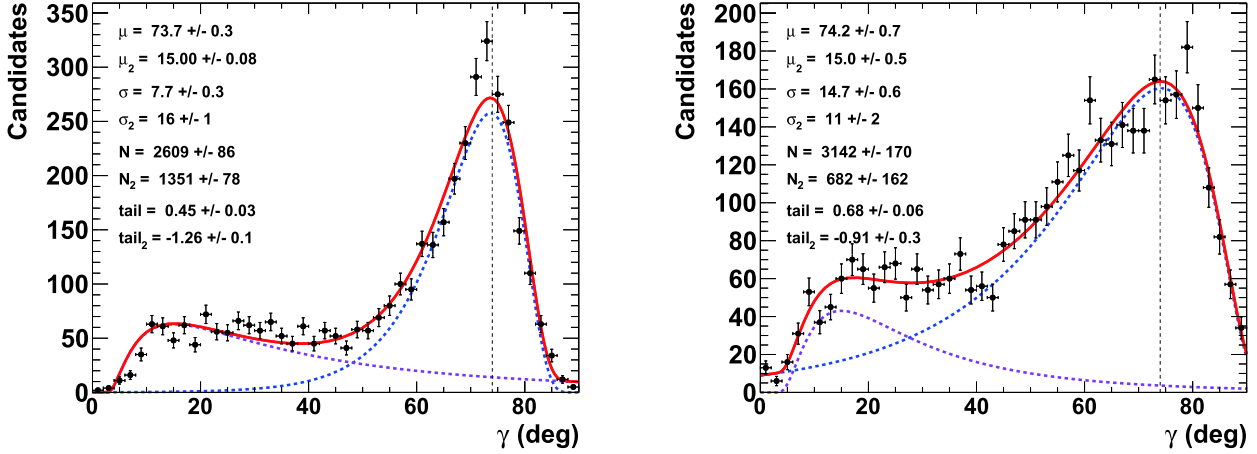
Appendix B: Case of γ equals 74° 

Fig. B1. (color online) Fit to distributions of nuisance parameters γ obtained from 4000 pseudoexperiments. The initial configuration is $\gamma = 74^\circ$, $r_B^{(*)} = 0.4$ (left) and 0.22 (right), $\delta_B = 171.9^\circ$ (3 rad), and $\delta_B^* = 114.6^\circ$ (2 rad). In the distributions, only the candidates with a value of $\gamma \in [0^\circ, 90^\circ]$ are considered. The purple dashed curve represents the tails generated by the correlations with the nuisance parameters $r_B^{(*)}$ and $\delta_B^{(*)}$, whereas the blue dashed curve indicates the core part of the distribution, and the plain red line is the sum of the two components of the fit.

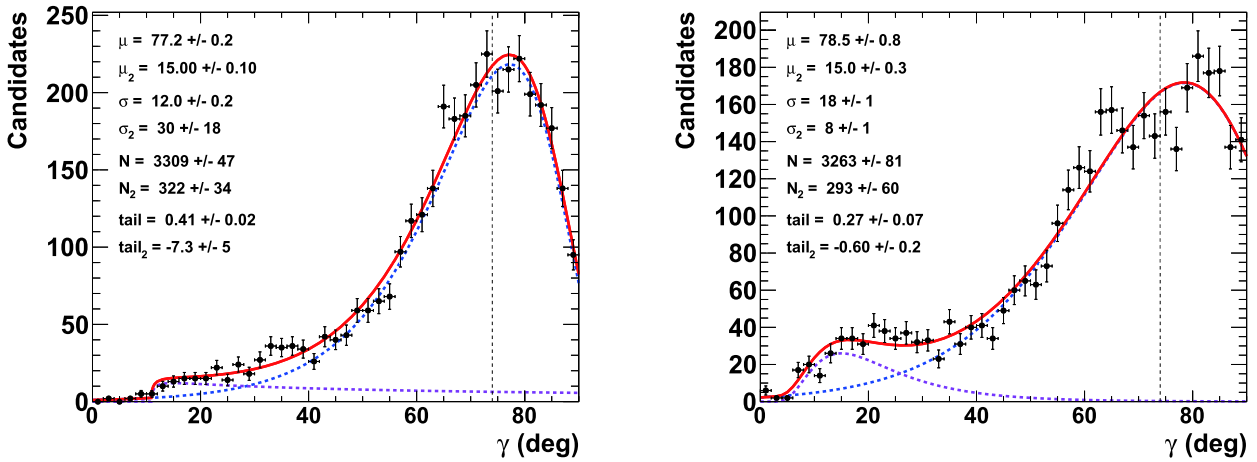


Fig. B2. (color online) Fit to distributions of nuisance parameters γ obtained from 4000 pseudoexperiments. The initial configuration is $\gamma = 74^\circ$, $r_B^{(*)} = 0.4$ (left) and 0.22 (right), $\delta_B = 57.9^\circ$ (1 rad), and $\delta_B^* = 286.5^\circ$ (5 rad). In the distributions, only the candidates with a value of $\gamma \in [0^\circ, 90^\circ]$ are considered. The purple dashed curve represents the tails generated by the correlations with the nuisance parameters $r_B^{(*)}$ and $\delta_B^{(*)}$, whereas the blue dashed curve indicates the core part of the distribution, and the plain red line is the sum of the two components of the fit.

Appendix C: Excluding $B_s^0 \rightarrow \tilde{D}^{(*)0}(\pi\pi)\phi$ and $B_s^0 \rightarrow \tilde{D}^{(*)0}(K\pi\pi^0)\phi$ decays

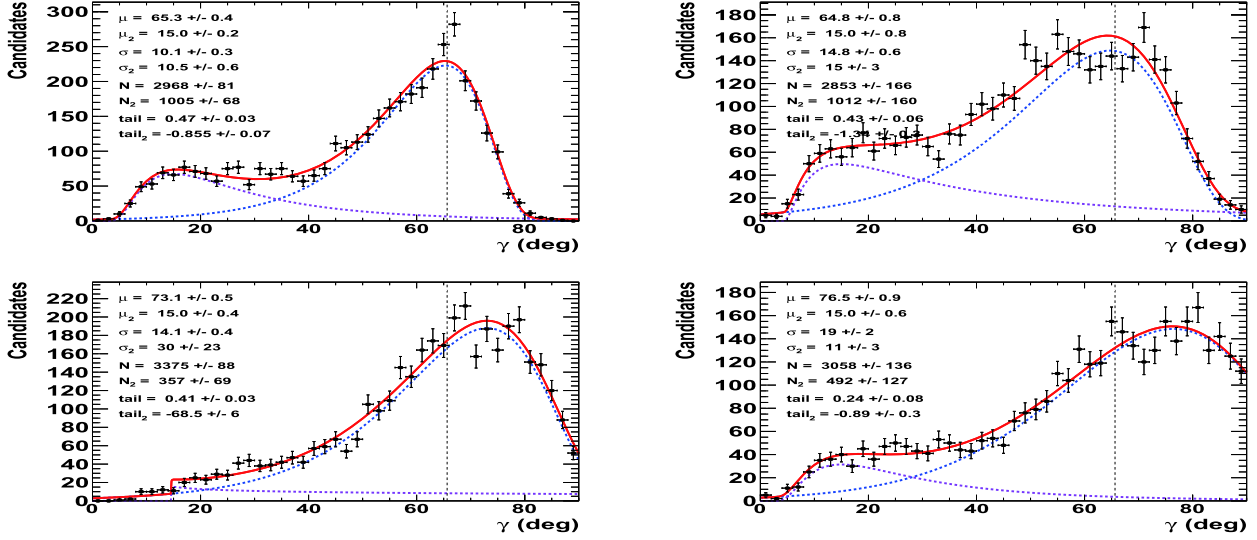


Fig. C1. (color online) Fit to distributions of γ obtained from 4000 pseudoexperiments for Run 1 & 2 LHCb dataset. The initial configuration is $\gamma = 65.66^\circ$, $r_B = 0.4$ (left) and 0.22 (right), and (top) $\delta_B = 171.9^\circ$ (3 rad) and $\delta_B^* = 114.6^\circ$ (2 rad) or (bottom) $\delta_B = 57.3^\circ$ (1 rad) and $\delta_B^* = 286.5^\circ$ (5 rad) (w/o $B_s^0 \rightarrow \tilde{D}^{(*)0}(\pi\pi)\phi$). The purple dashed curve represents the tails generated by the correlations with the nuisance parameters $r_B^{(*)}$ and $\delta_B^{(*)}$, whereas the blue dashed curve is the core part of the distribution, and the plain red line is the sum of the two components of the fit.

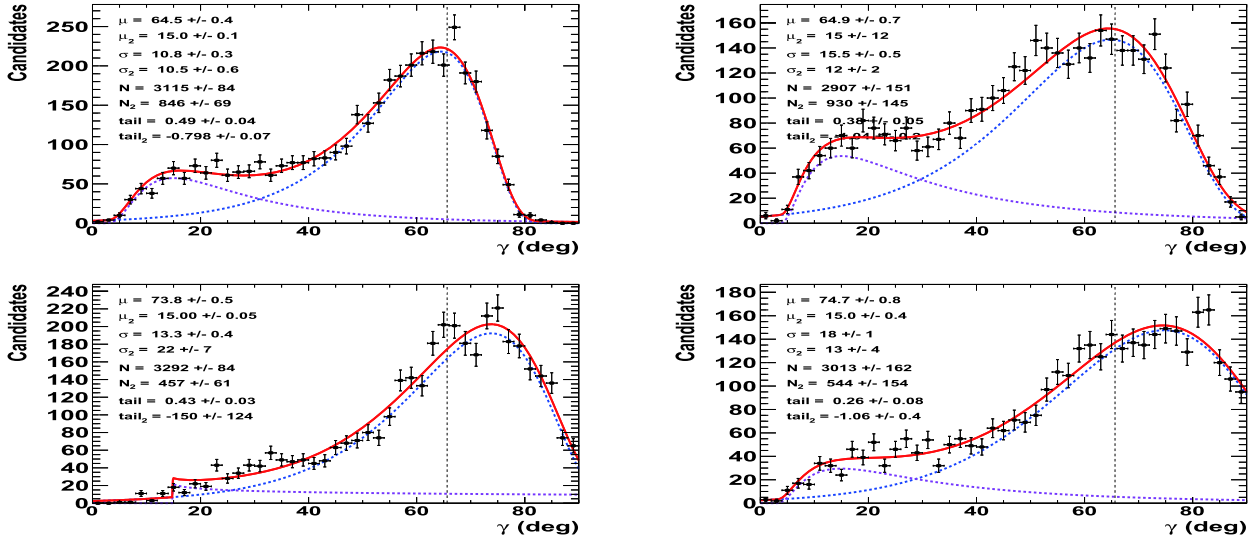


Fig. C2. (color online) Fit to distributions of γ obtained from 4000 pseudoexperiments for Run 1 & 2 LHCb dataset. The initial configuration is $\gamma = 65.66^\circ$, $r_B = 0.4$ (left) and 0.22 (right), and (top) $\delta_B = 171.9^\circ$ (3 rad) and $\delta_B^* = 114.6^\circ$ (2 rad) or (bottom) $\delta_B = 57.3^\circ$ (1 rad) and $\delta_B^* = 286.5^\circ$ (5 rad) (w/o $B_s^0 \rightarrow \tilde{D}^{(*)0}(K\pi\pi^0)\phi$). The purple dashed curve represents the tails generated by the correlations with the nuisance parameters $r_B^{(*)}$ and $\delta_B^{(*)}$, whereas the blue dashed curve is the core part of the distribution, and the plain red line is the sum of the two components of the fit.

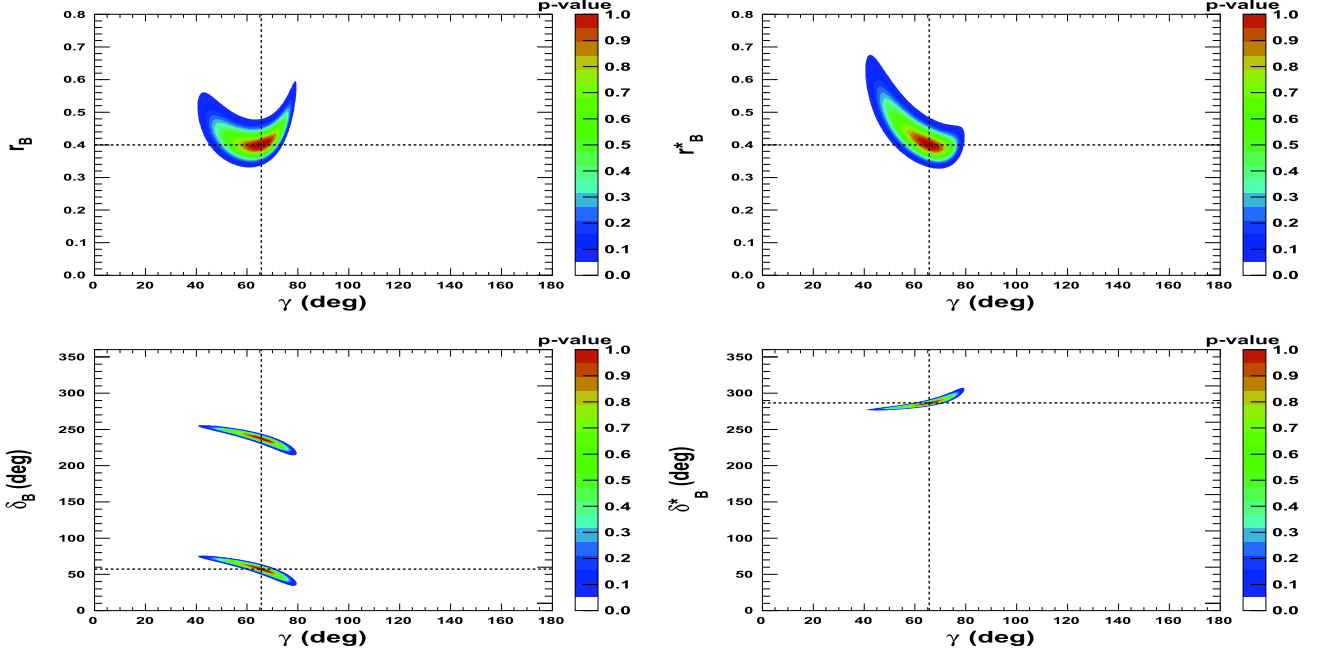
Appendix D: Other examples of 2-D p -value profiles for full HL-LHC LHCb dataset

Fig. D1. (color online) 2-D p -value profiles of nuisance parameters $r_B^{(*)}$ and $\delta_B^{(*)}$ for full HL-LHC LHCb dataset as a function of γ . In each figure, the dashed black lines indicate the initial $r_B^{(*)}$ and $\delta_B^{(*)}$ (γ) true values: $\gamma = 65.66^\circ$ (1.146 rad), $\delta_B = 57.3^\circ$ (1.0 rad), and $\delta_B^* = 286.5^\circ$ (5.0 rad), as well as $r_B^{(*)} = 0.4$.

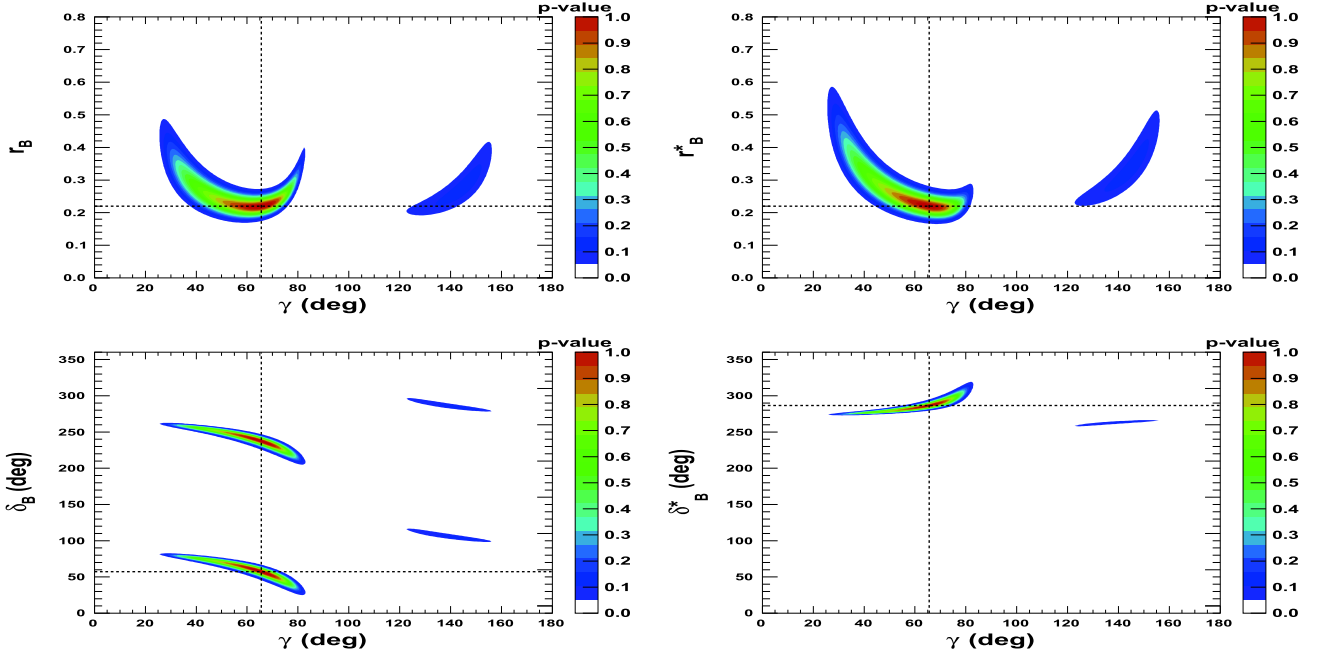


Fig. D2. (color online) 2-D p -value profiles of nuisance parameters $r_B^{(*)}$ and $\delta_B^{(*)}$ for full HL-LHC LHCb dataset as a function of γ . In each figure, the dashed black lines indicate the initial true values $\gamma = 65.66^\circ$ (1.146 rad), $\delta_B = 57.3^\circ$ (1.0 rad), and $\delta_B^* = 286.5^\circ$ (5.0 rad), as well as $r_B^{(*)} = 0.22$.

Appendix E: Half of 68.3% CL intervals of 1-D p -value profiles of γ

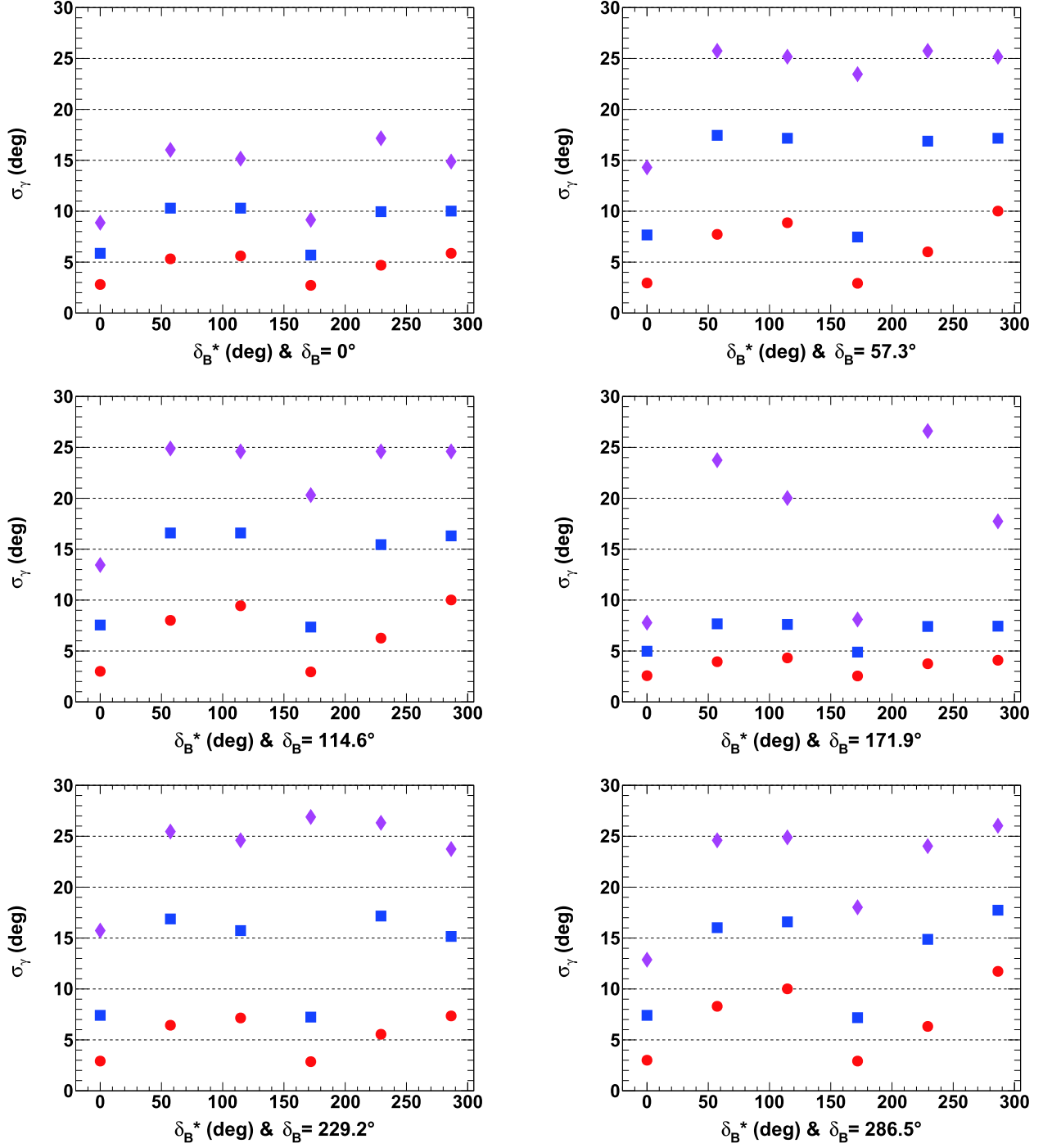


Fig. E1. (color online) Half of 68.3% CL intervals of 1-D p -value profiles of γ for Run 1 & 2 (pink lozenges), Run 1–3 (blue squares), and full HL-LHC (red circles) LHCb dataset as a function of δ_B^* , for $r_B^{(*)} = 0.4$ and initial true value of 65.66° . In each figure, the horizontal dashed black lines are guides for the eye.

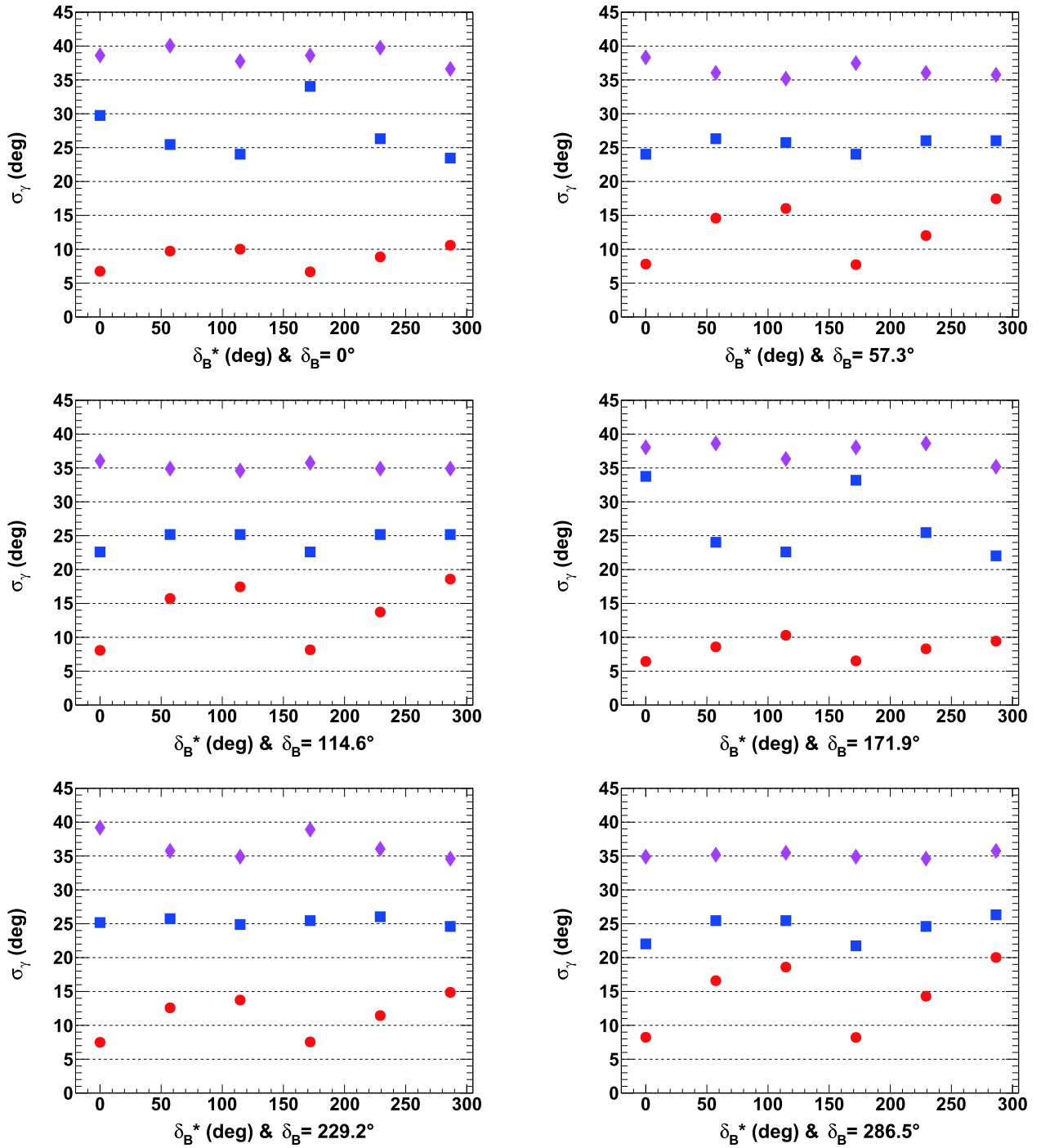


Fig. E2. (color online) Half of 68.3% CL intervals of 1-D p -value profiles of γ for Run 1 & 2 (pink lozenges), Run 1-3 (blue squares), and full HL-LHC (red circles) LHCb dataset as a function of δ_B^* , for $r_B^{(*)} = 0.22$ and initial true value of 65.66° . In each figure, the horizontal dashed black lines are guides for the eye.

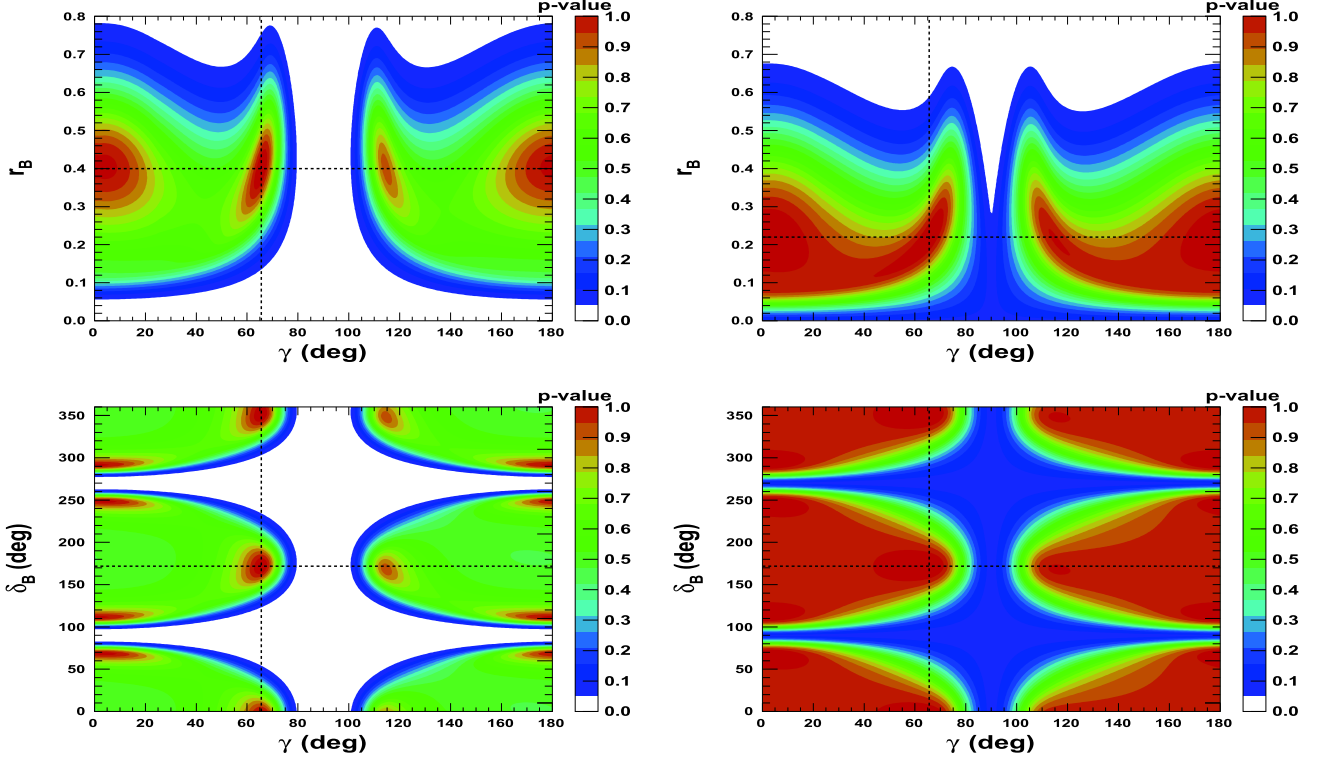
Appendix F: Excluding $B_s^0 \rightarrow \tilde{D}^{*0} \phi$ decays

Fig. F1. (color online) 2-D p -value profiles of nuisance parameters r_B and δ_B , for the Run 1 & 2 LHCb dataset, as a function of γ . In each figure, the dashed black lines indicate the initial true values $\gamma = 65.66^\circ$ (1.146 rad), $\delta_B = 171.9^\circ$ (3.0 rad), and $r_B = 0.4$ (left) and 0.22 (right) (w/o $B_s^0 \rightarrow D^{*0} \phi$).

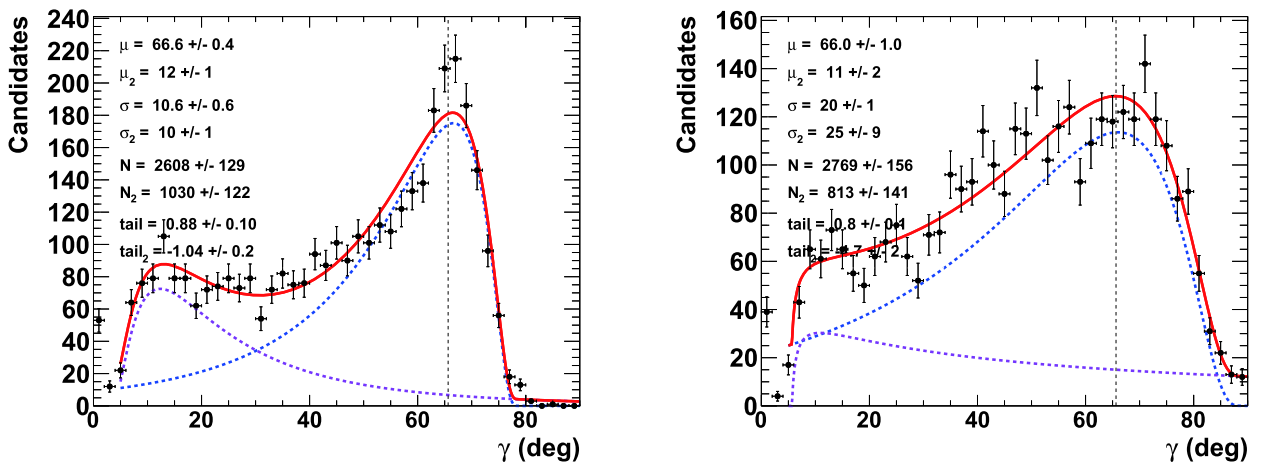


Fig. F2. (color online) Fit to distributions of γ obtained from 4000 pseudoexperiments for Run 1 & 2 LHCb dataset. The initial configuration is $\gamma = 65.66^\circ$, $r_B = 0.4$ (left) and 0.22 (right), and $\delta_B = 171.9^\circ$ (3 rad) (w/o $B_s^0 \rightarrow D^{*0} \phi$). The purple dashed curve represents the tails generated by the correlations with the nuisance parameters $r_B^{(*)}$ and $\delta_B^{(*)}$, whereas the blue dashed curve indicates the core part of the distribution, and the plain red line is the sum of the two components of the fit.

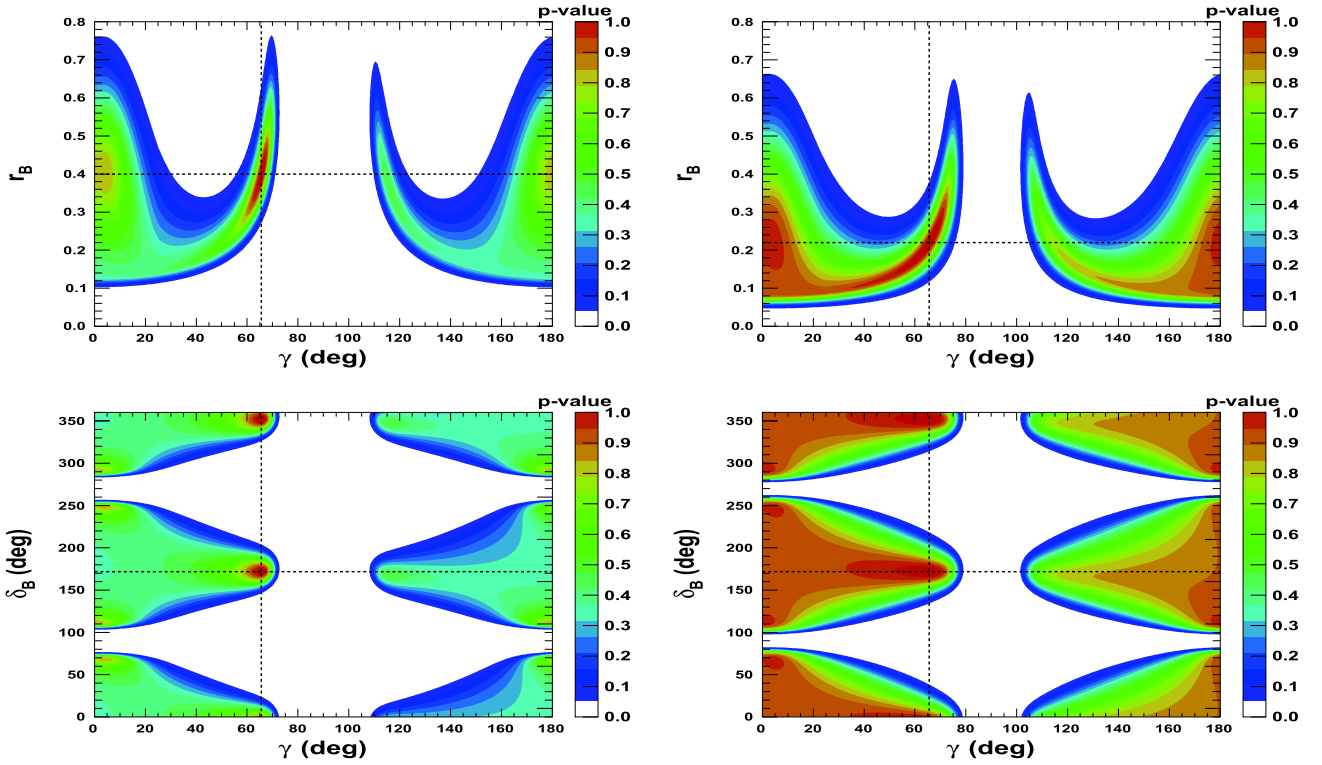


Fig. F3. (color online) 2-D p -value profiles of nuisance parameters r_B and δ_B (Run 1–3 LHCb) as function of γ . In each figure, the dashed black lines indicate the initial true values $\gamma = 65.66^\circ$ (1.146 rad), $\delta_B = 171.9^\circ$ (3.0 rad), and $\delta_B^* = 114.6^\circ$ (2.0 rad), as well as $r_B = 0.4$ (left) and 0.22 (right) (w/o $B_s^0 \rightarrow D^{*0}\phi$).

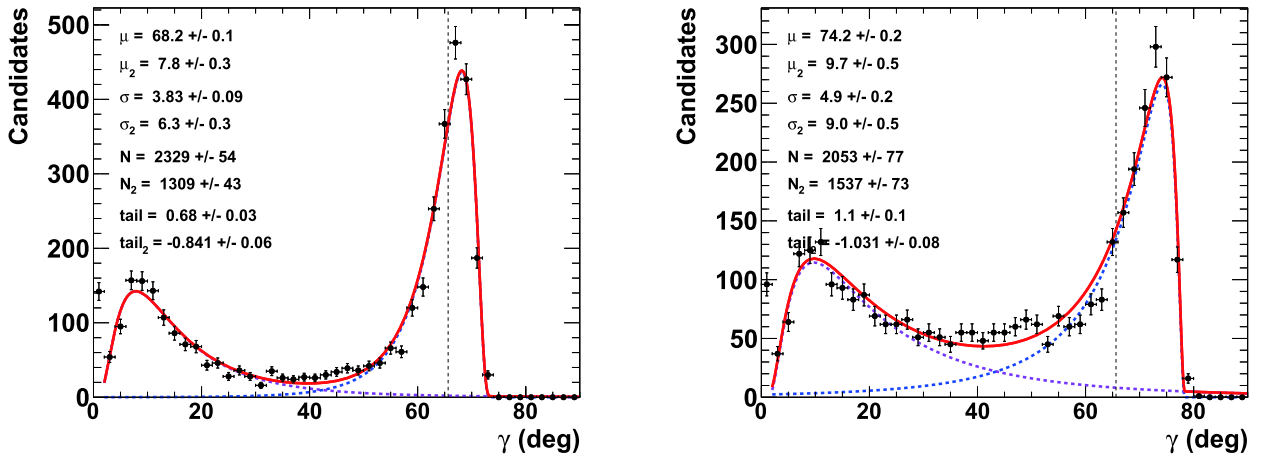


Fig. F4. (color online) Fit to distributions of γ obtained from 4000 pseudoexperiments (Run 1–3 LHCb). The initial configuration is $\gamma = 65.66^\circ$, $r_B = 0.4$ (left) and 0.22 (right), and $\delta_B = 171.9^\circ$ (3 rad) (w/o $B_s^0 \rightarrow D^{*0}\phi$). The purple dashed curve represents the tails generated by the correlations with the nuisance parameters $r_B^{(*)}$ and $\delta_B^{(*)}$, whereas the blue dashed curve indicates the core part of the distribution, and the plain red line is the sum of the two components of the fit.

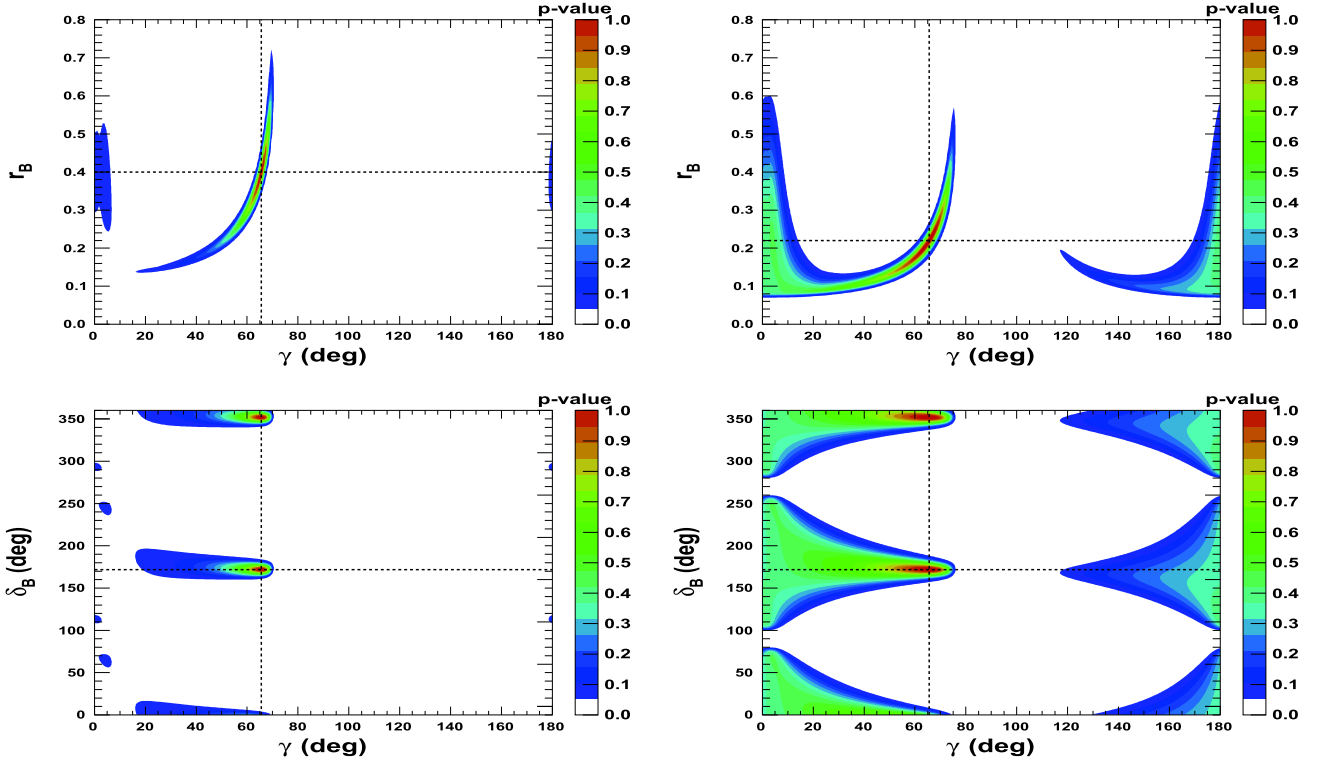


Fig. F5. (color online) 2-D p -value profiles of nuisance parameters r_B and δ_B (full HL-LHC LHCb) as function of γ . In each figure, the dashed black lines indicate the initial true values $\gamma = 65.66^\circ$ (1.146 rad) and $\delta_B = 171.9^\circ$ (3.0 rad), as well as $r_B = 0.4$ (left) and 0.22 (right) (w/o $B_s^0 \rightarrow D^{*0} \phi$).

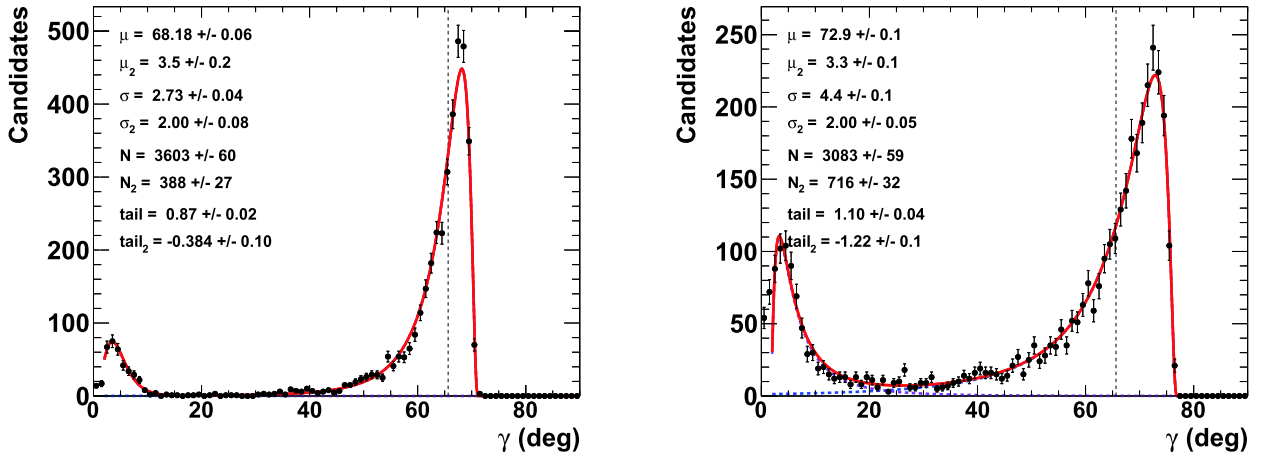


Fig. F6. (color online) Fit to distributions of γ obtained from 4000 pseudoexperiments (full HL-LHC LHCb). The initial configuration is $\gamma = 65.66^\circ$, $r_B = 0.4$ (left) and 0.22 (right), and $\delta_B = 171.9^\circ$ (3 rad) (w/o $B_s^0 \rightarrow D^{*0} \phi$). The purple dashed curve represents the tails generated by the correlations with the nuisance parameters $r_B^{(s)}$ and $\delta_B^{(s)}$, whereas the blue dashed curve indicates the core part of the distribution, and the plain red line is the sum of the two components of the fit.

References

- [1] M. Kobayashi and T. Maskawa, *Prog. Theor. Phys.* **49**, 652 (1973)
- [2] I. Dunietz, *Phys. Lett. B* **270**, 75 (1991)
- [3] M. Gronau and D. London, *Phys. Lett. B* **253**, 483 (1991)
- [4] M. Gronau and D. Wyler, *Phys. Lett. B* **265**, 172 (1991)
- [5] D. Atwood, I. Dunietz, and A. Soni, *Phys. Rev. Lett.* **78**, 3257 (1997), arXiv:[hep-ph/9612433](#)
- [6] D. Atwood, I. Dunietz, and A. Soni, *Phys. Rev. D* **63**, 036005 (2001)
- [7] A. Bondar, *Proceedings of BINP special analysis meeting on Dalitz analysis, 24-26 Sep. 2002*, unpublished;
- [8] A. Giri, Yu. Grossman, A. Soffer *et al.*, *Phys. Rev. D* **68**, 054018 (2003), arXiv:[hep-ph/0303187](#)
- [9] A. Poluektov *et al.* (Belle Collaboration), *Phys. Rev. D* **70**, 072003 (2004), arXiv:[hep-ex/0406067](#)
- [10] Yu. Grossman, Z. Ligeti, and A. Soffer, *Phys. Rev. D* **67**, 071301 (2003), arXiv:[hep-ph/0210433](#)
- [11] A. Ceccucci, T. Gershon, M. Kenzie *et al.*, arXiv: 2006.12404 [physics.hist-ph]
- [12] M. W. Kenzie and M. P. Withead (on behalf of the LHCb Collaboration), LHCb-CONF-2018-002, CERN-LHCb-CONF-2018-002
- [13] R. Aaij *et al.* (LHCb Collaboration), LHCb-PAPER-2020-019, CERN-EP-2020-175, arXiv: 2010.08483 [hep-ex]
- [14] R. Aaij *et al.* (LHCb Collaboration), *J. High Energy Phys.* **1803**, 059 (2018), arXiv: 1712.07428[hep-ex].
- [15] M. Schiller (on behalf of the LHCb Collaboration), *CERN LHC seminar*, and LHCb-PAPER-2020-030 in preparation.
- [16] M. W. Kenzie and M. P. Withead (on behalf of the LHCb Collaboration), LHCb-CONF-2020-003, CERN-LHCb-CONF-2020-003
- [17] R. Aaij *et al.* (LHCb Collaboration), *J. High Energy Phys.* **08**, 137 (2016), arXiv:[1605.01082\[hep-ex\]](#)
- [18] R. Aaij *et al.* (LHCb Collaboration), *J. High Energy Phys.* **08**, 041 (2019), arXiv:[1906.08297\[hep-ex\]](#)
- [19] E. Kou *et al.* (Belle II Collaboration), *Prog. Theor. Exp. Phys.*, (2019), arXiv:[1808.10567\[hep-ex\]](#)
- [20] I. Bediaga *et al.* (LHCb Collaboration), CERN-LHCC-2018-027, LHCb-PUB-2018-009, arXiv: 1808.08865 [hep-ex]
- [21] R. Aaij *et al.* (LHCb Collaboration), *Phys. Lett. B* **727**, 403 (2013), arXiv:[1308.4583\[hep-ex\]](#)
- [22] R. Aaij *et al.* (LHCb Collaboration), *Phys. Rev. D* **98**, 071103 (2018), arXiv:[1807.01892\[hep-ex\]](#)
- [23] R. Aaij *et al.* (LHCb Collaboration), *Phys. Lett. B* **777**, 16 (2017), arXiv: 1708.06370 [hep-ex] And update in LHCb-PAPER-2020-036, in preparation
- [24] M. Gronau, Y. Grossman, N. Shuhmaher *et al.*, *Phys. Rev. D* **69**, 113003 (2004), arXiv:[hep-ph/0402055](#)
- [25] M. Gronau, Y. Grossman, Z. Surujon *et al.*, *Phys. Lett. B* **649**, 61 (2007), arXiv:[hep-ph/0702011](#)
- [26] S. Ricciardi, LHCb-PUB-2010-005, CERN-LHCb-PUB-2010-005
- [27] Y. Amhis *et al.* (Heavy Flavor Averaging Group (HFLAV)), arXiv: 1909.12524 [hep-ex] and online updates at [hflav.web.cern.ch](#)
- [28] R. Aaij *et al.* (LHCb Collaboration), *Phys. Lett. B* **760**, 117 (2016), arXiv:[1603.08993\[hep-ex\]](#)
- [29] R. Aaij *et al.* (LHCb Collaboration), *Phys. Rev. D* **91**, 112014 (2015), arXiv:[1504.05442\[hep-ex\]](#)
- [30] Y. Grossman, A. Sofer, and J. Zupan, *Phys. Rev. D* **72**, 031501 (2005), arXiv:[hep-ph/0505270](#)
- [31] M. Martone and J. Zupan, *Phys. Rev. D* **87**, 034005 (2013), arXiv:[1212.0165\[hep-ph\]](#)
- [32] M. Tanabashi *et al.* (Particle Data Group), *Phys. Rev. D* **98**, 030001 (2018)
- [33] M. Gronau, Y. Grossman, Z. Surujon *et al.*, *Phys. Lett. B* **649**, 61 (2007)
- [34] R. Aaij *et al.* (LHCb Collaboration), *Phys. Rev. Lett.* **108**, 101803 (2012), arXiv:[1112.3183\[hep-ex\]](#)
- [35] R. Aaij *et al.* (LHCb Collaboration), *J. High Energy Phys.* **04**, 001 (2013), arXiv: 1301.5286 [hep-ex]; the f_1/f_d value was updated in the report LHCb-CONF-2013-011, CERN-LHCb-CONF-2013-011
- [36] T. Evans, S. Harnew, J. Libby *et al.*, *Phys. Lett. B* **757**, 520 (2016) and Erratum *ibid* **B 765**, 402 (2017), arXiv: 1602.07430 [hep-ex]
- [37] A. Bondar and T. Gershon, *Phys. Rev. D* **70**, 091503 (2004), arXiv:[hep-ph/0409281](#)
- [38] The LHCb Collaboration public page
- [39] R. Aaij *et al.* (LHCb Collaboration), *J. High Energy Phys.* **1308**, 117 (2013), arXiv:[1306.3663\[hep-ex\]](#)
- [40] R. Aaij *et al.* (LHCb Collaboration), *Phys. Rev. Lett.* **118**, 052002 (2017) [Erratum *ibid* **119**, 169901 (2017)], arXiv: 1612.05140 [hep-ex]
- [41] R. Aaij *et al.* (LHCb Collaboration), *J. High Energy Phys.* **10**, 097 (2014), arXiv:[1408.2748\[hep-ex\]](#)
- [42] J. Charles *et al.* (The CKMfitter Group), CKMfitter Summer 2019 update
- [43] A. Bondar and A. Poluektov, *Eur. Phys. J. C* **47**, 347 (2006), arXiv: hep-ph/0510246 and *Eur. Phys. J. C* **55**, 51 (2008), arXiv: 0801.0840 [hep-ex]
- [44] J. Libby *et al.* (BES-III Collaboration), *Phys. Rev. D* **82**, 112006 (2010), arXiv:[1010.2817\[hep-ex\]](#)
- [45] M. Ablikim *et al.* (BES-III Collaboration), *Phys. Rev. D* **101**, 112002 (2020), arXiv: 2003.00091 [hep-ex] and *Phys. Rev. D* **102**, 052008 (2020), arXiv: 2007.07959 [hep-ex]
- [46] I. Adachi *et al.* (BaBar and Belle Collaboration), *Phys. Rev. D* **98**, 110212 (2018)
- [47] J. Charles *et al.* (The CKMfitter Group), *Eur. Phys. J. C* **41**, 1 (2005), arXiv: hep-ph/0406184, updated at [ckmfitter.in2p3.fr]
- [48] J. P. Lees *et al.* (BaBar Collaboration), *Phys. Rev. D* **84**, 112007 (2011) and Erratum *ibid* **D 87**, 039901 (2013), arXiv: 1107.5751 [hep-ex]
- [49] V. Tisserand (on behalf of the BaBar and Belle Collaborations), eConf **C070512**, 009 (2007), arXiv:[0706.2786\[hep-ex\]](#)
- [50] B. Sen, M. Walker, and M. Woodroffe, *Statistica Sinica* **19**, 301-314 (2009)
- [51] G. Cowan (for the Particle Data Group), *review on statistic in Phys. Rev. D* **98**, 030001 (2018) and 2019 online update
- [52] T. Evans, J. Libby, S. Malde *et al.*, *Phys. Lett. B* **802**, 135188 (2020), arXiv:[1909.10196\[hep-ex\]](#)
- [53] H. Ikeda *et al.* (Belle Collaboration), *Nucl. Instrum. Meth. A* **441**, 401-426 (2000)
- [54] D. M. Asner *et al.*, *Int. J. Mod. Phys. A* **24**, S1-794 (2009), arXiv: 0809.1869 [hep-ex]
- [55] R. Aaij *et al.* (LHCb Collaboration), *Phys. Rev. D* **98**, 072006 (2018), arXiv:[1807.01891\[hep-ex\]](#)
- [56] S. Nandi and D. London, *Phys. Rev. D* **85**, 114015 (2012), arXiv:[1108.5769\[hep-ph\]](#)
- [57] H. Sheng Chen, *Nucl. Phys.- Proceedings Supplements B* **59**(13), 316-323 (1997)
- [58] S. Eidelman, *Nucl. and Part. Phys. Proceedings* **260**, 238-241 (2015)
- [59] *Joint Workshop of future tau-charm factory (2018) Orsay, France and Joint Workshop on future charm-tau Factory (2019) Moscow, Russia.*